DEVELOPMENT OF CALIBRATION, STRIDE TRACKING, AND ACTIVITY RECOGNITION ALGORITHMS USING INERTIAL MEASUREMENT UNITS TOWARD LONG-TERM OUT-OF-LAB GAIT MEASUREMENTS

A Thesis

Presented to

the faculty of the School of Engineering and Applied Science

University of Virginia

In Partial Fulfillment

of the requirements for the Degree

Master of Science (Mechanical Engineering)

by

Travis Simpson

May, 2014

APPROVAL SHEET

The thesis is submitted in partial fulfillment of the requirements

for the degree of

Master of Science (Mechanical Engineering)

Travis Simpson
Author

This thesis has been read and approved by the examining Committee:

Brad Bennett
Advisor

Silvia Blemker

John Lach

Shawn Russell

Accepted for the School of Engineering and Applied Science:

Dean, School of Engineering and Applied Science

May, 2014

Clinical gait analysis can provide valuable information about walking pathologies experienced in neuromuscular conditions such as cerebral palsy. However, the motion capture based gait analysis commonly used is not without its limitations. In particular, most subject visits are short and may repeat yearly or even less often. During this span, the effectiveness of interventions and pathological progression can be difficult to assess. Recent developments in sensor technology have made gait analysis using accelerometers, gyroscopes, and other sensors feasible. The development of new analytical tools could provide never before seen insight into pathology and its propagation in everyday activity. As a potential solution, this work proposes comprehensive methods for sensor signal preparation and processing applied to a wireless, remote gait sensing platform.

A validated framework will be presented for creation of a gait observation system for everyday activities, particularly walking and running. Elaboration of spatio-temporal methodology ascends from the lowest level of design as follows: sensor calibration; coordinate frame alignment; gait event detection; spectrum analysis of static and dynamic activity; sensor orientation; and stride motion. Methods are validated using data collected on five healthy participants wearing a sensor embedded ankle-foot-orthosis. Each level of validation produced comparable, if not superior accuracy relative to claims of singular studies in the literature. The work is concluded with a follow-up collection on a single subject, on which this work's all-inclusive capabilities are demonstrated by successfully pairing the spatio-temporal methodology with a modified adaptation of a previously validated activity recognition approach**.** Ultimately, the proposed framework proved capable of high fidelity gait identification and tracking in healthy subjects with potential extensibility to the clinical gait analysis of disorders such as cerebral palsy.

TABLE OF CONTENTS

LIST OF FIGURES

LIST OF TABLES

INTRODUCTION

Motion analysis has tremendous applications in many fields, particularly athletics and medicine. Labs using optical motion capture (motion analysis/gait labs) have become the gold standard for measuring human kinematics and with force plate data, kinetics. However, these systems are expensive and data collected in the lab may not correlate with actual performance in daily life. To address this concern, researchers and to a limited extent clinicians have begun to use inertial measurement units (IMUs) to record movements in and out of the lab.

Initial work with IMUs has been performed in the lab or at locations where data could be sent via Bluetooth to a local computer. However, such systems, which can be less expensive and more portable than optical motion capture systems, do not address the challenge of measuring out-of-lab naturally occurring movement over extended periods of time. Some additional work has been started to improve these systems by integrating local data storage, removing the need for a nearby collecting computer.

This thesis presents work that is part of a project to develop the ability to measure movement, i.e. gait, over periods of months where the IMUs are mounted in an ankle foot orthosis (AFO). Specifically, this work addresses the calibration of accelerometers and gyroscopes, the development of algorithms to compute stride kinematics in walking and running, and corresponding validation so that such systems are all-inclusive and available for use in the field.

While disciplines as diverse as athletics and ergonomics can benefit from out-of-lab movement measurement, the ultimate goal here is to measure children's gait as affected by cerebral palsy (CP), which is often assisted by AFOs. A primary reason for prescribing these

devices to these children is preventing contractures of the plantar flexors of the ankle. To date, there has been no unequivocal evidence indicating whether AFOs prevent contractures or under what conditions/use they could prevent contractures of the plantar flexors of the ankle. In addition, previous work in our lab has shown that AFOs do not always improve the gait of children with CP.[1] The development of the instrumentation and associated algorithms will for the first time allow testing of the hypothesis that AFO use can prevent these contractures during functional, everyday use, as well as how everyday gait changes as a result. In particular, observation of walking on a stride by stride basis can provide relevant clinical information and will be the primary focus of this work, along with general activity recognition.

PROPOSED SOLUTION TO REMOTE GAIT ANALYSIS

In summary this thesis describes the development of algorithms and procedures to create a high fidelity inertial based gait system, as well an analytical framework by which similar systems could be constructed. A bottom-up approach is used to identify and expound upon key operations necessary to produce an accurate system. Solutions for calibration and conversion; coordinate frame alignment; noise compensation; stride detection and segmentation; stride kinematics; and activity recognition toward long-term, self-contained gait analysis are cohesively demonstrated using TEMPO (Technology Enabled Medical Precision Observation) IMUs developed by the Inertia Team at the UVA Center for Wireless Health. For cerebral palsy subjects, individual TEMPO nodes were strapped to the legs and feet. Additionally, a deployable custom AFO was manufactured and fit to an average adult foot by UVA Health's Prosthetics and Orthotics and tested on healthy adult subjects. The individual sections' results were comparable and in many cases more accurate

than those presented in previous literature. Additionally, the methods presented function together to provide identification and quantitative characterization of walking and running without any user supervision. The system is proven to be comparable to motion capture in accuracy without many of its limitations, rivaling previous attempts in the literature to produce a validated high accuracy remote gait analysis platform.

The remainder of this thesis is organized in the following manner. First related background is explored. This includes a basic description of human gait, the characteristics of available micro-electro-mechanical sensors/systems (MEMS), the UVA TEMPO nodes that were used, and signal processing algorithms previously employed by other researchers. Next the calibration process for both the accelerometers and gyroscopes is discussed. In order to produce accurate and precise estimations, removal of undesirable characteristics of sensors is essential. Since the framework for stride tracking is purely physical based, sensor measurements need to be as ideal as possible; this involved removal of constant biases, imperfect orthogonality, and axis inter-dependence. Calibration is followed by a description of how the local axes of the instruments are aligned with a known global coordinate system to establish clinically relevant measurements.

Then the method by which gait events, e.g. foot contact and foot off, are detected. This allows for segmentation and framing of results consistent with traditional motion capture and clinical analysis. Subsequent estimation methods for kinematics and gait metrics also require this detection and segmentation process. Since much of the error in the original sensor signals cannot be removed via calibration, noise can further be reduced by choosing filtering cutoffs carefully with frequency analysis during static and active periods of interest. Furthermore, a spectral analysis of accelerometer and gyroscope signals is also presented to

optimize signal filtering with respect to static and active periods, as well as gain insight into frequency content of gait.

Finally, the computational algorithms for kinematics and gait metrics based on a first principle approach are described. Specifically, sagittal rotation (flexion/extension) and stride speed on a treadmill are validated to provide accuracy and precision measures. A first principle approach is implemented to allow for highly generalized results with extensibility to a large number of applications. Additionally, sample by sample kinematic measurements are retrievable due to this implementation, since only physically related processing and corrections are performed as opposed to methods such as linear regression or machine learning. This spatio-temporal body of work is then combined with a modified version of Archer's activity recognition method.[2] The modified method is tested on a returning subject to demonstrate its potential as a gait analysis tool. In conclusion, the work is summarized and discussed with respect to application, limitations, and future work.

BACKGROUND

This thesis outlines a framework for acquiring quantitative spatio-temporal gait information from IMUs mounted in AFOs. This work includes using activity recognition methods previously developed in conjunction with the spatio-temporal methods of this research. This section begins with a basic description of gait biomechanics and the sensors used in IMUs including a description of the TEMPO devices. Next the methods used to interpret the IMU signals are described. Lastly, research applying such methods to pathological gait is discussed.

GAIT BIOMECHANICS

The purpose of modern day motion analysis is to measure kinematics and/or kinetics to gain insight into human movement. Biomechanics parameters are measured depending upon the application as movement examination is used both in research and the clinic with walking, running, jumping, and many other athletic motions. For clinical assessments of pathological gait, certain metrics are commonly used to frame normal walking kinematics. Using these metrics, a subject's gait is often compared to that of healthy individuals to narrow what deficiencies could be causing pathological patterns. The following section will briefly outline some of these metrics and details of the gait cycle.

Gait Cycle

The "gait cycle" is a term which describes the repetitive mechanical processes of the lower body which propel the body center of mass (COM) forward during walking or running. Because walking is the most efficient form of locomotion on level terrain, most humans have very similar gait patterns. The gait cycle encompasses a full stride, or a single stride by both the left and right legs, and consists of phases of double support, stance, and swing.

Figure 1 shows a full human gait cycle.[3] Double support phases are defined by periods when both feet contact the ground. The stance phase for a leg is defined by the period when the foot touches the ground. The stance phase for each leg encompasses both the double support phase and the swing phase of the opposite leg. Swing phase for a leg is defined by the period when the foot is not in contact with the ground, and it coincides entirely with the stance phase of the opposite leg.

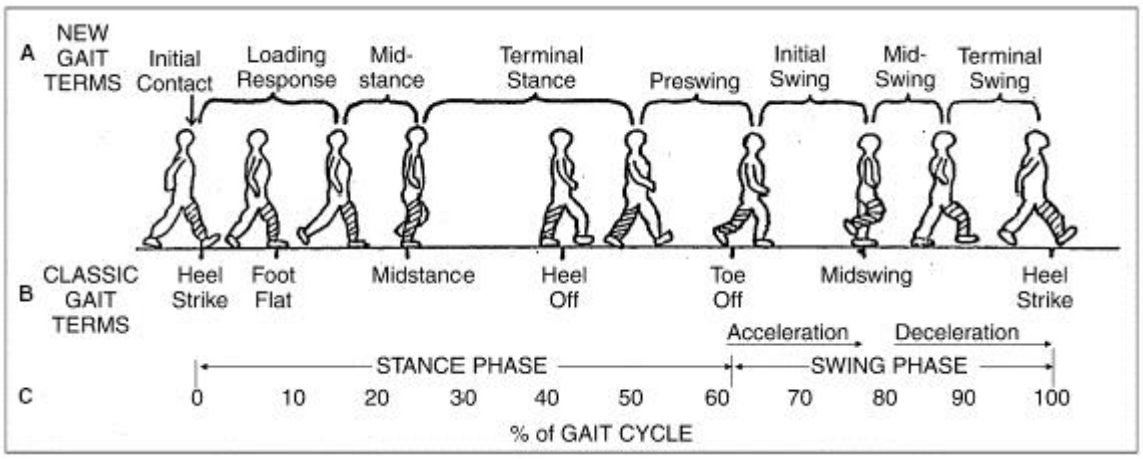

Figure 1. Common gait cycle event terminology with approximate percentage of stance and swing phase. Taken from Cuccurollo.

Most clinicians choose the beginning of the gait cycle to be defined by foot contact of the forward leg. In this discussion, the initial forward leg will be the right leg. At this point the rearward (left) leg will still be in contact with the ground, so the gait cycle begins in an initial double support phase. During the initial double support phase, the anchoring of the right leg results in a deceleration of the COM, with most of the weight of the body shifting to the right leg[4]. As the weight shifts forward, the left leg supports less and less weight, and the left ankle alternates from dorsiflexion to plantarflexion in typical subjects. This plantarflexion of the rear foot provides the majority of the propulsive power in the gait

cycle. However, the presence and extent of plantarflexion and dorsiflexion may vary and be more unpredictable in pathological gait patterns.

Gait Metrics

Locomotion is also of clinical significance, especially in cases of CP, injury rehabilitation and traumatic brain injury.[5–7] The most common measures examined by clinicians, biomechanics, and researchers include joint angle, step or stride length, step or stride, cadence, and step or stride speed. As far as joint angles, sagittal rotations are typically of the most interest as they are the primary driving motion related to walking and running motions. For gait analysis, sagittal knee and ankle angle are of particular interest to biomechanists. In the case of cerebral palsy, sagittal ankle angle is particularly informative for clinicians as it indicates extent of plantar/dorsiflexion in subjects.

Often times, stride speed or distance is used as a parameter to test rehabilitative progress at physician and therapist visits. Additionally, speed, distance, and time of strides and steps are performance measures in sports such as running. Step and stride related metrics deal with single leg and combined leg motion during walking, respectively. Remaining consistent with the gait cycle, a step begins with a heel strike and ends with a contralateral heel strike. A stride begins with a heel strike and ends with an ipsilateral heel strike. Length of steps and strides are calculated as the distance covered between the beginning and ending condition. Similarly, cadence is the time it takes to complete one such sequence. Speed is calculated by distance times cadence on a per step or per stride basis.

LIMITATIONS OF CLINICAL GAIT ANALYSIS

Although traditional gait analysis in neurological disorders such as CP is the gold standard, there is significant room for improvement. From the patient's standpoint, even scheduling an appointment can be challenging due to the travel time and costs of medical visits for patients and their families. This immediately limits the practical frequency at which gait analysis can be performed. Even so, there is no work providing perspective on how a subject's gait or even general activity may change in continuous, everyday settings. Attempts to assess changes in pathology over multiple lab visits are the closest studies have come to long-term analysis. Insight into repeated everyday activity could provide valuable information about treatment options and effectiveness of interventions but is currently unavailable with traditional gait analysis. In particular, the effectiveness of ankle-foot-orthoses is difficult to assess given the spacing of medical visits and controlled environment in an in-lab gait analysis. A gait sensing system that is unobtrusive but constantly collecting data every day could potentially determine the effectiveness of AFOs in improving functional gait as compared to no corrective devices.

Motion capture gait analysis is based on the premises that results are both representative of "normal" functioning of the subject on an everyday basis and superior to human observation alone. The first premise is very difficult to assess since an out-of-lab to in-lab activity comparison is not yet possible, although the foundation for such work is being laid by this and other research. Although this premise may not be presumed by experts or clinicians, a system that could identify in-lab to out-of-lab relationships would be useful. The second premise may be true in some regards but a gait expert could hypothetically observe much of what is occurring pathologically without the assistance of an automated, computer based method provided by motion capture systems such as Vicon. In some instances,

biomechanists, physicians or physical therapists are knowledgeable enough to function as gait experts, making quantitative gait analysis via motion capture somewhat redundant from a practical, treatment standpoint. This is not to say that motion capture based gait analysis is not useful but that even with automated computer algorithms, it is still an expert supervised process.

Thus, an ideal system would allow remote, unsupervised collection that would otherwise be impossible with motion capture. If validated and proven to produce accurate results, such a system would dispel any controversy related to the aforementioned premises involved with traditional motion capture. In particular, gait experts could not possibly observe and analyze a subject over the course of a day, nor would the "normal" functioning of the participants be in question since the data would be collected over long periods of time. Additionally, this would complement traditional motion capture by providing supplementary information to in-lab analysis to assess longitudinal change continuously. Zatsiorsky's book on human gait can provide extensive insight into gait metrics and common conventions.[8]

SENSING OPTIONS

For the design of a system small enough to be implanted in an AFO without affecting gait, a sensor system must be small, efficient, self-contained, and comparable to the accuracy and precision of traditional methods of gait analysis. Modern micro-electro-mechanical systems (MEMS) assembled into IMUs fit all these requirements, enabling research into topics such as this thesis. Although MEMS magnetometers and GPS are sometimes used in navigation systems, the present work only employed accelerometers and gyroscopes. An overview of

the advantages, disadvantages, operational characteristics and motivation for the design choices made in this work is presented below.

MEMS Accelerometers

An accelerometer measures the proper acceleration of the small fixed area of which it is attache. There are both digital and analog varieties of accelerometers. Practically, both types will be functionally consubstantial since analog accelerometers are conventionally converted to digital signals. Most commonly, digital outputs (ADC values) correspond to voltages experienced by each axis within the accelerometer structure. Therefore, calibration models must be used to convert the digital signal to a conventional unit. Accelerometers are designed to have linear conversions from ADC to conventional units. Due to manufacturing limitations, there are relatively small interactions between each sensing axis of the accelerometer modeled by cross-axis sensitivities. Similarly, the axes are not perfectly orthogonal. Manufacturers provide specifications of the manufacturing tolerances for these factors, as well as sensitivities (scale factor) and biases (offsets) for converting digital output to g's or some other conventional unit. High-frequency, zero-mean noise is present in MEMS accelerometers due to their internal mechanisms. Temperature also affects sensor output but the relationship is not usually modeled for room temperature applications. Energy consumption for MEMS accelerometers is considerably lower than gyroscopes, leading to some attempts to replace gyroscopes with rigid accelerometer arrays.[9,10]

MEMS Gyroscopes

From a practical standpoint, gyroscopes function comparably to accelerometers, except that they measure angular velocity instead of linear acceleration. They can be produced in both digital and analog forms. Manufacturers account for a linear conversion model with

sensitivities, biases, and misalignment tolerances. Temperature dependence is usually treated the same as with accelerometers, although power consumption is much higher which can result in larger internal gradients. Consequently, low-frequency drift is a common characteristic of MEMS gyroscopes, most notably directly following turn-on. High-frequency noise is less prevalent than in accelerometers, leading to better results for integration if low-frequency biases are removed. A further complication arises from many commercially available gyroscopes being limited to bi-axial or uniaxial configurations, forcing users to manually align a uniaxial and biaxial gyroscope for a triaxial system.

MEMS Magnetometer

Magnetometers are commonly used in modern navigation systems to yield sensor orientation in highly dynamic periods of motion. Since accelerometers can only accurately yield orientation during static periods and gyroscopes may drift when integrated for orientation, magnetometers can counteract the error accumulated by integration drift through feedback systems such as Kalman filters. However, as they measure magnetic field, they are sensitive to changes in location and metal interactions. Additionally, they tend to sample much slower than accelerometers and gyroscopes making them unreliable at exclusively tracking orientation during high frequency activity. Ultimately, difficulty in obtaining a compatible 9-axis (accelerometer, magnetometer, and gyroscope) solution led to the use of a 6-axis IMU (accelerometer and gyroscope) in this work. A better solution would include a magnetometer considering its physical and energy footprint are a relatively small addition.

GPS

Global Positioning Systems (GPS) have also been used for navigation systems, notably for military or automotive purposes. A GPS receiver is located by orbiting satellites providing a

global position trajectory at a specified sampling rate. Its effectiveness over long-distances and in varied circumstances is the biggest advantage of this system, as long as the GPS receiver can be seen by four or more satellites. However, GPS precision can vary more than local, self-contained solutions such as gyroscopes, accelerometers, and magnetometers, particularly over small distances. Navigation solutions adding GPS to 6- or 9-axis systems have been well researched, showing little advantage at the scale needed for gait analysis. This along with the added size requirement deemed GPS inappropriate for this work. GPS is also occasionally used as validation when motion capture is unavailable. Due to the aforementioned issues, its use as a high fidelity validation tool is inferior to motion capture in a lab setting.

TEMPO SOLUTION

TEMPO 3.1 and 3.2f are custom body sensor platforms designed and built by researchers of the University of Virginia's Inertia Team. TEMPO body sensor networks (BSNs) incorporate an accelerometer and gyroscope in the form factor of a wristwatch to enable kinematic data collection. These systems have been previously used in assessing human motion and gait pathology. Specifically, the sensors have been used to assess tremor in individuals with Parkinson's disease[11], differentiating normal and "shuffling" gait[12], fall detection[13], and spatio-temporal gait feature extraction[14,15]. These studies have demonstrated success in using TEMPO sensors to quantify and classify normal and pathological movement and gait, and provide additional support to the concept of AFO sensor mounting as a means of quantifying and classifying gait in AFO users such as children with CP.

TEMPO BSNs are particularly attractive for use with AFOs because they are wireless, capable of Bluetooth real-time data receiving (TEMPO 3.1), as well as long-term

Flash memory storage (TEMPO 3.2f). Their small form factor allows them to be discreetly mounted within modified AFOs with no discomfort to the wearer. To test the efficacy of each version, integrated AFO solutions were created for both 3.1 and 3.2f versions of TEMPO.

General AFO Design

Two versions of the AFO instrumentation were created similarly in design and execution. The two systems were meant to be compared, validated and assessed for advantages and disadvantages. The primary practical difference between the two versions was wireless data collection (3.1 version) vs. flash storage (3.2f version). Left and right AFOs were molded to size US 10.5 male feet for 3.2f and 3.1 versions, respectively, thanks to UVA Health's Prosthetics and Orthotics group. Two sensors were placed in each AFO corresponding to areas proximal of the instep of the foot (slave sensor) and posterior shank (master sensor). A rechargeable battery was placed posterior to the shank sensor and directly wired to both sensors. A single, unified USB breakout for data download and charging was created inferior to the shank sensor and superior to the ankle.

TEMPO 3.1 AFO

The TEMPO 3.1 solution incorporated a mixed-signal processor (TI MSP430F1611) to facilitate digital signal processing and a Bluetooth 2.0 transceiver (Roving Networks RN-41) for wireless communication to a PC or smart phone. The shank and foot sensors functioned independently, each requiring wireless connection and emission for data collection; this design was not optimal given that a recording computer was required to continually receive the data. Freescale MMA7261 tri-axial, monolithic, micro-machined accelerometer records accelerations at a selected sensitivity of ±10g to accommodate a wide range of human

movement applications. Two micro-machined gyroscopes, the InvenSense IDG-300 (dual axis) and Analog Devices ADXRS610 (single axis), capture triaxial angular velocity to up to ±500 degrees per second. Experimentation on running trials indicate angular velocity in the shank and foot may approach 400 degrees per second, indicating the need for such ranges for high intensity observation.

Sensor outputs were conditioned by single-pole low-pass filters with 60 Hz cutoff frequencies. The six signals were captured by 12-bit analog to digital converter (ADC) channels. Conditioned signals were sampled at 128 Hz – a bandwidth far exceeding the characteristic response of human movement. The MSP430 processor operated at 4 MHz by a digitally-controlled oscillator synchronized to a low-power 32 kHz crystal. For a complete introduction to TEMPO 3.1 BSNs, see the seminal work by Barth et al[16].

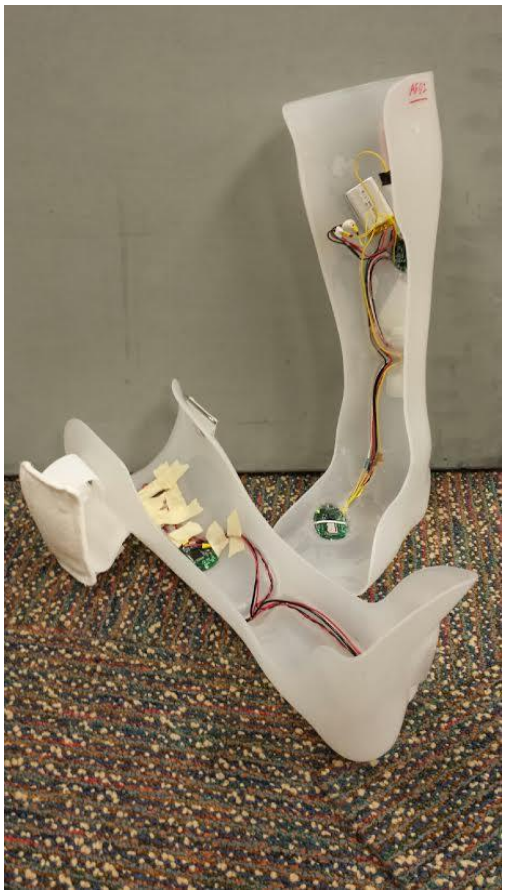

Figure 2. Prototypes for 3.1 (left) and 3.2f (right) AFOs.

TEMPO 3.2f AFO

TEMPO 3.2f utilized the aforementioned MSP430 with improved sensors and local data collection. A flash card was placed directly on the PCB board along with the sensors and processor; Bluetooth capabilities were omitted. Accelerometry was performed with a tri-axial Freescale MMA7331LC set to ±9g. A biaxial (InvenSense IDG-650) and uniaxial (InvenSense ISZ-650) gyroscope combined to make a tri-axial gyroscope set to sense bounds

of ±2000°/sec, improving upon the sensor used in the 3.1 version. These sensors were superior to those of TEMPO 3.1 in energy consumption as well as precision. Figure 2 shows the final prototype for the TEMPO 3.1 and 3.2f AFO.

SIGNAL PROCESSING FOR WIRELESS GAIT ANALYSIS

Sensors provide valuable real-word observations when the proper measures are taken to synthesize raw data. For a self-contained wireless gait analysis tool, important gait events, as well as kinematic information must be recoverable. The background for these topics will be presented in the following section.

Activity Recognition

Activity recognition of human motion from IMU signals is a dense field with many methods for probabilistic determination of gestures and movement patterns.[17] Feature selection is particularly appropriate for pathological gait analysis, given that the kinematic basis for walking or any activity may be highly variable between participants due to neuromuscular conditions. One such hierarchical feature selection based method, k-Nearest Neighbor (kNN), was validated by Archer et al.[2] on an IMU AFO system as a supplementary approach to this thesis. This technique required computation of 23 features for the training and test data sets.

A six level kNN decision tree aided computational load and reduced false positives. As shown in Figure 3, specific designations of types of walking, running, and basic postural gestures were determined throughout the decision tree. Sensitivities for recognition of annotated activities surpassed 90% using less than 5 minutes of training data. A training partition of that data at 120 seconds was chosen as a benchmark for high sensitivity and

specificity. However, stair walking sensitivity faltered relative to level walking, incline walking, and basic gestures. To address specificity, a declassification algorithm was also developed. For more background information and further details on this algorithm, see Archer's thesis.[18]

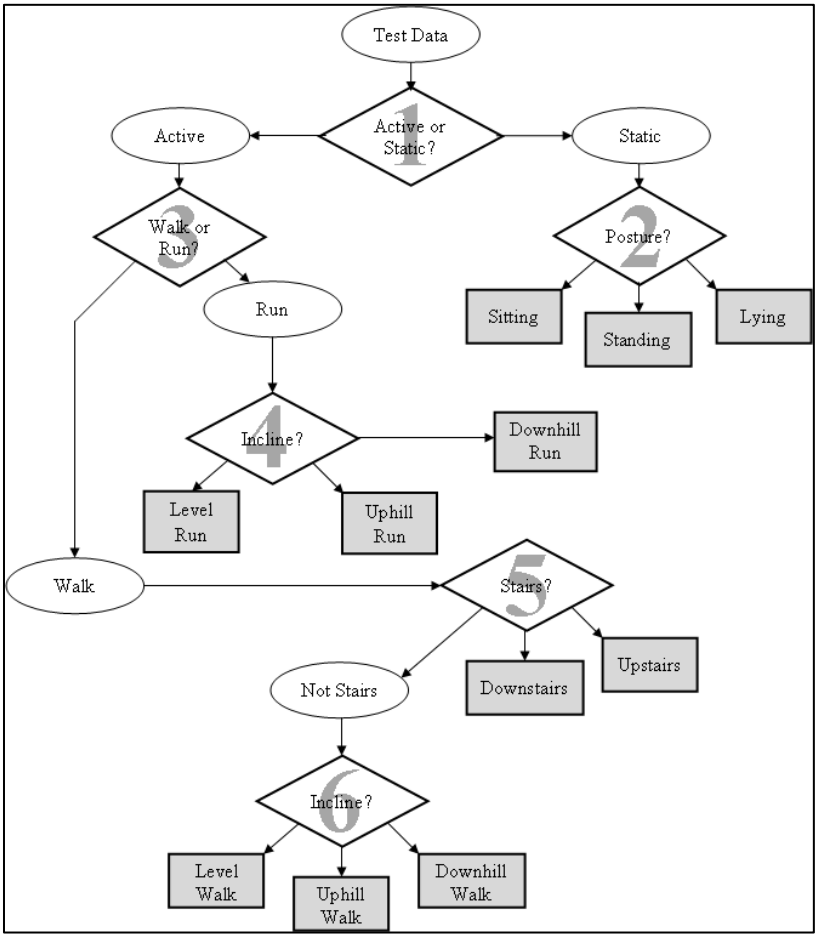

Figure 3. Hierarchical decision tree for Archer et. al's kNN method. Diamonds represent decisions and grey boxes show possible classifications. Taken from Archer et al.

Spatio-Temporal Gait Parameter Determination

Different methods and order of operations may be implemented with sensor systems to observe gait. For example, machine learning coupled with regression can provide spatio-

temporal estimations without the need for precisely calibrated sensors but may not observe pathological scenarios accurately. For most first principle methods, calibration is performed separately and prior to other measures, following which activities and spatio-temporal parameters are identified. The following section will build upon this order, leading up to more comprehensive literature in a bottom-up fashion.

SENSOR CALIBRATION

For sensors to be used with physical models, it is important that they are calibrated as accurately as possible to some known measures. Often times, this process is ignored in favor of manufacturer's conversion values with little to no validation. However, sensors will vary at least slightly with time due to startup and wear. Additionally, manufacturer's specifications are designed to fall within specified manufacturing tolerances so maximum precision and accuracy for an individual unit will likely not be achieved without a user calibration. Given the capabilities of accelerometers and gyroscopes, user calibrations can be performed in various ways. Conversion models for the sensors are most commonly linear but non-linear models have been proposed as well. To be clear, the problems required to solve for conversion model constants are usually non-linear, regardless of the linearity of the conversion model.

Some models have attempted to characterize nonlinearities which may be present. Non-linear models are more difficult to use than linear and often require large amounts of highly accurate relatable data. Additionally, non-linear models are disadvantageous due to the added complexity and cost of constructing an accurate test setup. As an alternate to more complex non-linear methods, Stakkeland et al. used non-linear Kalman filters with a non-linear conversion model to account for high frequency vibrations using validation from a

position sensor, and compared to a linear model.[19] The linear model provided the most accurate and precise calibration of the accelerometer, despite presence of high frequency vibrations. Although not considered in their work, a low-pass filter could partially if not fully negate high frequency noise and vibration. Another similar method, used a rate table to force an accelerometer into a variety of known orientations to account for a non-linear model.[20] Experimental validation was provided but root mean square error (RMSE) was not reported. The method appeared to work very effectively but explicit error measures were not provided and convergence was not addressed. Cai et al. proposed a further improved non-linear model using a single non-linear scale factor calibrated over 24 positions.[21] GPS data was compared to accelerometer integration for vehicle driving trajectories which indicated an abundance of calibration positions. The addition of the non-linear scale factor reduced maximum positions error. Generally, gyroscope models are more difficult or time consuming to fit since relatable data is more difficult to obtain. Potentially as a result of this, work with non-linear conversion models could not be found for gyroscopes.

Linear conversion models are more commonly used for their ease of calculation and repeatability, considering recalibration may occur many times over the life of a sensor. For accelerometers, many procedures have been devised to manipulate knowledge of the gravity vector to solve for linear constants. These vary from methods using only the magnitude of gravity,[22] only the orientation of gravity, or a combination of both. Fitting data to the magnitude is the most common method, as demonstrated by Won & Golnaraghi.[23] Their tri-axial linear models had 6 conversion constants (scale factor and offset for each axis). They solved for these constants in 3 or less iterations of a non-linear problem. Using unique static positions, an RMSE lower than 0.09 m/s^2 was observed when each position was compared

to the magnitude of gravity. Grip and Sabourova designed a non-iterative solution for a 6 constant model by fitting accelerometer data to the magnitude of gravity for 6 unique positions.[24] Simulations including noise yielded no more than 0.016% error in sensitivity and offset calculations. Another non-iterative solution for a 6 constant model involving 3-d ellipsoid fitting was proposed by Gietzelt, et. al[25] and performed similarly to other methods. As an alternative or complementary measure to offline calibrations, Beravs, et. al demonstrated the ability to calibrate data real time using a Kalman filter with results comparable to offline least squares methods by using a typical six parameter model with an additional three parameters for cross-axis sensitivity[26].

Similar to accelerometers, most gyroscope models use six parameters and are solved using cost functions relating rate table outputs to those of the gyroscopes. Depending on how the problem is formulated, a linear cost function can be more feasible than with accelerometers. Nevertheless, non-linear cost functions are normally posed, as they can provide a more robust problem statement. A nine parameter model was proposed by Zhang et al. to account for axis misalignment, in addition to the normal principal scale factors and offsets.[27] This model was applied to both accelerometers and gyroscopes and compared to the typical approach using a 6 parameter model. RMS errors for the accelerometer method were below 15μg and 30 μg, respectively. Gyroscope RMSE did not vary significantly between the two methods, with an RMSE below 0.075°/h. An alternative method foregoing a rate table was introduced by Olivares and Olivares.[28] An accelerometer-gyroscope package was placed on a spinning bicycle wheel. Sinusoidal behavior of the accelerometer was used to determine rotational velocity of the wheel and fit to a 6 parameter model. This clever setup worked with a biaxial gyroscope but the addition of a third axis could cause

complications. Additionally, the rotational velocity during one 360° period is not constant as their problem assumes. Although this method is clever and good for practical use, it is not a high precision, well validated calibration option. The largest linear conversion model in the literature involved 12 parameters, which extended the 9 parameter model with 3 non-symmetric axis misalignment terms.[29] This method appears to be accurate and performed well in Monte Carlo simulations but real data was untested. Comparisons to other models were also not provided. Much of the calibration analysis to be performed in this work is related to this work by Skog & Händel. Additional information on proposed calibration methods can be explored by Fong et al.'s survey.[30]

The work presented in this thesis compares six, nine, and 12 parameter models similar to the aforementioned previous studies. Additionally, least squares methods and number of positional data are compared with respect to the models. Determination of positions and assessment of algorithm effectiveness are performed with respect to two wireless sensors implanted in an AFO.

EVENT DETECTION

Similar to activity recognition, gait events must be reliably tracked on a stride by stride basis to allow for parallelism with common gait analysis terminology. The most common techniques for event detection during known walking periods are machine learning methods and peak detection. One method for using machine learning was proposed by Park and Suh to detect zero velocity intervals through angular velocity[31]. Their Hidden Markov Model is useful for integration boundary conditions, although it lacks direct translation to gait terminology such as foot flat, heel strike, and toe off. Peak detection algorithms have been found to be equally robust and easier to implement and compute. In fact, the one study

using IMUs to measure gait in children with CP successfully used peak detection algorithms applied to foot sensors.[32] In general, peak detection methods can use data from single accelerometers, gyroscopes, or can combine both sensors. An algorithm tested in two studies was developed and validated with high accuracy results using threshold based methods.[33,34] However, force sensitive resistors were placed under the foot and used in conjunction with gyroscopes for event detection. Kose et al employed a unique extension of peak detection methods by using wavelet decomposition of accelerometer data with a waist sensor to achieve 96% accuracy of heel strike identification.[35]

COMPUTATION OF SEGMENT & JOINT ANGLES

Gyroscopes provide true angular velocity and theoretically should be able to produce sensor orientation at each sample. However, noise limits the accuracy and precision with which angles are reproducible by integration alone. Accelerometers can make up for this deficiency to some extent by providing orientation during static (stationary) periods. As dynamic motion mixes with the gravity vector, orientation via accelerometry becomes more inaccurate. While accelerometers have been used to exclusively track angular velocity and orientation of low frequency movement, they do not provide the fidelity required for a gait analysis system.[36] In fact, accelerometers are limited to only providing 2 of the 3 Tait-Bryan or Euler angles desired.[37] Without a magnetometer, perfect removal of gyroscope integration drift from the heading angle (yaw) is very challenging.

Gyroscope drift has been removed using a variety of methods. Detrending data between two known boundary conditions is commonly used. The corresponding events are often heel strike, foot flat, or toe-off. The boundary conditions are either user-defined assumptions or provided by other sensors such as accelerometers and/or magnetometers.

The other most common method utilizes digital filters and possibly knowledge of noise characteristics to reduce drift. A complementary filter provides a simple filter implementation for 6-axis systems. This filter weights and combines low-passed acceleration with high-passed angular velocity to estimate sensor orientation to reduce offset bias. Chalmers et. al compared various implementations of a complementary filter, demonstrating superiority of adaptively weighting a complementary filter.[38] Kalman filters are also commonly used to combine multiple observation models to reduce orientation error using predict-update cycles for each sample given a noise covariance matrix. Although Kalman filters can be implemented using gyroscopes and accelerometers, they are most effective when including magnetometers as shown by various studies.[39–42] Highly accurate Kalman filter methods for angle tracking have been proposed that assume the knee is a perfect hinge.[43,44] However, the knee and ankle are far from perfect hinges which must be accounted for when analyzing frontal and transverse rotations during a stride. Favre et. al developed a Kalman filter to reliably track sagittal and transverse orientations using only accelerometers and gyroscopes.[45]

Comprehensive angle calculation comparisons were performed by Olivares et.al[46] and Öhberg et al.[47] Both studies found that over long periods of time, standard Kalman filters will not converge as they only update based on quasi-static periods, similar to complementary filters. Olivares et al.'s comparison between various least squares and Kalman filters found recursive least squares schemes to be optimal. Öhberg et al. extended a similar study comparing a number of methods which supported Olivares et al.'s results and proposed an modified Kalman filter (similar to a complementary filter) for superior results. Another Kalman filter for accelerometers and gyroscopes similar to the previous was

proposed by Mazzà et al, which includes a quasi-static threshold for switching between accelerometer and gyroscope proximal to the trunk as the most trusted sensor.[48]

WALKING ESTIMATION

Many studies have attempted to estimate walking speed or stride length from inertial sensors, as reviewed by Yang et al.[49] Sensors are commonly placed on the shank, foot, or even the waist to determine segment and/or center-of-mass motion of the body. For first principal methods, a zero-velocity update (ZVU) has commonly been added as a boundary condition for acceleration integration. Since heel strikes are an important event in gait analysis, many studies segment integration periods at these events and argue zero velocity at boundaries. Peruzzi et al performed a comparative study on sensor placement and accuracy of ZVU at heel strike[50]. They found velocity varies over at eight different sensor placements (shank, ankle, and 6 foot locations), with the shank having much higher velocity than foot or ankle placements. Considering many studies find consistent underestimates of stride length, non-zero velocity boundary conditions that are ignored could significantly affect accuracy. Therefore, more robust methods have used accelerometers and/or magnetometers for quantification of boundary conditions and choose different segmentation events.

Treadmill walking speed is commonly tested due to its prescribed walking direction, easy validation, and potential for collecting many strides. Sabatini et al varied treadmill speed and incline while using a biaxial accelerometer and uniaxial gyroscope. Gait cycles were averaged and compared to treadmill speed (no motion capture validation) to produce a coefficient of variation (CV) of 4% and RMSE = 0.18 km/h on five normal subjects at six different speeds[51]. An RMSE of 1.52% was found for their method of determining incline. Although the accelerometer was trusted for initial conditions, segmentation was performed

between heel strikes. Similar to our AFO design, the sensor resided on the instep of the foot. Li validated a walking speed estimation algorithm based on shank-mounted sensors at different level inclines. Mean percent error reached as high as 10% and was commonly above 5% in estimation of speed using a hinge model.[52] Yang et al performed a similar experiment with shank mounted sensors to assess the best signal processing approach.[53] A biaxial accelerometer and uniaxial gyroscope were used. Gait cycles were segmented by mid-stance. Accelerometer tilt provided boundary condition orientation. Boundary conditions for velocity were provided by $\omega * L$ to correct for known non-zero velocity; L was the distance from the sensor to the ankle and ω was the angular velocity from the uniaxial gyroscope positioned sagittally. Treadmill speed RMSE% (RMSE/Treadmill Speed) totaled 3.5% over 5 different walking speeds on a treadmill. As with the previous study, there was no motion capture validation and RMSE was calculated by root-mean-squaring the *mean walking speed – treadmill speed* for each period. Another significant limitation to these studies and most regarding walking speed is the assumption of the knee as a perfect hinge. This is problematic because the knee is not a perfect hinge (in particular can experience internal/external rotation) and assuming so also limits the feasibility of 3-d walking trajectories. A more general model should not assume the nature of a joint, especially considering the need for local and global segment angles, as well as other fully articulating joint angles such as ankle angle.

Using an integration method proposed by Zok et al,[54] Kose et al validated an alternative approach with waist-mounted sensors (tri-axial accelerometer and gyroscope) for heel strike accuracy and distance estimation.[35] Over nine trials, their estimation of 75 m distances varied from -1.11% to 1.12%, centered on -0.02%. Despite using a waist sensor,

heel strike was detected within a margin no larger than 50 ms. Although this method was relatively accurate, any angular information about the lower body is irretrievable because of sensor location. Kose et al extended this method with another paper in determining each step length during 30 m walks. Mean error for this study ranged between about -3% and 3% mean error for each step.[55] Yang et al proposed a foot based system including a triaxial accelerometer, gyroscope, and magnetometer for estimating track walking. An adaptive gain complementary filter was used to keep track of orientation and global frame rotations. Using validation from GPS, no more than 1.1% distance error was reported.

RUNNING ESTIMATION

Other than use as a temporal identifier or pedometer as described by Lee et al,[56] validation of running with inertial sensors is limited in the literature. Yang et al.[57] used a shank mounted triaxial acclererometer and gyroscope, although only sagittal motions were considered. Two separate gait segmentations were made to satisfy observable boundary conditions for orientation and velocity, respectively. For acceleration integration, toe-off boundaries are set with the same $\omega * L$ velocity boundary condition as used in their walking study. Angle boundaries were provided by detection of shank vertical and set to $\theta=0$. Seven subjects ran at four speeds. RMSE was calculated identically to the last study and found to range from 2.87% to 5.85%; this equated to an overall RMSE of 4.1% and absolute means ranging from 0.08 to 0.11 m/s. Calculated stride length was consistently underestimated which can be attributed to their analysis of only the sagittal plane, as well as initial velocity and initial angle miscalculations. A couple other methods have proposed modeling techniques for spatio-temporal tracking of gait but no validation was provided.[58,59] Ultimately, robust methods regarding spatio-temporal parameters of running using inertial sensors are scarce.

PATHOLOGICAL SPECIFIC STUDIES

Despite the need for wireless sensing methods in clinical gait assessment, only a few studies have validated spatio-temporal, first principal methods on pathological gait. Chalmers et al presented methods for tracking sagittal foot angle in idiopathic toe walking similar to those previously mentioned.[38] The most effective method (predict-update: similar to a Kalman filter) was evaluated on both normal and idiopathic subjects with RMS (*mean*) errors of 4.9° (*3.4°*) and 6.5° (*4.5°*), respectively. A normal complementary filter produced slightly more error than the predict-update algorithm.

The only cerebral palsy (CP) study to date using spatio-temporal methods was conducted by Bourgeois et al and used a pre-validated, commercial inertial measurement unit by Physilog.[32] Fourteen CP and 15 normal subjects straight-line walked for a total of 1490 gait cycles, with Vicon motion capture providing validation. Their study validated many different kinematic parameters (error: *mean±std, %mean/actual*) in CP but most notably stride length (3.4±*4.6 cm, 2.8%*), speed (*4.3±4.2 cm/s, 3.8%*), and strike angle (*0.5±2.9°, 20%*). RMSE values were not provided and angle calculations other than at boundaries (foot strike, foot off) were not validated or provided. ZVUs were applied at stance. Although this study is the only of its kind using CP, the motion capture validation was not quite up to par with previous studies examining normal gait and angle variation throughout the stride was not even considered. The algorithm also only considered sagittal angles and the nature of the algorithms used were not made entirely clear.

Hemiparetic gait has also been quantified using inertial sensors by Yang et al.[53] Walking speed using sagittal accelerometer and gyroscope readings and the velocity update correction proposed in their previous papers was validated with a stopwatch. Walking speed

seemed unaffected by which leg was analyzed (paretic or non-paretic), with paretic leg stride errors of 0.00 ±0.9 m/s, given the precision of the stopwatch and user error. The lack of motion capture validation and 3-d analysis limit the extensibility of this method to comprehensive gait analysis modules.

The current work attempts to provide consistently accurate and precise observation measurements for all types of gait. Unlike much of the literature, 3-d angular and linear motion will be employed in an attempt to observe as many features of gait as possible. Although a magnetometer is not employed, this work is capable of extracting yaw components of motion. Additionally, an activity recognition method will be employed that complements and enables first principal spatio-temporal gait analysis.

SENSOR CALIBRATION

This section describes the need for and design of a simple new calibrating process for the TEMPO IMUs mounted in an AFO. The calibration process produces a conversion model to change raw sensor digital output (ADC) to a recognized unit such as g's or °/s. Previously used methods may provide sufficient accuracy for machine learning or less precise analyses but the first principal model to be presented in following sections requires high accuracy conversions to real world values. Normal TEMPO nodes, as shown in Figure 4, are traditionally calibrated prior to deployment but rely on proper sensor alignment with testing orientations. The methods recommended here can circumvent this requirement with much higher accuracy and convergence, despite minimal additional work on the part of user.

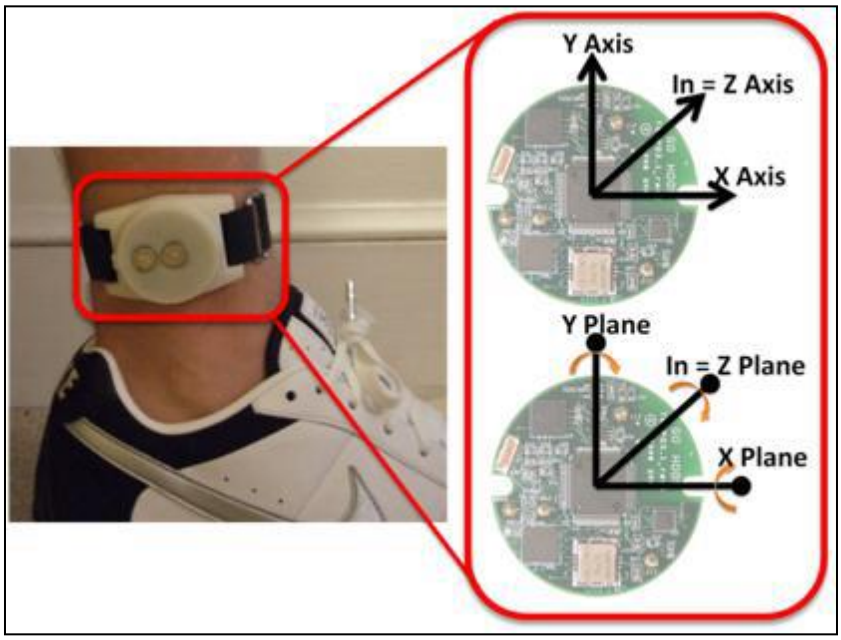

Figure 4. Wristwatch style TEMPO nodes commonly used by UVA Center for Wireless Health[15]

TRADITIONAL TEMPO SPECIFIC CALIBRATION

For the accelerometer calibration, the node is placed in six positions corresponding to alignment with principal axes and solved for a six parameter linear model using a gravity magnitude based non-linear cost function. This cost function y is a scalar function of the error between the estimated acceleration data in g's ($\hat{A}$) and the ground truth (1 g acceleration at static periods).

$$y = \sum_{i=1}^{p} \left(\left\| \hat{A}_i \right\|_2 - 1 \right)^2, \qquad p = length\ of data$$

The explicit calculation of estimated acceleration will be a function of the six parameters and will be addressed later. The cost function is then minimized by a non-linear iterative Gauss-Newton method.

The gyroscope is calibrated by rotation on a rate table at ±33 1/3 RPM along the approximate axes of the gyroscope then solved for a six parameter linear model identical to the accelerometer. However, instead of comparing gravity, the linear cost function relates each directional angular velocity. Gyroscope parameters are determined simply by connecting positive and negative 33 1/3 RPM rotations for each principal axis to determine sensitivities (slopes) and offsets (biases).

These calibration methods do not provide the fidelity required for the work presented here for a number of reasons. In the AFO implementation of these nodes, both sensors, particularly the gyroscope, are hard to calibrate given that both nodes are connected by brittle wires and have a peripheral battery. Even if a method was designed to efficiently

and accurate calibrate the sensors in this form, once they are built-in the AFO, the method would not be repeatable since it was not designed for sensors mounted in an AFO.

The other reasons stem from inaccuracy and unreliable convergence. The accelerometer cost function is non-linear, yet only 6 positions are provided to solve for 6 parameters, making the equation barely solvable and not robust, as will be demonstrated. Additionally, the simplified Gauss-Newton method used can have difficulty converging given the details of the algorithm and the small number of positions provided.

Gyroscope calibration is limited severely by the need to align the sensors' principal axis with axis of rotation. Any error in this alignment, which is sure to occur, will skew the results. The gyroscopes used here are biaxial+uniaxial configurations so axis misalignment is more likely to be present and cannot be accounted for with a 6 parameter model. Also, the rate table used is capable of ±45 and ±78 RPM for additional validation information, yet only ±33 RPM is used.

MANUFACTURER'S SPECIFICATIONS

Another consideration is the use of manufacturer's specifications for conversions to some unit, e.g. m/s^2. For less demanding applications, their specifications may be sufficient for producing ball-park results with minimal work. However, it is important to realize manufacturer's sensitivities and offsets are estimates based on electromechanical relationships in the accelerometer. Their specified sensitivity errors are chosen to account for general variability during life of the sensor and manufacturing tolerances. Since the model proposed in this work is based on first principle methods, achieving the highest raw sensor exactness possible will reduce sources of error and improve reliability. Manufacturer's specifications will be used as a starting point for further methods.

CONVERSION MODELS

The goal of calibration is to provide parameters for a conversion model to produce an ideal standardized measure of acceleration, as shown in Figure 5. Sensor noise primarily occurs from electromechanical and temperature related artifacts.

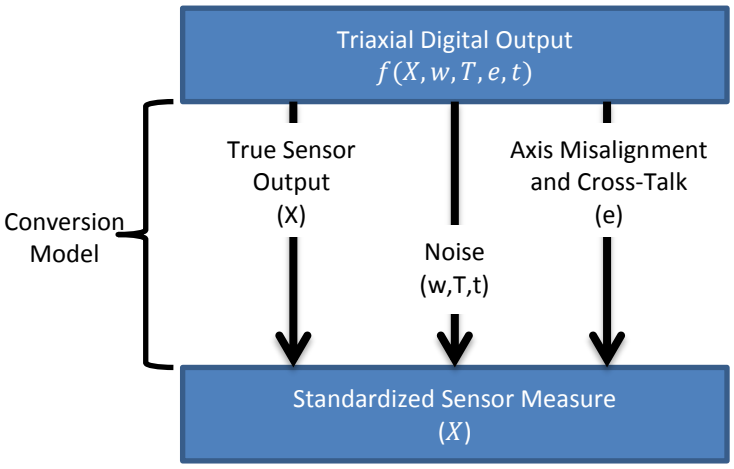

Figure 5. Conversion model overview. Note, noise may be a function of time (t), temperature (T), and white noise (w).

As mentioned, accelerometer noise is generally zero-mean and high-frequency, while gyroscope noise is mostly low-frequency and drifting with time. Although temperature does affect drift, temperature is assumed constant, as explicitly correcting for it is very challenging and all of this work is performed at room temperature. Similarly, over time sensor parameters will change due to mechanical wear. However, this error will be assumed negligible between calibrations. Random, white noise produced at high frequencies can be treated by filtering. Therefore, the resulting conversion model ignores sources of noise, i.e. $digital\ sensor\ output \approx f(X,e)$.

The effectiveness of three models – six, nine, and 12 parameter models were examined. These models are not new developments but a comprehensive comparison between them has not been performed.[29]

The 6 parameter model is a simple linear fit with a scale factor (S_{xx}, S_{yy}, S_{zz}) and bias (O_x, O_y, O_z) for each axis. Variable *X* represents sensor measurement for either a gyroscope or accelerometer.

$$X_i^{6*} = S_{ij}^{6*} ADC_j + O_i,$$

$$ADC = \begin{bmatrix} ADC_x \\ ADC_y \\ ADC_z \end{bmatrix}, \quad S^{6*} = \begin{bmatrix} S_{xx} & 0 & 0 \\ 0 & S_{yy} & 0 \\ 0 & 0 & S_{zz} \end{bmatrix}, \quad O = \begin{bmatrix} O_x \\ O_y \\ O_z \end{bmatrix}$$

Note, principal components of S correspond to the inverse of the principal sensitivites provided by the manufacturer.

Due to internal mechanisms, each axis has dependence on the others resulting in cross-axis sensitivity. The 9 parameter model adds 3 symmetric cross-axis sensitivities (S_{xy}, S_{xz}, S_{yz}) to the 6 parameter model.

$$X_i^{9*} = S_{ij}^{9*} ADC_j + O_i,$$

$$S^{9*} = \begin{bmatrix} S_{xx} & S_{xy} & S_{xz} \\ S_{yx} & S_{yy} & S_{yz} \\ S_{xz} & S_{yz} & S_{zz} \end{bmatrix}$$

Since, sensor axes are based on physical positioning of componentry ADC output never corresponds to perfectly orthogonal axes. The 12 parameter method adds 3 new misalignment constants (m_{xy}, m_{xz}, m_{yz}) to further reduce sources of error. Note this model now converts ADC using a non-symmetric matrix.

$$X_i^{12*} = M_{ij} S_{ij}^{9*} ADC_j + O_i$$

$$M_{ij} = \begin{bmatrix} 1 & m_{xy} & m_{xz} \\ 1 & 1 & m_{yz} \\ 1 & 1 & 1 \end{bmatrix}$$

ACCELEROMETER CALIBRATION

Two possible validation solutions were considered for accelerometer calibration. The simplest used verification of static magnitude during a number of stationary periods. The second included sensor orientation validated by Vicon motion capture in addition to the static magnitude verification. Below are the relative advantages and disadvantages of the solutions.

Static Magnitude Verification

Relative Pros

- Ground truth is a direct physical quantity
- No secondary system
- Easy sensor model implementation with cost function

Relative Cons

- Only magnitude is verified
- Orientation accuracy is unassessed

Sensor Orientation Verification

Relative Pros

- Highly specific and unique ground truth info
- Angle based verification

Relative Cons

- Increased model complexity
- Time onsuming
- Verification with black box system (motion capture)
- …or very specific, prearranged test setup

Due to the demands for repeatability and simplicity, sensor orientation was omitted in favor of static magnitude verification. Although a sensor orientation based method could provide even more precise results, the following section will demonstrate the high levels of precision obtainable by a robust static magnitude verification method.

Gravity Based Least Squares

A procedure was established to place the AFO in 14 unique static positions (Figure 6). This number was chosen to provide an excess of required positions for the 12 parameter model and provide comparisons between using the minimal number of positions for each model increasing up to the maximum of 14. The 14 positions are unique but can be arbitrarily chosen as long as there is sufficient differentiation between them. The resulting error vector is as follows.

$$\hat{A}_i = X_i^{6*}, X_i^{9*}, or\ X_i^{12*}$$

$$e_j = \left(\left\|\hat{A}_j\right\|_2 - 1\right), \quad j = 1,2,3,\dots p, \quad p = \#\ of\ positions$$

The p ADC outputs are determined by averaging the entire static period during each corresponding annotation.

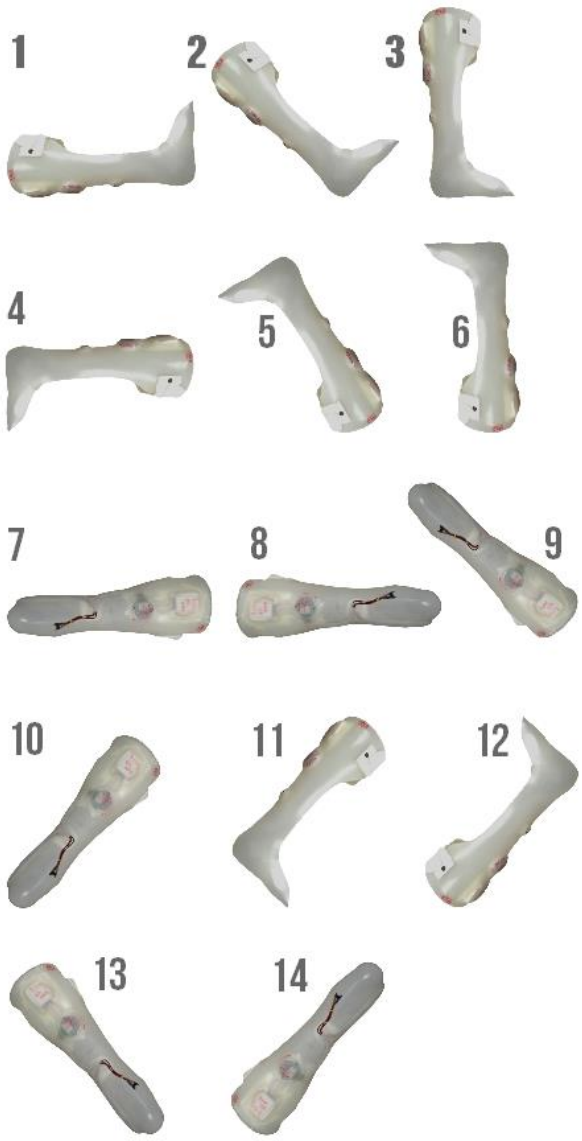

Figure 6. Diagram of static positions used for accelerometer calibration.

LEAST SQUARES METHODS

The non-linear least squares problem to select n (6, 9, or 12) constants c is:

$$\min(y), \quad y = f(c_1, c_2, c_3, \ldots c_n)$$

In addition to varying parameter models and positions, three least squares methods were compared for exactness and convergence. Initial guess (*i=0*) for each method was supplied by manufacturer's specification. Iterations were performed by augmenting the last guess by a correction size *h*, which was determined by each least squares method.

$$\hat{c}_{i+1} = \hat{c}_i + he_i, \quad i = 0,1,2,3 \dots imax - 1, \;\; imax = max\ \#\ of\ iterations$$

$$\hat{c} = vector\ of\ predicted\ constants\ c_1, c_2, c_3, \dots c_n)$$

Gauss-Newton (GN)

The standard Gauss-Newton method only considered the number of positions equal to the number of parameters to be solved for, e.g. 6 parameter model could be solved by GN only when using 6 positions. From the Jacobian *J* the correction size was determined by:

$$h = -\alpha(J'J)^{-1}J'e,$$

$$J = \frac{\partial e_i}{\partial c_j},$$

$$i = 1,2,3, \dots p, \quad p = \#\ of\ positions$$

$$j = 1,2,3, \dots n, \quad n = \#\ of\ parameters$$

The error matrix and Jacobian were evaluated at each iteration to find *h*. A divergence tolerance of 10^4 for the norm of the correction would trigger a replacing of the current correction with a sign change*2 of the previous correction to avoid divergent solutions and local minima. A scaling factor α was introduced to minimize false convergence and set empirically to 0.9. Note use of the Hessian was tested but far too unstable to be used as is the case for most least squares applications.

Gauss-Newton Matrix Rank Partition (GN-MRP)

This least squares algorithm was identical to GN. However, the number of positions could be larger than the number of constants to be solved for. This was achieved by extracting the full rank portion of the Jacobian at each iteration and passing it through GN. Automatic reduction to row echelon form yielded the rank matrix. Zero tolerance of 10^{-9} was used to improve invertability.

Levenberg-Marquardt (LM)

Levenberg-Marquardt least squares was performed through MATLAB's function *lsqnonlin*. Error tolerance (10^{-9}) was chosen identical to GN and GN-MRP methods. Correction size calculation was modified to include a damping factor λ set to 0.1. This damping factor modifies the gradient of descent to improve convergence and circumvent misleading gradients. Often times this step formulation is regarded as a trust region step, as it will only follow the gradient so far.

$$h = -(J'J + \lambda I)^{-1}J'e$$

Data Collection and Analysis

In order to compare and validate the effectiveness of these methods, five separate sessions were recorded and analyzed with the 3.2f AFO. The AFO was left still during the first few minutes of collection to remove startup drift. Following which, the AFO was placed in the proper 14 unique positions (split 1). After around a couple of hours, another calibration procedure was performed prior to ending the session (split 2).

Each least squares method and parameter model was performed for the entire range of possible input positions to compare models, least squares methods, and required

positions. Data was analyzed as a whole, as well as with respect to time of calibration. The 12 parameter model was only performed using LM, as will be justified later. Also, GN-MRP methods were not performed at the minimum positions per parameter model, since they would produce identical results to the GN method.

A number of constraints were imposed on all the methods. After each iteration, if the error tolerance (10^{-6}) exceeded y, a solution was found. This low tolerance was chosen in order to produce the best results possible, even though most local minima found could not achieve this accuracy. The GN methods needed significantly more iterations than the LM methods to find a local minimum. It is worth noting, LM was vastly superior at converging to a minimum within 20 iterations.

Since these calibrations were not performed often, absolute accuracy was deemed more important than computational efficiency. Furthermore, max iterations were limited to 50 in order to improve convergence of GN methods. If a reasonable solution ($y < 5$) could not be found in 50 iterations, the method was said to be divergent. Additionally, false convergence could occur due to the lack of an acceleration directionality component in the Jacobian. To identify if this happened, a standard deviation tolerance for the static periods was introduced and manually verified. Since the sensors have an inherent noise floor, standard deviation measures also have a floor which could only be surpassed by false convergence. Empirically, the threshold was chosen to be 1% standard deviation from the mean for the entirety of the static periods, per axis.

The manufacturer supplied initial parameters for conversion to g's were as follows:

$$S_{xx} = S_{yy} = S_{zz} = 0.0083$$

$$S_{xy} = S_{xz} = S_{yz} = 0.0004$$

Another analysis which will not be explicitly presented indicated GN and GN-MRP methods were highly sensitive to which positions were provided to the algorithm (e.g., for 9 position input to 6 position model, the different combinations of 9 positions could be constructed from the total of 14). The LM method was vastly superior in this regard and could produce high accuracy results with positions that would not converge with GN and GN-MRP methods. More than likely, this is a result of the damping factor included in the LM method. Since the less unique combinations of positions caused the most problems, the Jacobians calculated at each iteration were poorly defined resulting in more unstable step sizes. The damping factor λ can compensate for step sizes that would be too big and otherwise skip over minima. Additionally, this was further justification for a scale factor α in the GN methods to improve convergence. The order of positions passed was empirically set to position numbers 1, 3, 4, 6, 7, 10, 5, 9, 11, 2, 8, 12, 13, and 14 (e.g. 9 required position simulations would pass 1, 3, 6, 7, 10, and 5 to the least squares method). This optimal ordering helped remove any potential issue related to the aforementioned sensitivity of Gauss-Newton to less than optimal positions.

Results

The LM approach was found to be the preferred method for determining the calibration coefficients. Root-mean-square error (RMSE) was calculated for each trial via the mean of each static period, i.e., each trial's RMSE was calculated using 14 values. For example, a 9 parameter LM method using 12 positions had an RMSE determined over all 14 positions to assess the importance of providing the algorithm with more positions than required. Figure 7 shows the RMSE results for the entirety of the data. Figure 8 and Figure 9 demonstrate

RMSE when examining the beginning (split 1) and end (split 2) of session calibrations, respectively. In general, increasing passed positions to any method and model decreased RMSE. The 9 parameter model is consistently superior to the 6 parameter model, regardless of changes to least squares methods. This is particularly prevalent for split 1. Furthermore, GN-MRP and LM perform very similarly with respect to RMSE. However, 9GN-MRP falters with a high percentage of diverging solutions as shown in Table 1. Additionally, one false convergence was found in split 2 with 9GN. All models' error increased during split 2 (end of session calibrations) with the 12 parameter model encountering the most significant increase in error; this model may have also needed more positions to converge to the proper misalignment values, as the other models seemed to converge to an error floor.

A number of conclusions can be made from this calibration analysis. Levenberg-Marquardt least squares method was by far the most robust and consistent method for any model and any number of passed positions. The nine parameter model was optimal in producing the smallest error in all cases. However, the 6 parameter was still effective and converged for every least squares method and passed positions. Twelve parameter results indicated an insufficient number of positions for ideal convergence.

Gauss-Newton, particularly the MRP version struggles with the 9 parameter model. Although looking at mean RMSE may suggest GN-MRP is more accurate than LM, this is not necessarily true as divergent groupings were not factored into this calculation; the groupings that were divergent for GN-MRP likely increased the relative mean RMSE for LM.

A possible explanation for the high divergence rate in 9GN-MRP lies within the step size h calculation. Since LM and GN-MRP are both gradient descent based methods,

depending on how positions are chosen and set, the Jacobian may not be optimally defined. LM accounts for this by using a damping factor which GN-MRP omits. Since an apparatus does not hold the AFO in the precisely same positions every calibration, significant variations in the line of descent between calibrations are expected. Furthermore, since the initial guesses were given by manufacturer's specifications and already close to the solution, a damped step size should not considerably affect rate of convergence.

For high fidelity applications, the Levenberg-Marquardt method was vastly superior to Gauss-Newton. A six parameter model is feasible but a higher parameter model is optimal and requires little additional computation. Whether to choose a 9 or 12 parameter model may depend on the manufacturing process of the sensor. In the case of triaxial accelerometers as shown here, axis misalignment is probably negligible relative to the order of RMSE achievable. Increasing number of passed positions was the most effective at reducing RMSE for 6 parameter models. Nine parameter models only saw a significant reduction in RMSE at 10 positions; further additional positions did not seem to affect RMSE but could still be useful if available. A maximum of only two extra positions were passed to the 12 parameter model. More positions would need to be added in order to assess this method's effectiveness.

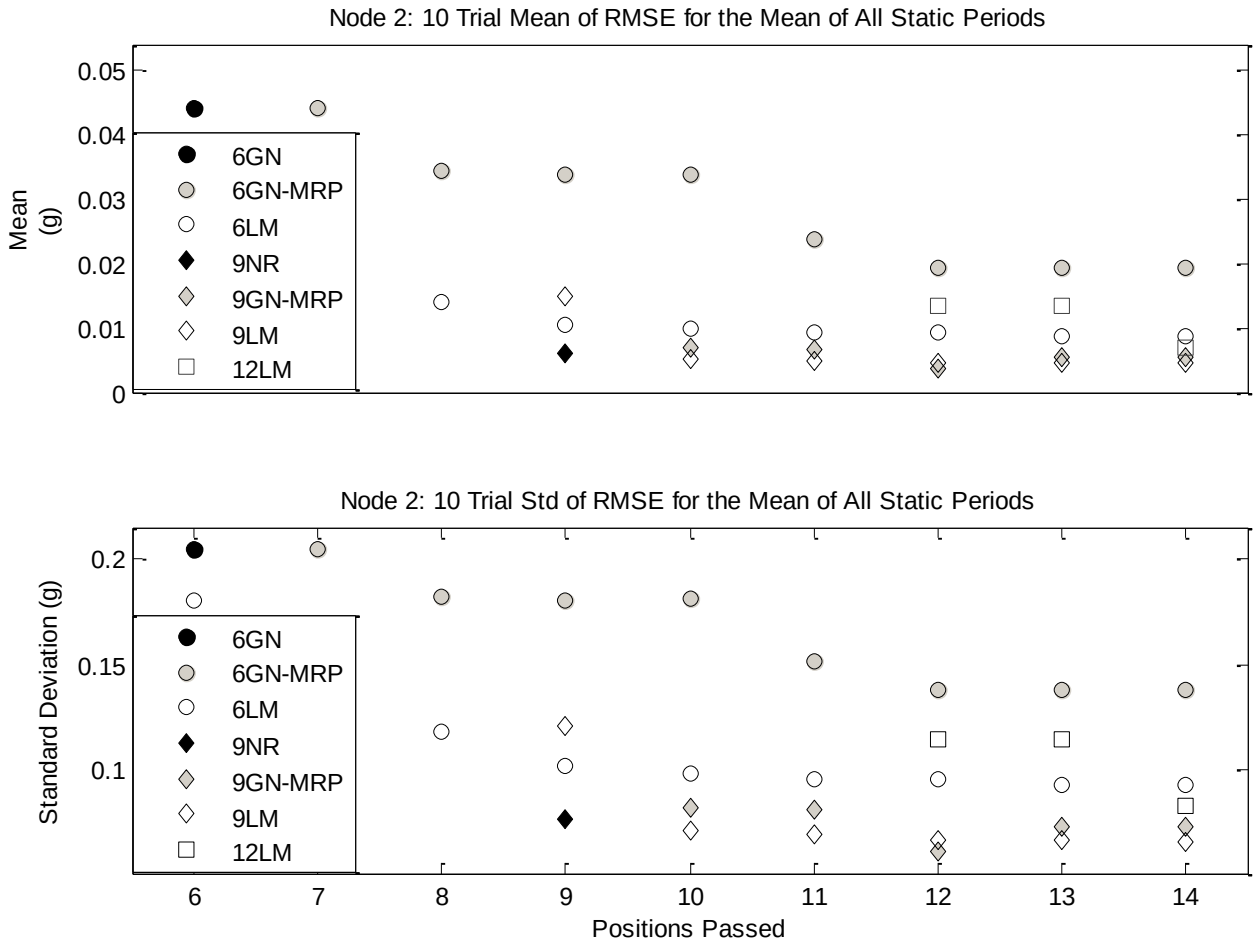

Figure 7. Distribution of RMSE for all trials and all groupings showing the superiority of the LM approaches. Note 9 and 12 parameter models can only be analyzed with greater than 9 and 12 positions passed, respectively, because these non-linear solving methods require data that is at least equal to the solvable parameters.

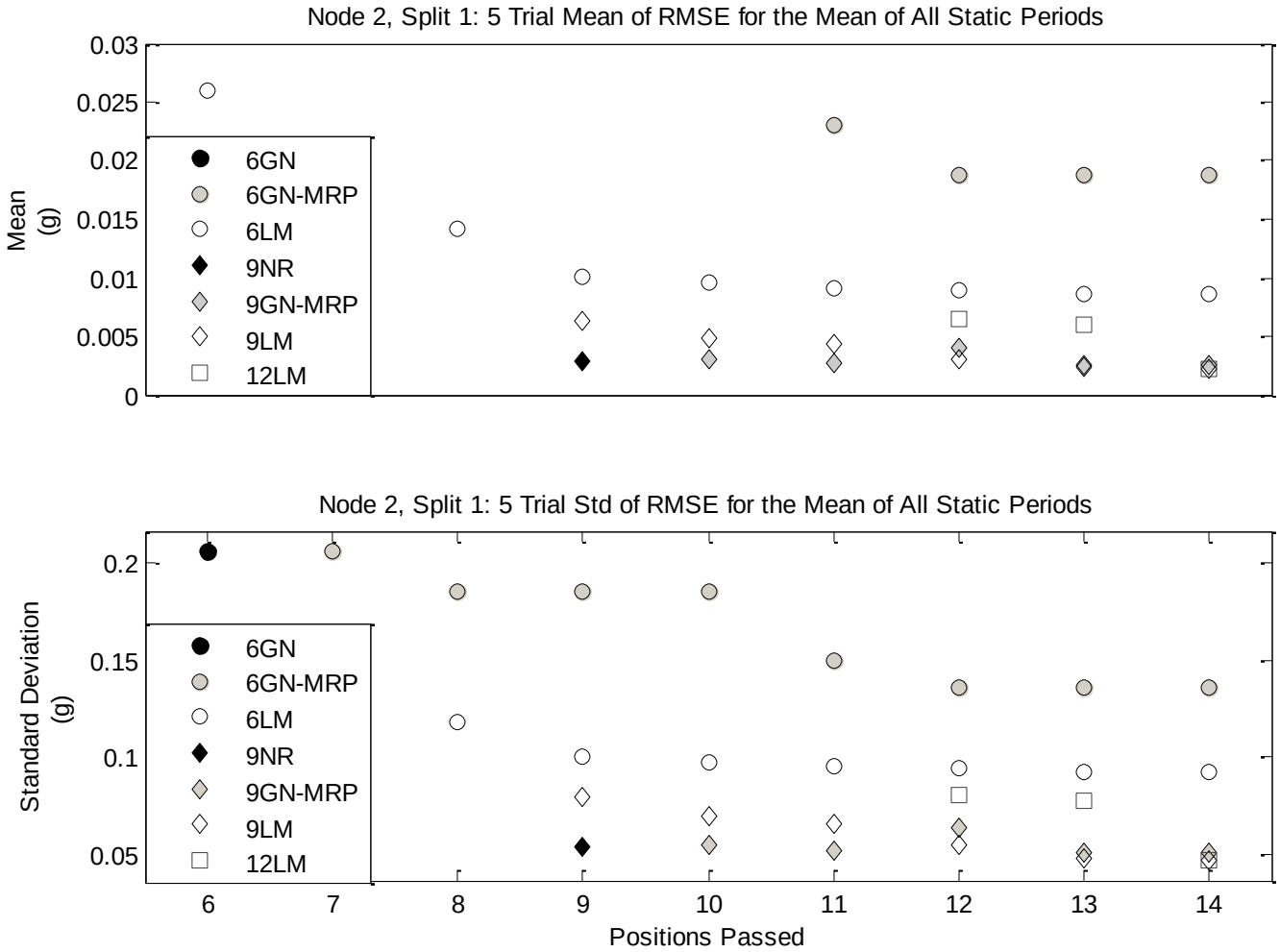

Figure 8. Distribution of RMSE for trials at the beginning of the session (split 1).

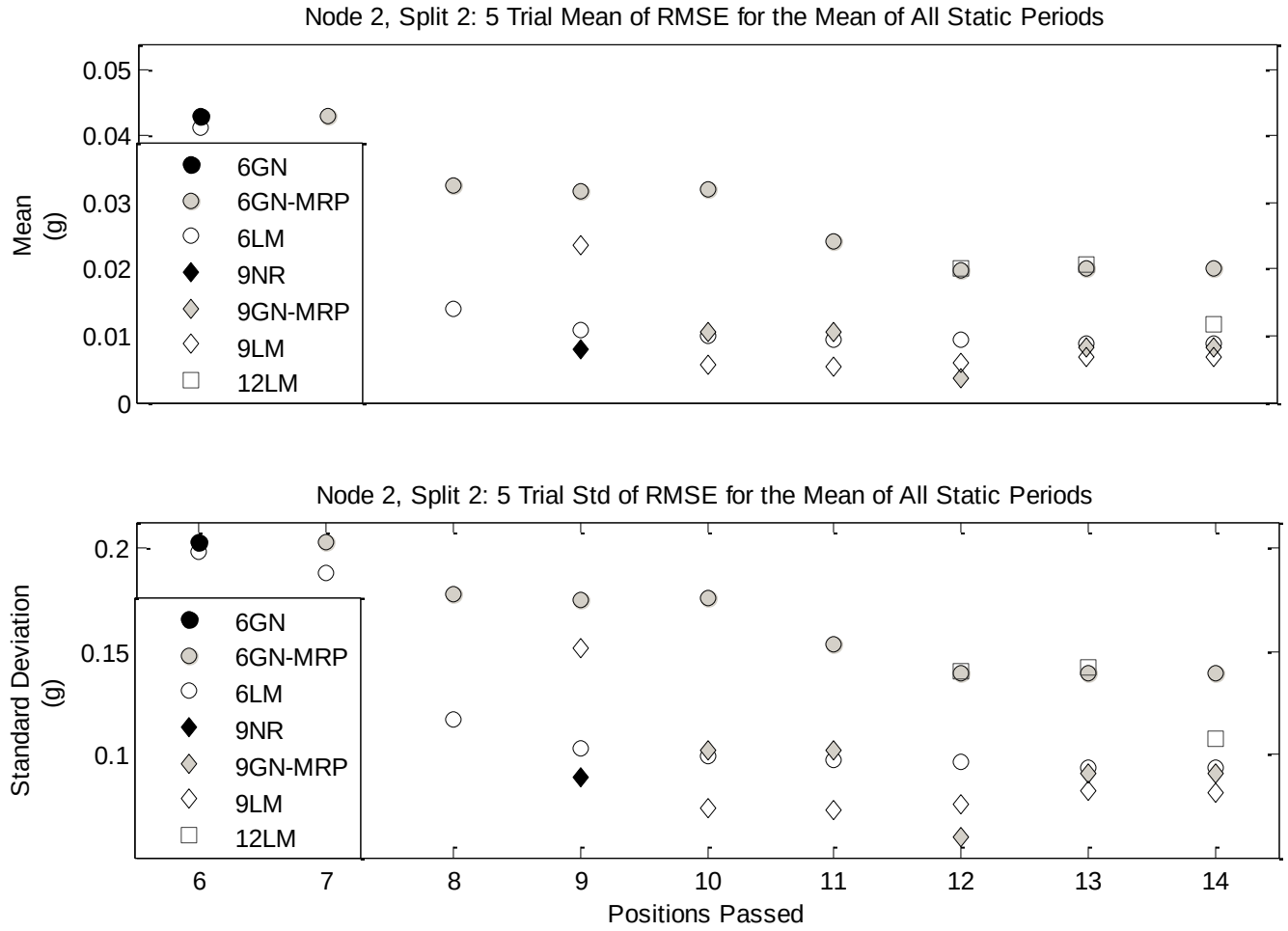

Figure 9. Distribution of RMSE for split 2 (calibration procedure at the end of session).

Table 1. Instances of divergence categorized by groupings and calibration times. Split 1 for beginning of session calibrations and split 2 for those at the end.

Divergences

	Positions Passed	6GN	6GN-MRP	6LM	9GN	9GN-MRP	9LM	12LM
Split 1	6	0	0	0	0	0	0	0
	7	0	0	0	0	0	0	0
	8	0	0	0	0	0	0	0
	9	0	0	0	3	0	0	0
	10	0	0	0	0	3	0	0
	11	0	0	0	0	3	0	0
	12	0	0	0	0	4	0	0
	13	0	0	0	0	3	0	0
	14	0	0	0	0	3	0	0
Split 2	6	0	0	0	0	0	0	0
	7	0	0	0	0	0	0	0
	8	0	0	0	0	0	0	0
	9	0	0	0	1	0	0	0
	10	0	0	0	0	3	0	0
	11	0	0	0	0	3	0	0
	12	0	0	0	0	3	0	0
	13	0	0	0	0	3	0	0
	14	0	0	0	0	3	0	0
Totals	(abs)	0	0	0	4	31	0	0
	(%)	0.00%	0.00%	0.00%	4.44%	34.44%	0.00%	0.00%

Individual Node Adaptation for CP group

For data collections involving individual 3.2f nodes strapped to cerebral palsy participants, the accelerometer calibration was modified slightly. Despite using 14 positions in the control group, the aforementioned analysis suggested any more positions than 12 produced negligible RMSE decrease. Thus, a 12-sided (dodecahedron) calibration rig was prototyped and used to calibrate accelerometers. Figure 10 shows the prototype prior to and following sensor placement within.

Figure 10. Dodecahedron calibration solution before and after assembly around a sensor.

Each side of the dodecahedron was numbered for ease of calibration. The rig and sensor within were both held in place by rubber bands as a temporary solution; a future prototype could use pins for easy closure and opening. The rig was then placed on all of its side to achieve unique static positions for each individual node accelerometer calibration. Results for one 3.2f node calibration are shown in Table 2 and are comparable to the analysis previously presented.

Table 2. Acceleration calibration results for individual 3.2f node 104.

Node	Axis	Fit RMSE (g)	Total Mean Drift (g)	Total RMSE (g)	LM Runtime (s)
104	Norm	0.0017	0.0023	0.0841	3.01

The calculated conversion model for g's was found to be:

$$A_{N104} = \begin{bmatrix} 0.008000 & -0.00000 & -0.00002 \\ -0.00000 & 0.008200 & -0.00003 \\ 0.00002 & 0.00002 & 0.00790 \end{bmatrix} (ADC_{N104} - \begin{bmatrix} 2067.1 \\ 2083.4 \\ 2027.2 \end{bmatrix})$$

Adaptation of LM methods used on the AFO produced similarly precise results on a single 3.2f node placed in 12 unique positions. Cross-axis terms in this particular instance were very small and probably negligible. However, use of those terms for robustness and generality over different sensors is essential.

GYROSCOPE CALIBRATION

Gyroscope calibration for TEMPO systems has typically been done by aligning the sensors in the direction of their principal axes and rotating at ±33 RPM on a turntable. Principal scale factors and offsets (6 parameter model) are then determined by the slope and y-intercept of the line connecting +33 and -33 RPM for each axis. This setup is problematic for a number of reasons. First, sensor axis alignment with the rotation axis is an educated guess. Sensor misalignment or transverse sensitivity is also ignored which additionally conflicts with the assumption that the sensor axes are perfectly aligned. Other external factors such as levelness of the turntable will always inadvertently limit the precision of this method. Lastly, the turntable is also capable of various rotation speeds although only one has been utilized in previous procedures. Two methods were devised to improve gyroscope calibration and address these issues.

Linear Least Squares, 6 Parameter

In order to improve the previously used procedure with minimal changes, some adjustments were made to the test setup and processing. Instead of only performing 33 RPM rotations, 45 and 78 RPM rotations were tested as well. Rotations at 78 RPM were found to be unstable with the housing platform used so rotations became ±33 and ±45 RPM. Following careful node setup to align axes, manual inspection of off axis rotation magnitude was necessary to ensure properly aligned axes. Three linear methods were compared. The first was identical to the original, which finds the line between +33 and -33 RPM rotations. The second makes a small adjustment by adding a 0 RPM period then finding sensitivities for the positive and negative spectrum via 33 RPM. The last method performed linear regression on -45, -33, 0, 33, and 45 RPM rotations.

Levenberg-Marquardt Least Squares, 9 Parameter

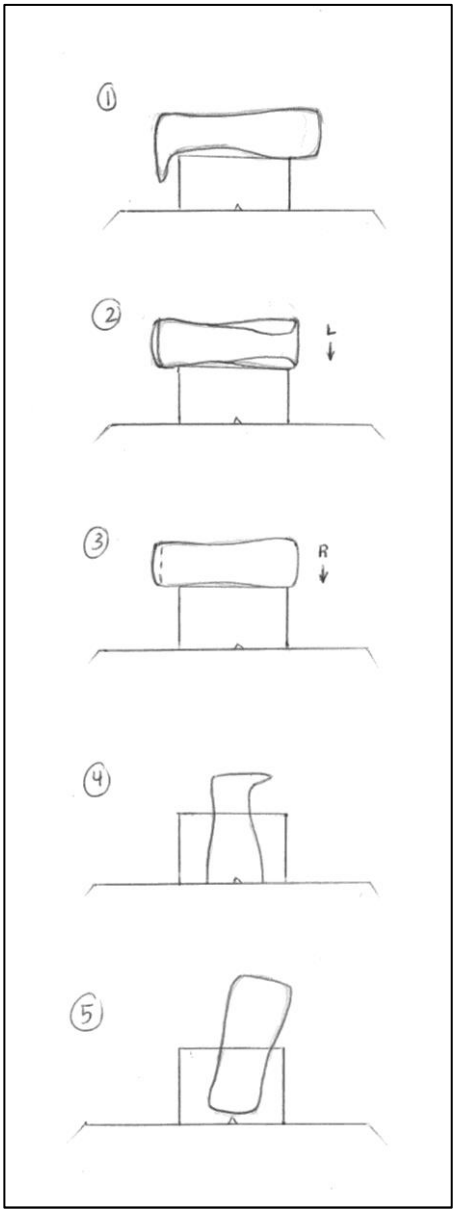

Figure 11. Diagram of configurations used to perform 33 and 45 RPM turntable rotations for gyroscope calibration

Although the regression technique improved upon the original TEMPO calibration procedure, many limitations of the original were unaddressed. Similar to the accelerometer calibration, a LM 12 parameter non-linear least squares problem was posed to reconcile the need for sensor axis alignment with the turntable. This conversion model has previously been discussed, this time being implemented for gyroscope output $\hat{G}$. One again, the digital output (ADC) is the convertible measure, this time produced by the gyroscop.e

$$\hat{G}_i = M_{ij} S_{ij}^{9*} ADC_j + O_i$$

$$S^{6*} = \begin{bmatrix} S_{xx} & 0 & 0 \\ 0 & S_{yy} & 0 \\ 0 & 0 & S_{zz} \end{bmatrix}, \quad O = \begin{bmatrix} O_x \\ O_y \\ O_z \end{bmatrix},$$

$$M_{ij} = \begin{bmatrix} 0 & m_{xy} & m_{xz} \\ 0 & 0 & m_{yz} \\ 0 & 0 & 0 \end{bmatrix}$$

The cost function was constructed similarly to that of the accelerometer. Since proper axis alignment with rotation direction was omitted, directionality of the known speed was impossible to validate. However, this did not limit effectiveness as directionality is ultimately preserved in the conversion model for each axis.

$$e_j = \left(\left\| \hat{G}_j \right\|_2 - Known\ Speed\ Magnitude \right),$$

$$j = 1,2,3, \ldots p,$$

$$p = \#\ of\ rotation\ configurations$$

$$y = \sum_{i=1}^{p} {e_i}^2$$

All further methodology involving LM least squares was preserved from the accelerometer technique. A total of 5 orientations at ±33 and ±45 RPM were enforced by a makeshift box, as shown in Figure 11. Along with a static, non-rotating period, a total of 21 unique combinations of orientation and speed were performed.

Calibration Validation

This section will validate and compare the proposed methods, as well as describe the calibration measures used in order to achieve upcoming kinematic results. Data was collected on a number of different subject groups. The gyroscope calibrations performed on each group were different, as well as performed sparingly but still produced results similar in precision. Different methods were performed due to necessity and evolving methodologies. The reason for sparing calibrations was two-fold. First, turntables were not feasible to access directly before recording a subject. Secondly, the most variable parameter for accelerometers and particularly gyroscopes is the resting voltage, which will vary over time and between startups. In these devices, the resting voltage will directly influence the bias for each axis. Although scale factors may change, they are less likely to in the short-term. Furthermore, compensation for bias accumulation in the gyroscope and accelerometer will be discussed

later. The following section will present the procedure and results for gyroscope calibration in each group.

CONTROL GROUP, PART A

The control group, part A (NOA) consisted of five subjects without any walking disabilities wearing the custom made 3.2f AFO. Prior to assembly of electronics into the custom made AFO, each sensor was rotated on the turntable per the principal axis alignment method previously described by *Linear Least Squares, 6 Parameter* section. This method was performed only once in late June 2013. The date of the last subject's collection (NOA05) was mid-December 2013. Despite half of a year separation between the calibration and last trial, there were no noticeable issues with the calibration parameters in upcoming gyroscope-related methods.

Prior to statistical analysis, highly linear nature of the gyroscope and biaxial+uniaxial related misalignment were obvious. The master in particular demonstrated nearly identical ADC output for two of the axes, as shown in Figure 12, and the only significant difference between the uniaxial and biaxial axes appears to be bias.

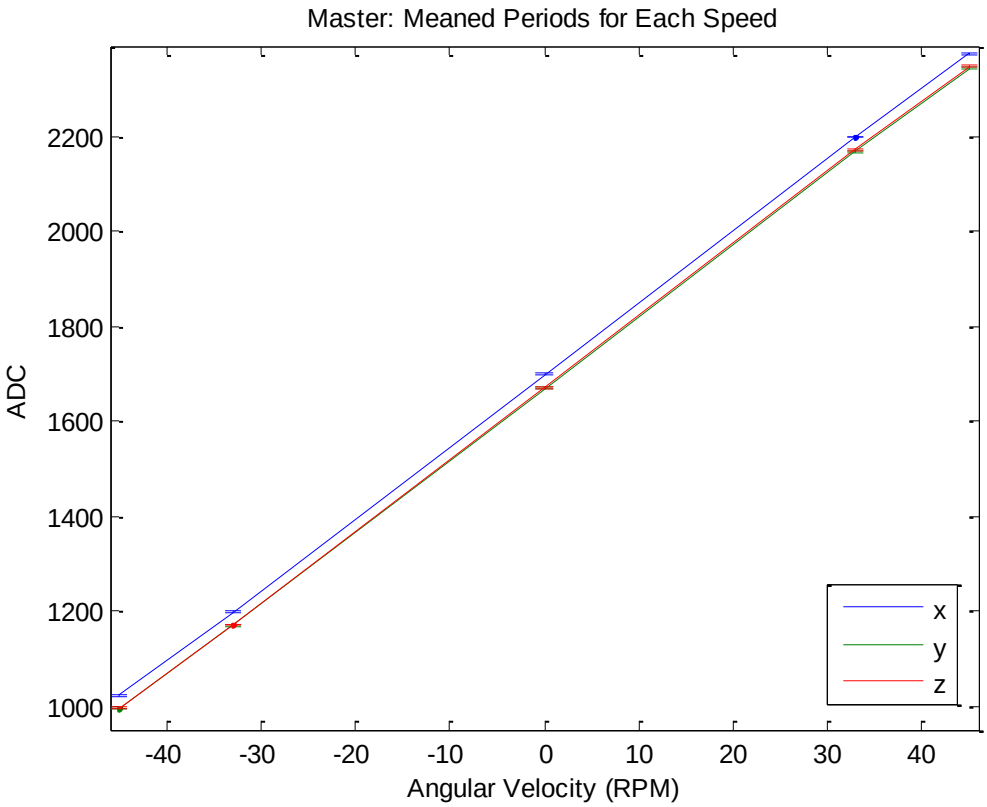

Figure 12. ADC vs. RPM for the master node of the custom 3.2f AFO showing the linear behavior of the gyroscope between -45 and 45 RPMs. Standard deviation bars are centered around the mean ADC for each annotated speed period. Note, y and z data are overlapping.

Upon analysis, very little differences were observed between the three methods (point to point linear methods and regression). Virtually no error was observed between positive and negative spectrum when creating two point to point lines (i.e. line from 0 to 33 RPM and line from -33 to 0 RPM) when compared to simply finding the slope and offset connecting -33 RPM and 33 RPM. Additionally, the 5-point regression provided statistically insignificant improvement over point to point methods. Furthermore, only results for the 5-point regression are provided via Table 3.

Table 3. Linear regression calibration results. These results only pertain to validation of converted sensor speed relative to known speed during annotated periods for the principal axis being rotated. Presence of off-axis rotation was deemed negligible.

Node	Axis	Fit RMSE (°/s)	Total Mean Drift (°/s)	Total RMSE (°/s)
Master	X	0.053	0.0001	0.303
	Y	0.135	0.0064	0.287
	Z	0.058	0.0005	0.256
Slave	X	0.041	0.0001	0.294
	Y	0.109	0.0003	0.274
	Z	0.128	0.0018	0.315

The parameters for conversion to degrees per second (DPS) were found as follows:

$$DPS_{master} = \begin{bmatrix} 0.400 \\ 0.400 \\ 0.398 \end{bmatrix} (ADC_{master} - \begin{bmatrix} 1698.2 \\ 1676.4 \\ 1673 \end{bmatrix})$$

$$DPS_{slave} = \begin{bmatrix} 0.403 \\ 0.401 \\ 0.406 \end{bmatrix} (ADC_{slave} - \begin{bmatrix} 1679.8 \\ 1660.5 \\ 1666.2 \end{bmatrix})$$

As compared to manufacturer's specifications (same for biaxial and uniaxial):

$$DPS_{manuf} = \begin{bmatrix} 0.5 \\ 0.5 \\ 0.5 \end{bmatrix} (ADC_{manuf} - \begin{bmatrix} 2700 \\ 2700 \\ 2700 \end{bmatrix})$$

For whatever reason, there is a larger discrepancy between manufacturing specifications and those produced by the calibration. The calibration tolerance provided by the manufacturer is 6%, which still cannot account for the differences shown above. A difference in the bias is expected since the manufacturer's reference voltage is 1350 mV and

the ADC output for the sensor axes analyzed is around 1670-1700 mV. However, the ~20% difference in sensitivity was unexpected.

These results indicate that the gyroscope sensors are highly linear and simple to calibrate, if principal axes can be isolated and rotated about on a turntable. However, if the axes orientations are unknown, this method will not work. Even so, approximated principal axis alignment on the turntable will inevitably introduce some error, as it cannot be explicitly known. Lastly, manufacturer's specifications were proven to be unreliable for the AFO application outlined in this paper. It is possible that assembly of the sensors (soldering, etc.) changed some thermal or electromechanical properties in the sensors. Regardless, this is a clear indication of the importance of manual calibration, if high precision outputs are desired.

CP GROUP AND CONTROL GROUP, PART B

Despite high accuracy results given in the linear calibration results, much of the error accumulated could not be tracked since off-axes outputs are assumed to be zero and have no axis misalignment. Additionally, linear calibration could only be performed when the sensor orientation was known prior to setup. The non-linear, Levenberg-Marquardt method was able to work around these issues and provide a more robust calibration for the CP group, A and control group, B. Since these groups used different sensor arrangements, the procedure and results for both will be demonstrated separately.

Control Group, Part B

This group used the same custom 3.2f AFO used in part A. Since the nodes were already placed in the AFO, a linear calibration would have required their removal and was not

feasible. Using the arrangements in Figure 11, 21 axial rotations are obtained in a data collection prior to control group B recordings. The Levenberg-Marquardt method was executed as previously defined. Fit RMSE calculated RMSE of meaned unique speed/orientation periods and represented least squares effectiveness. Total mean drift and RMSE are calculated from the entirety of each period and is more indicative of sensor characteristics. Table 4 shows the results for both nodes. Figure 13 depicts the gyroscope calibration for the master (shank node).

Table 4. Results for NOA LM calibration. Note, axial* calculations are artificial calculations used to estimate axial error for comparison to linear methods. $\boldsymbol{Norm = \sqrt{3 * Axial^{*2}}}$

Node	Axis	Fit RMSE (°/s)	Total Mean Drift (°/s)	Total RMSE (°/s)	LM Runtime (s)
Master	Norm	0.207	0.061	1.873	2.25
	Axial*	0.120	0.035	1.081	
Slave	Norm	0.264	0.061	0.715	1.07
	Axial*	0.152	0.036	0.413	

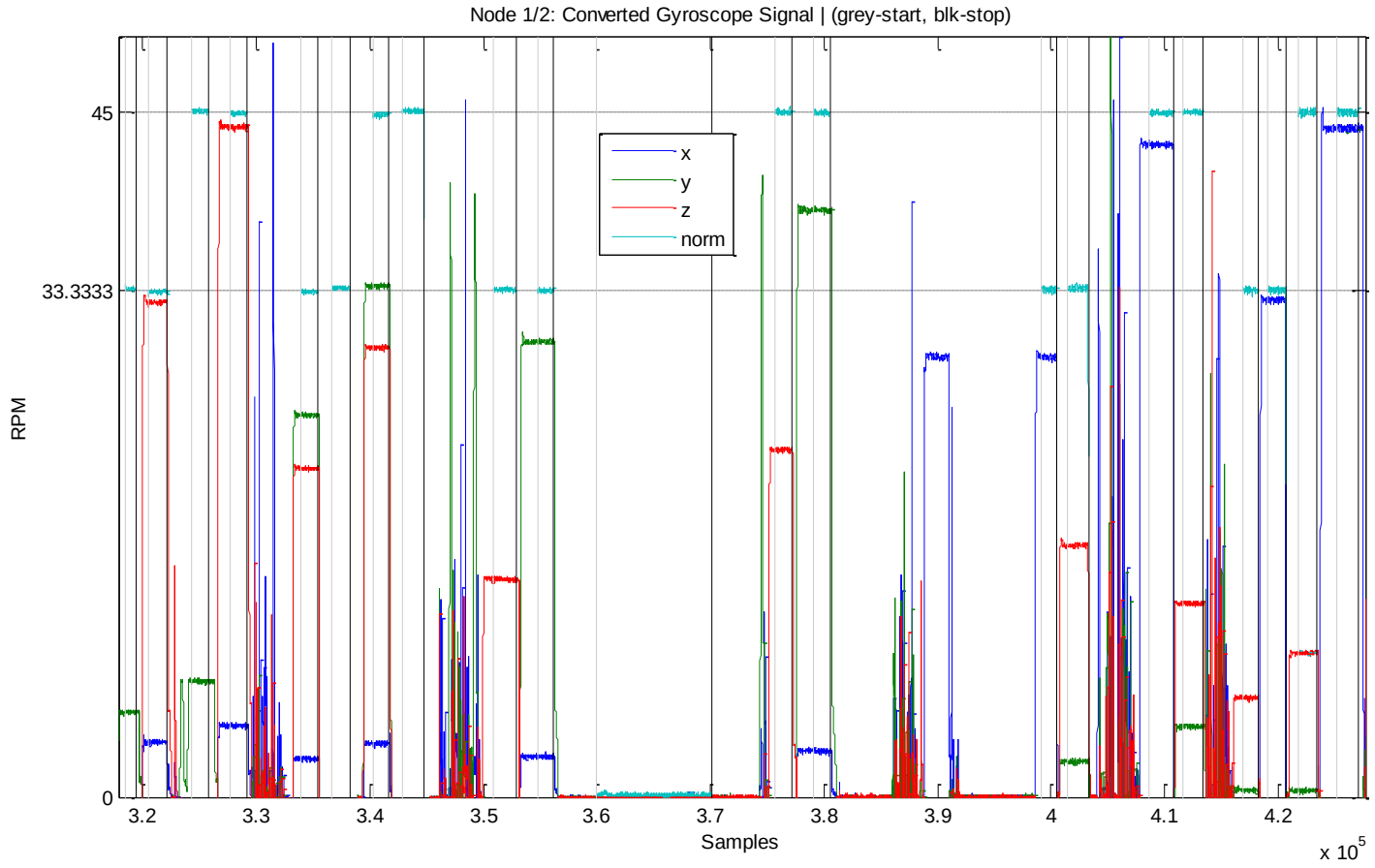

Figure 13. Gyroscope (master node) data after using LM least squares with turntable calibration at ±33 and ±45 RPM rotations over 5 positions. Annotated periods are marked between grey and black lines, during which turntable rotations were performed at constant speeds. Upon examination, the axial components of each rotation period appear to be unique as desired. Note negative range was cut off to more clearly display norm values.

As would be expected, the precision of the calibration was not as high as in the linear calibration. This is not an indicator of a less accurate calibration but instead more comprehensive error accounting. In this sense, the two methods were directly comparable, although axial error approximations would indicate the data still has a very low error ceiling. The slave produced better RMSE with faster convergence time than the master. Since the total mean drifts and fit RMSE were nearly identical between the nodes, the difference in RMSE was independent of the LM method used. The slave annotated data was less noisy than that of the master. This could be a direct result of sensor characteristics but was more than likely caused by movement and vibration within the master's housing in the AFO or inconsistent turntable rotations. Additional filtering, which will be analyzed, will be able to correct any unwanted high frequency vibration in the nodes. Concerns that some of the position-rotation combinations would not be unique enough were dispelled by both the slave and the master node data. Figure 13 depicts uniqueness of each position in the master node, which is also representative of the slave. The parameters for conversion to degrees per second (DPS) were found as follows for a 12 parameter model:

$$DPS_{master} = \begin{bmatrix} 0.0666 & 0.0005 & -0.001 \\ 0.0008 & 0.0666 & 0.0005 \\ -0.0005 & 0.0003 & 0.0671 \end{bmatrix} (ADC_{master} - \begin{bmatrix} 1696.831 \\ 1676.893 \\ 1670.147 \end{bmatrix})$$

$$m_{master,xy} = -0.0037, \;\; m_{master,xz} = -0.0105, \;\; m_{master,yz} = -0.0017$$

$$DPS_{slave} = \begin{bmatrix} 0.0674 & 0.0009 & 0.0005 \\ 0.0007 & 0.0665 & 0.0005 \\ 0.0004 & 0.0005 & 0.0683 \end{bmatrix} (ADC_{slave} - \begin{bmatrix} 1678.071 \\ 1649.285 \\ 1666.999 \end{bmatrix})$$

$$m_{slave,xy} = -0.0017, \;\; m_{slave,xz} = -0.0015, \;\; m_{slave,yz} = -0.0007$$

In general, cross-axis terms were very small and less than 2% of the principal scale factors in the master and slave. The x-z misalignment factor $m_{master,xz}$ for the master was ~15% of the principal scale factor indicating significant axis misalignment correction. The slave only produced a maximum misalignment percentage relative to the principal scale factor of ~2.5% for the x-y axis.

This LM procedure was highly effective and much easier than the linear calibration to physically setup. Any rigid sensor array could be calibrated in the same fashion as described here, with no limitations for embedded sensors. Direct accuracy comparisons between LM and the linear calibration are not possible with this data and are grounds for future work. This was not directly possible here as the linear regression collection requirements were not performed concurrently with that of the LM method. Ideally, the two methods could be performed together and the results from each individual method could be compared with the ground truths obtained by the other method, as the data would be unique.

CP Group

For cerebral palsy data collection, individual 3.2f nodes were placed on the foot and shank of the participant. Since individual nodes were used, the manual axis alignment method was not feasible. Despite sensors identical to the custom AFO, the previous tested LM setup had to be modified for a practical calibration due to the footprint of the nodes. The exact orientations used for the AFO were difficult to reproduce with the individual nodes, without some external hardware. Instead, these nodes were placed in 4 unique positions and rotated at the same speeds as previously defined, resulting in 17 unique orientation-speed combinations. The positions were arranged in such a way to produce large magnitude

contributions from each axis at a given speed. The specific orientations will not be provided as they were determined ad hoc and may vary for each sensor used. Data treatment was identical to that presented for the control group, part B. The results for one node's calibration are presented in Table 5. Figure 14 shows the converted data and relative uniqueness of each position.

Table 5. Results for CPA LM calibration. Note, axial* calculations are artificial calculations used to estimate axial error for comparison to linear methods. $\boldsymbol{Norm = \sqrt{3 * Axial^{*2}}}$

Node	Axis	Fit RMSE (°/s)	Total Mean Drift (°/s)	Total RMSE (°/s)	LM Runtime (s)
120	Norm	0.096	-0.115	0.4918	2.4
	Axial*	0.055	0.066	0.284	

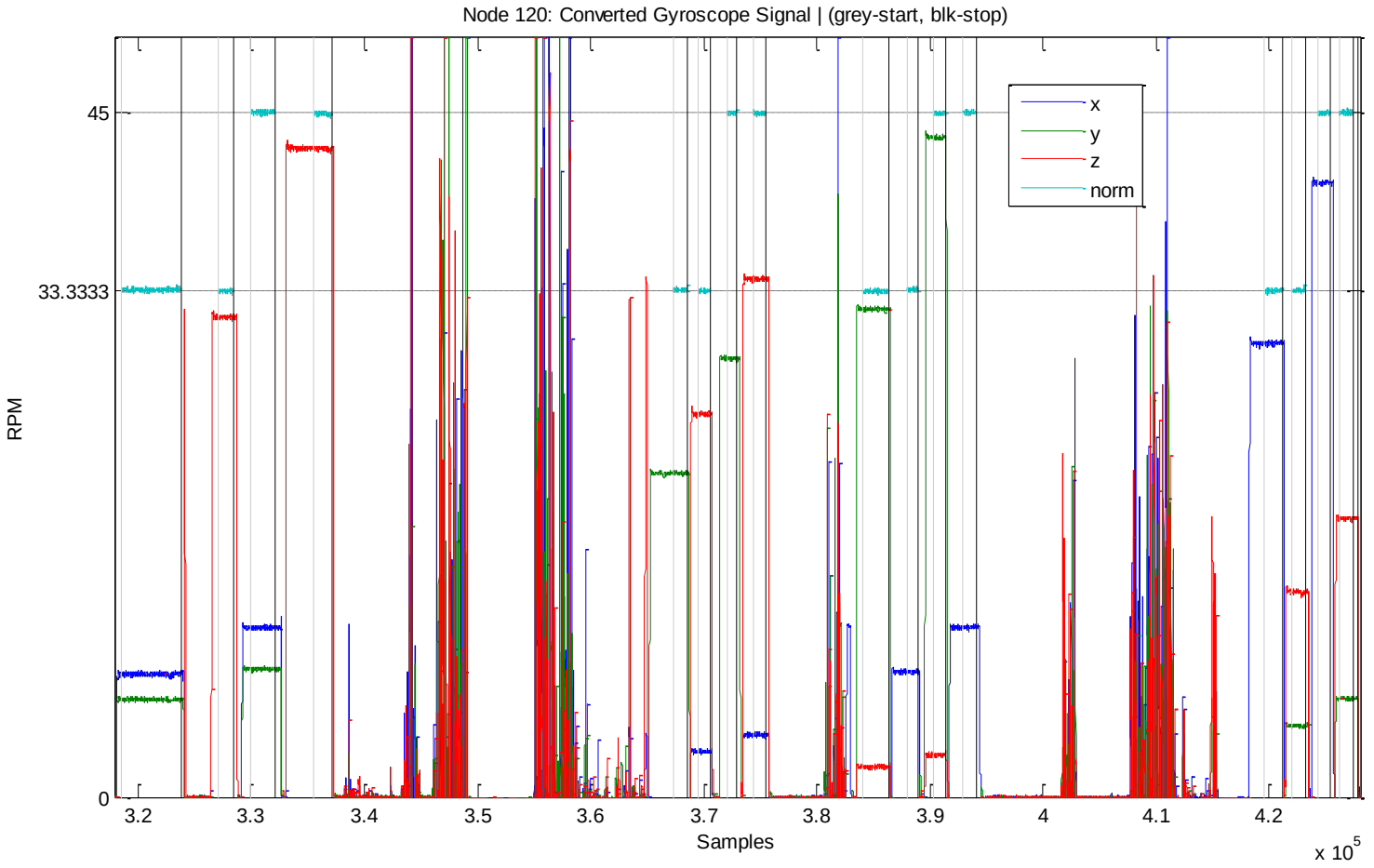

Figure 14. Gyroscope (individual node 120) data after using LM least squares with turntable calibration at ±33 and ±45 RPM rotations over 5 positions. Note the negative range was cut off to more clearly display norm values.

The results were similar to the NOB group. Direct comparisons show this particular calibration was slightly less accurate (total mean drift) but more precise (fit and total RMSE). Such variations were expected, given that the individual nodes were calibrated in their hard, tight fitting cases and the AFO housing is slightly less rigid and roomier. The subsequently reduced vibrations can account for the increased precision or decreased noise ceiling seen in the individual nodes. Additionally, only 17 unique validations were passed through LM, while the AFO method passed 21. Since there is less validation data, the accuracy and precision could presumably be higher. As with the previous group, more comparative experiments would need to be carried out to gauge the importance of method procedure and parameters. The conversion model to degrees per second (DPS) was found as follows for node 120:

$$DPS_{N120} = \begin{bmatrix} 0.0666 & 0.0005 & -0.001 \\ 0.0008 & 0.0666 & 0.0005 \\ -0.0005 & 0.0003 & 0.0671 \end{bmatrix} (ADC_{N120} - \begin{bmatrix} 1696.831 \\ 1676.893 \\ 1670.147 \end{bmatrix})$$

$$m_{N120,xy} = -0.0037, \;\; m_{N120,xz} = -0.0105, \;\; m_{N120,yz} = -0.0017$$

Cross-axis sensitivities were consistently small relative to principal sensitivities. Similar to a previous slave calibration, x-z misalignment was corrected by a factor of ~16% of the principal scale factor.

SUMMARY OF CALIBRATION ANALYSIS

This section outlined high precision methods for calibrating rigid accelerometer and gyroscope arrays. For the accelerometer, an instrumented AFO was propped in 14 unique, pre-defined static positions, which takes approximately two minutes and requires no external equipment. Other high accuracy models may involve validation systems such as motion capture or mechanical rigs, while the model presented requires only the accelerometer array and something to prop it against. Offloaded accelerometer data is passed to a non-linear least squares solver requiring an initial guess of sensor parameters, which was provided by manufacture's specifications. The method was validated using five trials, each containing two calibration procedures spaced out by approximately two hours. Least squares methods, number of positions passed, and parameter models were varied and compared for an optimal solution. A nine parameter Levenberg-Marquardt model demonstrated 100% convergence for every procedure with a mean RMSE < 0.005 g for 12 passed positions, with a marginal decrease of RMSE at 13 and 14 positions. Calibration occurring at the beginning of each session produced lower RMSE than the end of session calibration, although the latter procedure for each session was still acceptable (RMSE < 0.01 g); this was likely due to accumulation of time and temperature related noise.

Given the effectiveness of the LM method on the accelerometer, a similar method was applied to constant angular velocities produced by the turntable. Given the known rotation magnitudes and using a 12 parameter model to correct for biaxial+uniaxial gyroscopes, the method was tested on individual 3.2f nodes, as well as the custom AFO. Accuracy and precision was not significantly affected by these different configurations, even with the individual nodes producing 4 less orientation-speed combinations than the AFO's 21. The AFO procedure was validated on both the shank and foot node which were aligned

in different orientations within the brace. This method produced RMSE less than 1°/s and negligible mean drift. In one instance, the RMSE approached 2°/s but was more than likely a result of vibrations that can be accounted for with a low-pass filter.

Use of external equipment was minimized with all calibration techniques. Accelerometer calibration required no external equipment in the case of the rigid sensor array. For the individual nodes, a dodecahedron accelerometer rig prototype was created which could easily be manufactured with 3-d printers or even cardboard. Simply rotating the dodecahedron onto each numbered side provided all needed static periods. Gyroscope calibration of the individual nodes was performed simply by propping the shell surrounded nodes in 4 positions, although a well-made dodecahedron for the accelerometer portion could double for the gyroscope calibration. A small, non-specific cardboard box kept the AFO propped during turntable rotations but otherwise only required a turntable. A digital stopwatch saved annotated periods for direct import into the calibration algorithms.

Similar approaches have been used in the literature to calibrate sensors but none have provided the comparative and subsequently optimized analysis shown here. This framework is directly applicable to any accelerometer and/or gyroscope array for calibration that need not be performed by an expert. For deployable instrumented AFOs in particular, field calibrations may need to be re-performed periodically and this approach is an ideal solution.

SENSOR ALIGNMENT AND REFERENCE FRAMES

Identification of the proper reference frames is crucial in extracting relevant anatomical gait information. Given that foot and shank sensor coordinate frames orientations are different and unknown, sensor orientation must be determined through an alignment procedure. Previously described calibrations convert the voltages to the proper acceleration or angular velocity. Now this information must be correctly aligned with known coordinate systems.

Gait analysis traditionally uses a body-centered reference frame corresponding to angular movements of flexion/extension, abduction/adduction, and internal/external rotation when dealing with limbs.[8] Segment angles come from sensor frame rotations relative to an initial attitude, normally determined by standing. Relative motion or joint angles are determined by differencing angles in adjacent limbs. To adhere to this terminology, sensor frame axes (x, y, z) are in the body directions of anterior, superior and medial/lateral, respectively. Similarly, the pseudo global frame (X, Y, Z) is aligned in the direction of the aforementioned sensor frame axes when the AFO is oriented vertically. Figure 15 visualizes the coordinate frames utilized in this work.

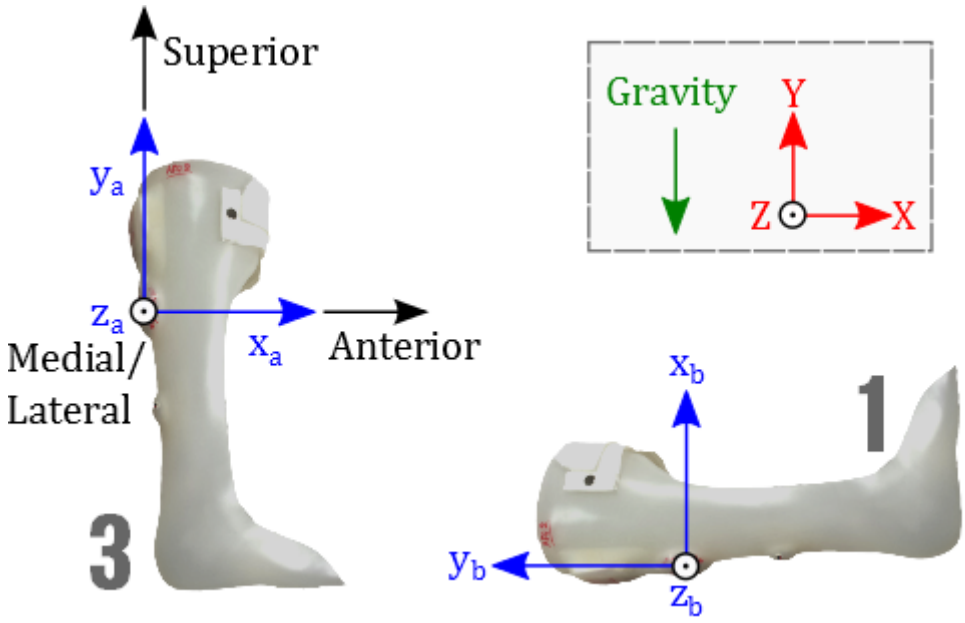

Figure 15. Depiction of coordinate frames. The two positions shown are used to create the proper coordinate systems. The body directionality of the *z* axis (exiting the screen) is dependent on whether the right or left sided AFO is considered – *z* is lateral for left, medial for right. Frames designated *a* and *b* indicate the same sensor axes *x, y, z* evaluated at different positions. Position 3 corresponds to instance *a*, position 1 to instance *b*.

SENSOR FRAME CONVENTION

A simple algorithm is applied to two of the accelerometer calibration positions to achieve rotations from the original sensor frame (x_0, y_0, z_0) to the desired sensor frame (x, y, z). Position *a* (standing AFO) and position *b* (lying AFO) (Figure 15) define a simple rotation (~90°) in flexion or the z direction. Additionally, since both of these positions are static, the magnitude of acceleration is well defined at 1 g. Using a method similar to Chen and Lach,[14] a rotation matrix R_0 converting original sensor frame acceleration normalized mean of each position (position *a*: $x_{0,a}, y_{0,a}, z_{0,a}$; position *b*: $x_{0,b}, y_{0,b}, z_{0,b}$) to the desired sensor frame accelerations ($x_a, y_a, z_a, x_b, y_b, z_b$) was constructed as follows:

$$\begin{bmatrix} x_a \\ y_a \\ z_a \end{bmatrix} = R_0 \begin{bmatrix} x_{o,a} \\ y_{o,a} \\ z_{o,a} \end{bmatrix}, \quad \begin{bmatrix} x_b \\ y_b \\ z_b \end{bmatrix} = R_0 \begin{bmatrix} x_{o,b} \\ y_{o,b} \\ z_{o,b} \end{bmatrix}$$

$$g_a = \begin{bmatrix} x_{o,a} \\ y_{o,a} \\ z_{o,a} \end{bmatrix}, \quad g_b = \begin{bmatrix} x_{o,b} \\ y_{o,b} \\ z_{o,b} \end{bmatrix}$$

$$R_0 = [(g_a \times g_b) \times g_a \quad g_a \quad g_a \times g_b]'$$

Following calculation of R_0, each recorded sample of acceleration and gyroscope is rotated to the new sensor frame. This assumes that any non-orthogonal axes of the sensors have been accounted for during calibration such that the accelerometer and gyroscope axes are perfectly orthogonal. The corresponding Tait-Bryan angles will be referred to as roll φ (rotation about x), pitch θ (rotation about z), and yaw γ (rotation about y).

One potential source of error is insufficient manufactured alignment between gyroscope and accelerometer units. If this occurred, the gyroscope sensor frame would not correspond to the accelerometer frame. Since many methods outlined in this work use both sensors complementarily, additional system error will be induced. Although this error will not be quantified, the effects of such misalignment would more than likely be negligible due the sensor attachment on a flat PCB board. However, bending of the board and sloppy manufacture could certainly result in errors in alignment between accelerometer and gyroscope.

WALKING FRAME CONVENTION

In order to convert accelerations to a global frame, accurate rotations at each sample must be obtained in three dimensions. Ideally, the gyroscope could provide this alone since perfect alignment with the accelerometer is assumed. However, as mentioned the gyroscope

has low-frequency noise components that are difficult to remove without losing valuable information. Given that the accelerometer can provide two angle corrections during static positions, gyroscope drift in all but one axis can be corrected periodically. Therefore, without a magnetometer or a perfect gyroscope, a pure global frame is impossible since one axis will have significant bias. If a pure global frame was approximated with bias accumulated yaw, results in the global frame would be inaccurate and unreliable from an axial (directional) point of view. Additionally, it is possible resultants could also be inaccurate given the computational methods used later in this work.

The alternative to a pure global frame proposed in this work was a "walking frame." Since the purpose of these methods is gait-specific observation, the sensor frame at mid-stance or foot flat period became the new "walking frame." Assuming such events can be observed and gait cycles are separable (which will be proved later), the walking frame will "reset" back to the mid-stance sensor frame at each foot flat. Even though the toe-out angle may be different at the start and end of each gait cycle, the walking frame will be aligned with the direction of the foot. The *X* direction will not necessarily be in the direction of walking, even though the norm of distances will still be accurate. Additionally, with this frame convention it is actually possible to estimate toe-out angle under the assumption that during a stride, the yaw angle at the beginning of the stride is equivalent to that at the end. As will be seen with the double integration technique, this approximate toe-out angle can be determined by the angle between the *X* and *Y* components of stride distance.

TAIT-BRYAN ROTATIONS

The rotation order used in this work is 132 or XZY for walking frame rotations, which will allow easy extraction of pitch and roll from static acceleration periods.

$$R = R_x R_z R_y$$

$$= \begin{bmatrix} cos\theta cos\gamma & -sin\theta & cos\theta sin\gamma \\ sin\phi sin\gamma + cos\theta cos\gamma sin\phi & cos\theta cos\phi & cos\phi sin\theta sin\gamma + sin\theta cos\gamma \\ sin\theta cos\gamma sin\phi - cos\phi cos\gamma & cos\theta sin\phi & cos\phi cos\gamma + sin\theta sin\gamma sin\phi \end{bmatrix}$$

Using this rotation matrix, initial orientation of the sensor unit relative to gravity can be related to a static acceleration reading (A_0), as follows:

$$\begin{bmatrix} A_{0,x} \\ A_{0,y} \\ A_{0,z} \end{bmatrix} = R \begin{bmatrix} 0 \\ 1 \\ 0 \end{bmatrix}$$

Solving this equation for accelerometer orientation yields the following Tait-Bryan angles.

$$\phi = atan\left(\frac{A_{0,z}}{A_{0,y}}\right), \qquad \theta = \text{atan}\left(\frac{-A_{0,x}}{\sqrt{A_{0,y}^2 + A_{0,z}^2}}\right)$$

These accelerometer orientations will be used later to correct gyroscope bias and improve rotations from the sensor frame to the walking frame.

EVENT DETECTION

Event detection is important to allow for determination of stride length and walking velocity. The method described below was validated by comparison with data captured by the Vicon motion capture system. While foot contact and foot off can be detected, foot flat detection and segmentation allows for a reset of the integration constants as described in an upcoming section, *Tracking Stride Motion*.

A simple and highly accurate method for event detection was developed using only the foot pitch rate (z sensor frame gyroscope data) for recognition of foot strikes, foot flats, and foot offs during walking or running. No discrimination between walking and running was required. No errors in peak detection were found for event detection of any stride cycle in level or inclined strides. This method's simplicity and congruence with activity recognition methods for walking and running periods yield an effective solution for an independent gait analysis system.

Walking and running periods were provided through manual annotations, although the method will ultimately be used in conjunction with an activity recognition method that determines walking and running periods. Furthermore, measures were included to remove false positives that may be results of errors in walking or running periods passed from an activity recognition method. Validation was performed at three walking speeds of 3, 4, and 5 km/h at 0° and 15° incline, and two running speeds for five healthy subjects. Additional exclusion conditions could be created to further minimize potential false positives, but were not found to be unnecessary. This method is as accurate as any previously provided in the literature, with a much simpler implementation and smaller computational load than machine learning techniques. Related methods have even been shown to work with children

with CP.[32] Further testing of this algorithm in more varied walking may require adjustments for removal of false positives.

Recent research has found acceleration to be most consistently 1 g during foot flat as opposed to heel strike during walking. Despite this fact, many studies have used heel strike as a static period. Acceleration during running at foot flat is not as close to static as walking but acceleration normalization can still produce reasonable orientation estimates.

Shank detection methods were ignored in favor of the foot since the instep is an instantaneous center of velocity at mid-stance, unless there is slipping. Pitch (sagittal) rate in the sensor coordinate frame was the only data used. Accelerometer input was deemed unnecessary, as well as yaw and roll of the foot, since most significant translational and rotational motion occurs in the y-x plane.

Figure 16 shows sample data for walking and running angular velocities using a foot sensor. Despite the different mechanics of walking and running, angular velocities trends are similar, particularly in pitch rate. Note, positive pitch rate indicates extension, while flexion occurs with negative pitch rate.

a)

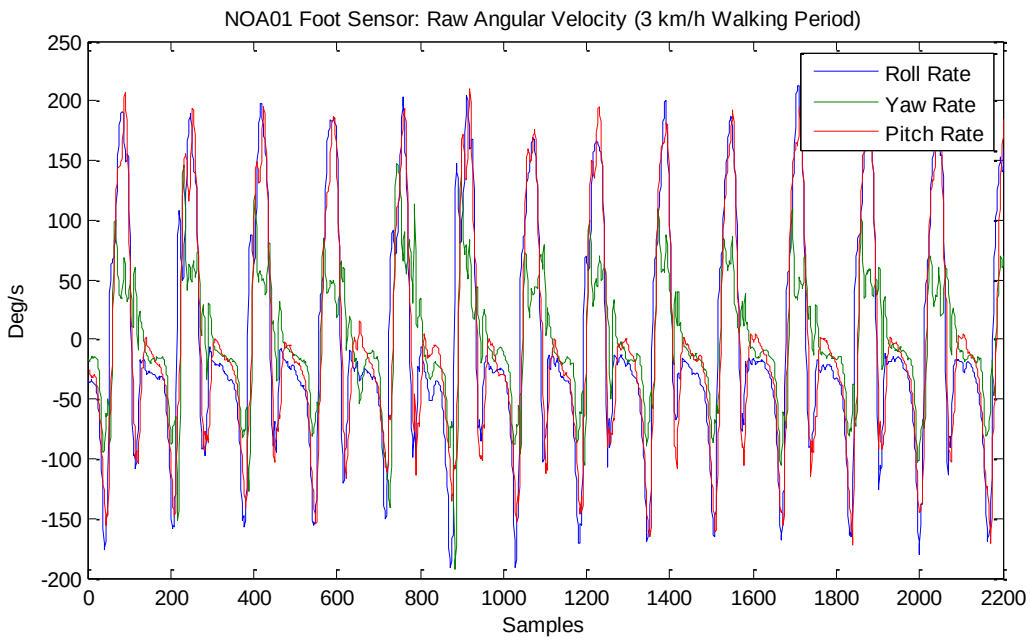

b)

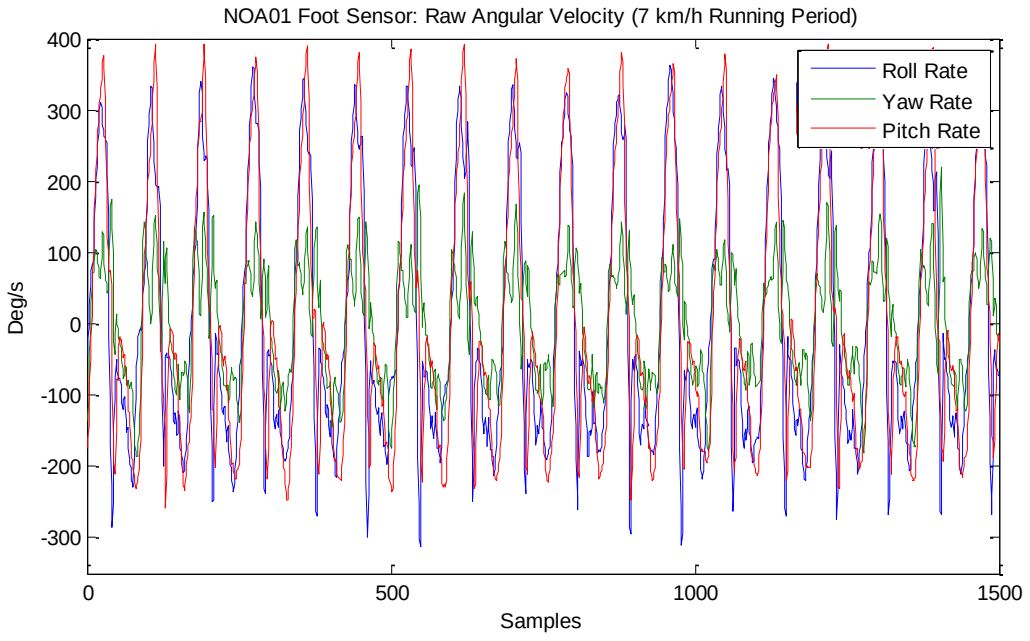

Figure 16. Sample sensor frame angular velocities showing the similarity of walking (a) and running (b).

Figure 16 shows foot pitch rate and acceleration norm during a representative walking strides and its relationship to foot strike, foot flat, and foot off. Angular velocity was filtered with a 3rd order Butterworth, zero-phase at 0.1 Hz (high-pass) and 20 Hz (low-pass). Acceleration data was low-passed only with a zero-phase, 3rd order 32 Hz Butterworth.

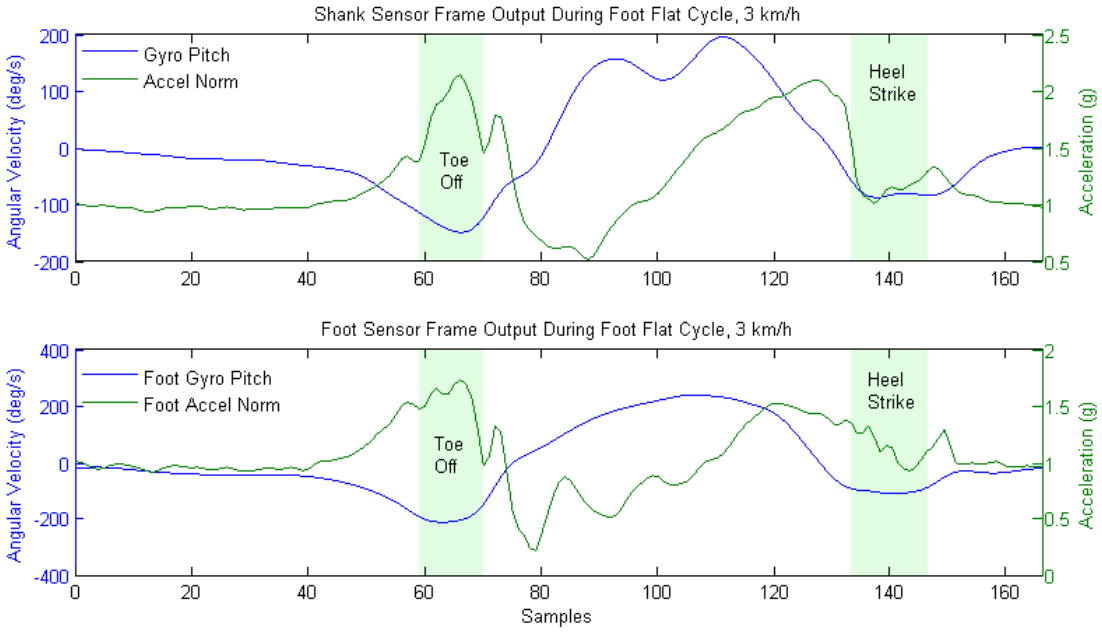

Figure 17. IMU outputs during a stride cycle. The cycle was segmented by foot flats, indicating the presence of foot flat at the beginning and end of the time series.

The large positive peaks in angular velocity indicate the foot has finished swinging through and is returning to the make contact with the ground. Furthermore, the following minimum coincides with foot strike. As the foot approaches a flat position, pitch rate approaches a maximum near zero before changing direction and pushing off. Foot off is the minimum preceding the large increase in pitch rate during swing-through. Historically, the specific peaks are used as absolute indicators of heel strike and toe off. However, validation that these events occur precisely at the peaks is very hard to produce, due to the difficulty of matching motion capture to the IMU data exactly. For further support of these claims refer

to Pappas et al[33] and Pappas et al[34]. The most important part of event detection is ensuring that foot period identification is consistent and meaningful in the context of future algorithms and interpretation. With this said, quantitative validation of event detection via motion capture will not be provided. Instead, proper identification of peaks will be used as the validation tool, i.e., the peak relationships shown in Figure 17.

Acceleration data during the stride cycle is also meaningful for future analyses. Use of foot flat or foot strike as integration boundaries has varied in the literature. Foot strike acceleration at foot flat and subsequent time stamps leading up to toe-off produce both foot and shank accelerations very near 1 g with little deviation. However, acceleration during heel strike is not consistently 1 g for the foot or shank accelerometers. Given the additional room for error and precision, foot flat is a far better boundary condition for updating sensor orientation to remove gyro bias. Additionally, foot flat is more attractive as a zero-velocity update for acceleration integration (see *Tracking Stride Motion*) for stride length than heel strike, given that much less motion occurs during mid-stance.

FOOT PHASE METHOD

The implementation of the determination of foot flat from foot gyroscope data was as follows:

1. Groups of continuous walking and running periods are passed to this method under one of the two conditions
    a. Activity recognition methods for walking and running content
    b. Annotated periods via data syncing and stopwatch, etc.
2. Filter pitch rate with a 3rd order 5 Hz low-passed Butterworth filter to remove minor peaks. (For this algorithm only)

3. A peak detection algorithm in MATLAB (*peakdet*) finds minimums preceded by a pitch rate greater than 5 deg/s.
4. To segment the trajectory by large peaks, peaks with less than 50 deg/s magnitudes are removed required.
5. An additional condition was added to reduce the possibility of false positives that could be a result of improper walking and running periods passed to this method by machine learning or annotations. All periods within minimums had to have at least 5 °/s standard deviation or those minimums were removed.
6. Given the relationships between angular velocity and gait events described by Pappas et al, foot strike, foot flat, and foot off could be determined:

   if (max between min *i* and min *i+1* > max of Walking Period *.5)

   ➔ Min *i* corresponds to foot off, Min *i+1* to foot strike

   else

   ➔ Min *i* corresponds to foot strike, Min *i+1* to foot off
7. If sequential foot off, foot strikes, or foot flats are found within half a second apart from the same event, the redundant event is removed.
8. Foot flats were classified within each foot strike to foot off sequence as the maximum only if the magnitude was less than 75°/s.
9. Finally, filtering at peaks was not completely zero-phase, despite the use of zero-phase filters. Since upcoming methods only utilized the 16 Hz low-passed gyroscope signal, the peaks identified with the 5 Hz cut-off exhibit a significant phase shift at higher speeds. To remove this shift, toe offs and heel strikes were refined by searching around the 5 Hz predicted peak. A 30 and 15 sample radius to the left and right, respectively, were used and if a peak value smaller than that produced from the

5 Hz predicted peak was found, the toe off/heel strike position was corrected. This refinement was deemed unnecessary for foot flat given that mid-stance lasts long enough for variations from phase shift to be negligible.

DETECTION VALIDATION

Five subjects walked and ran on a treadmill for approximately thirty seconds per speed. Walking speeds of 3, 4 and 5 km/h were performed on a level and inclined surface. Additional speeds of 7 and 8 km/h were tested with all subjects self-selecting running on level ground only. The foot phase method was tested on all annotated periods recorded from a digital time keeper. A total of 891 level foot flats and 359 incline foot flats were observable, with the breakdown shown in Table 6.

Table 6. Breakdown of observable foot flats for all normal subjects. Note incline treadmill feature was broken during NOA03 collection.

	Foot Flats Analyzed								
	Level Treadmill Walking					~15° Incline Treadmill Walking			*Subject Totals*
	level3	level4	level5	level7	level8	incline3	incline4	incline5	
NOA01	14	20	30	43	31	17	28	31	214
NOA02	25	32	32	52	43	47	27	30	288
NOA03	35	35	52	65	42	N/A	N/A	N/A	229
NOA04	31	34	37	47	41	36	29	34	289
NOA05	21	24	27	38	40	26	25	29	230
NOA Totals	126	145	178	245	197	126	109	124	**1250** *All Total*

Toe-off events that occurred first during walking periods were ignored. Manual inspection of the peaks for every cycle resulted in 100% sensitivity for foot flats and heel strikes. The only errors found in toe offs were for NOA05 during 5 km/h incline. In four instances during this period the toe offs were misidentified due to unexpected peak detection function, as shown in Figure 18. However, over such a large dataset, errors in a threshold based peak detection method are to be expected. Further conditions could be added to remedy this issue but due to the already high sensitivity and relative unimportance for toe off in coming algorithms, no adjustments were made. Specificity experiments were not carried out, given walking and running periods should be directly accessible with high specificity through Archer et al.'s work. Figure 19(a-e) and Figure 20(a-c) demonstrate representative effectiveness of this method on level treadmill and incline treadmill locomotion, respectively, by subject one (NOA01).

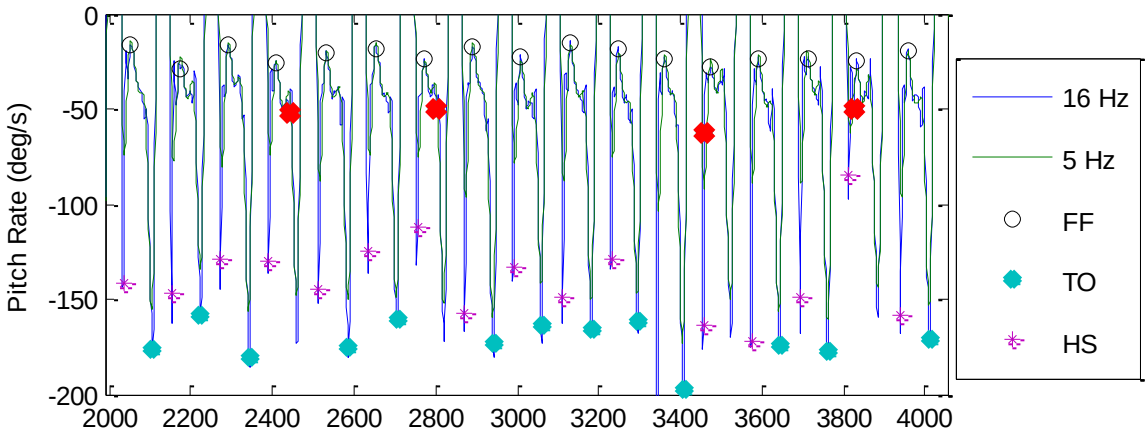

Figure 18. Depiction of toe-off errors found during 5 km/h incline walking for NOA05. Enlarged red circles indicate the incorrectly identified toe-offs.

a)

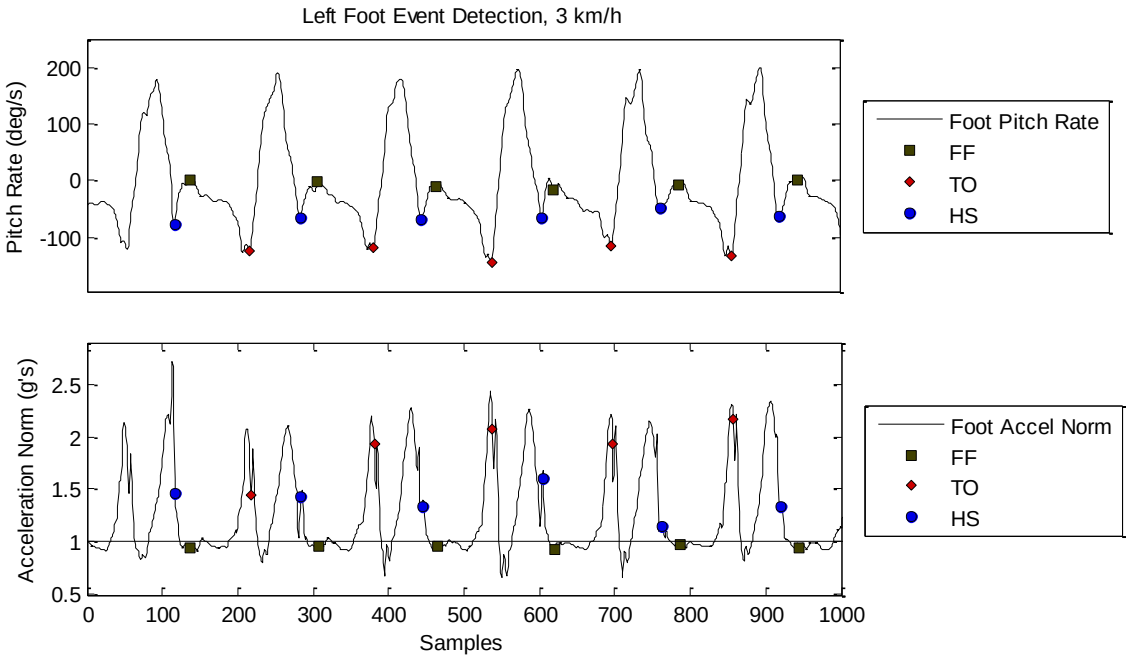
Left Foot Event Detection, 3 km/h
Pitch Rate (deg/s)
200
100
0
-100
Foot Pitch Rate
FF
TO
HS
Acceleration Norm (g's)
2.5
2
1.5
1
0.5
Foot Accel Norm
FF
TO
HS
0
100
200
300
400
500
600
700
800
900
1000
Samples

b)

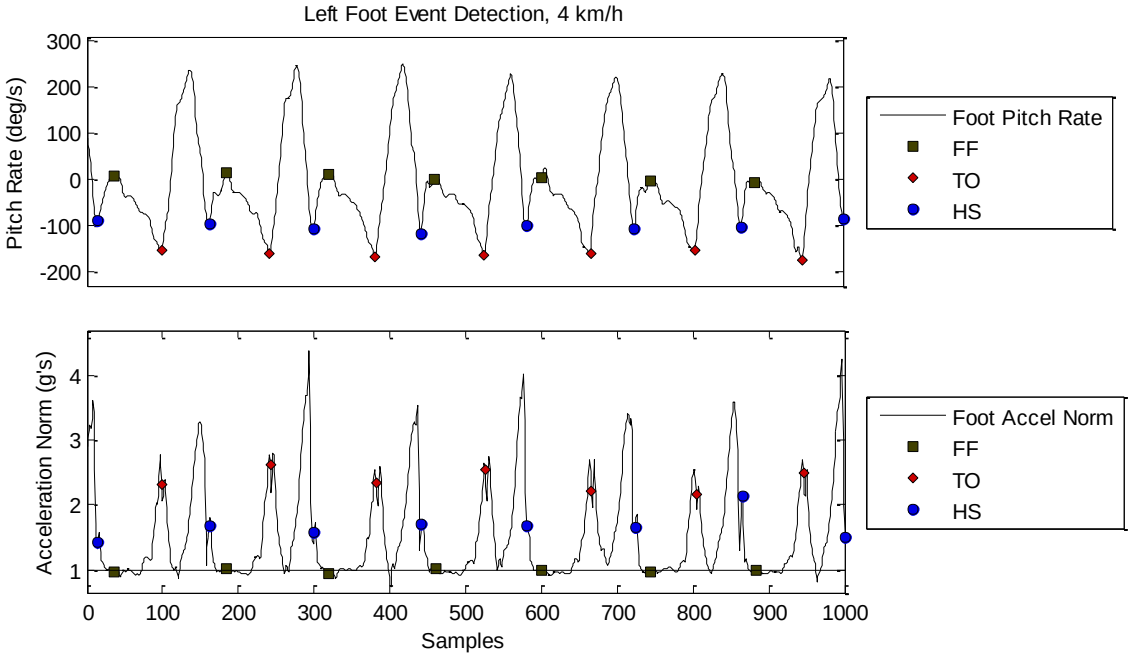
Left Foot Event Detection, 4 km/h
Pitch Rate (deg/s)
300
200
100
0
-100
-200
Foot Pitch Rate
FF
TO
HS
Acceleration Norm (g's)
4
3
2
1
Foot Accel Norm
FF
TO
HS
0
100
200
300
400
500
600
700
800
900
1000
Samples

c)

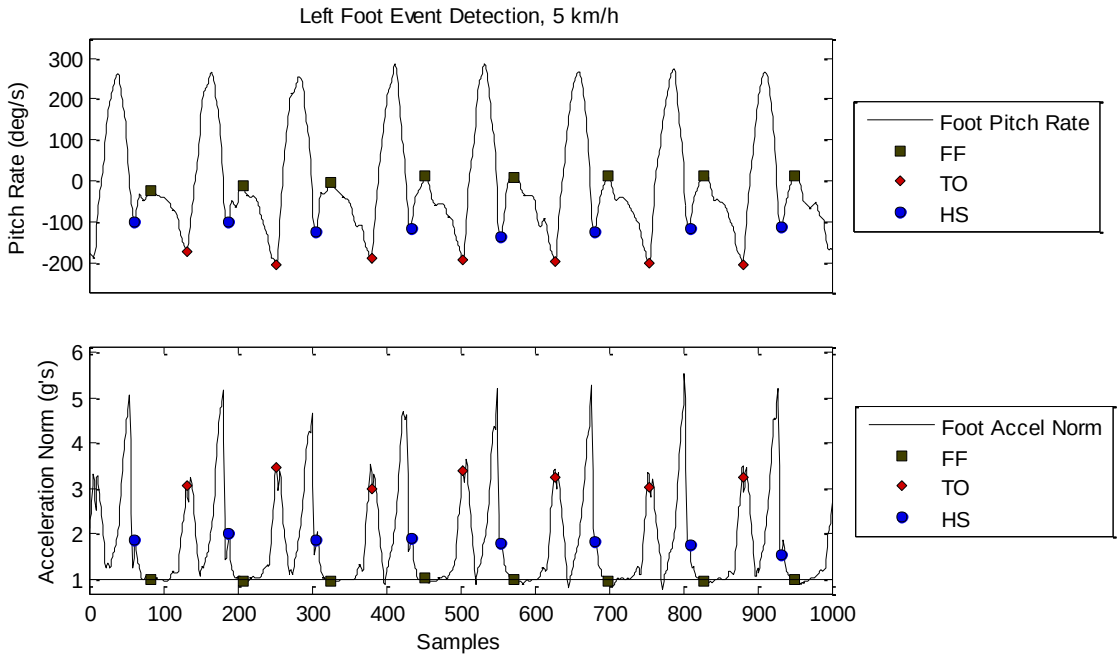
Left Foot Event Detection, 5 km/h
Pitch Rate (deg/s)
300
200
100
0
-100
-200
Foot Pitch Rate
FF
TO
HS
Acceleration Norm (g's)
6
5
4
3
2
1
Foot Accel Norm
FF
TO
HS
0
100
200
300
400
500
600
700
800
900
1000
Samples

d)

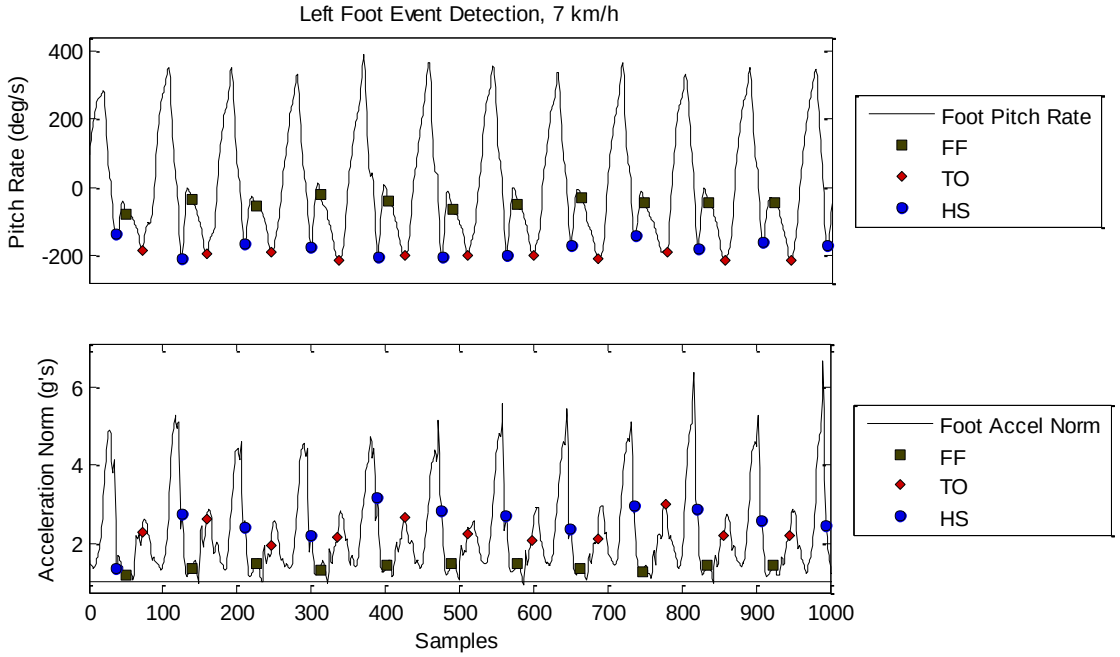
Left Foot Event Detection, 7 km/h
Pitch Rate (deg/s)
400
200
0
-200
Foot Pitch Rate
FF
TO
HS
Acceleration Norm (g's)
6
4
2
Foot Accel Norm
FF
TO
HS
0
100
200
300
400
500
600
700
800
900
1000
Samples

e)

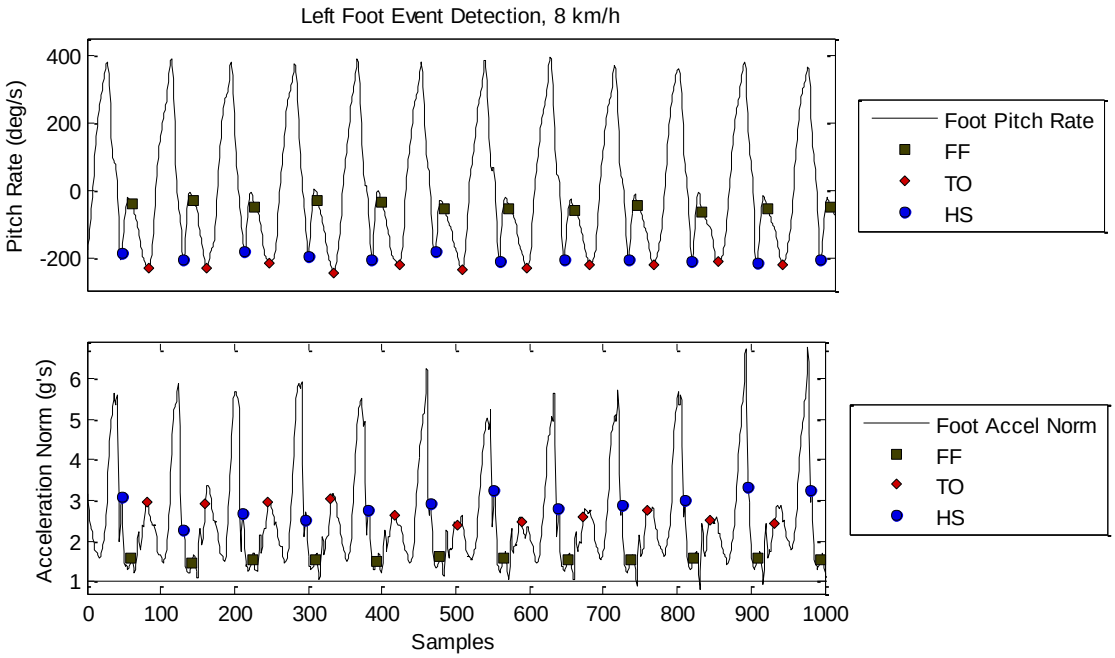

Figure 19(a-e). An example progression of level treadmill speeds for a subject and its effect on acceleration and pitch rate.

a)

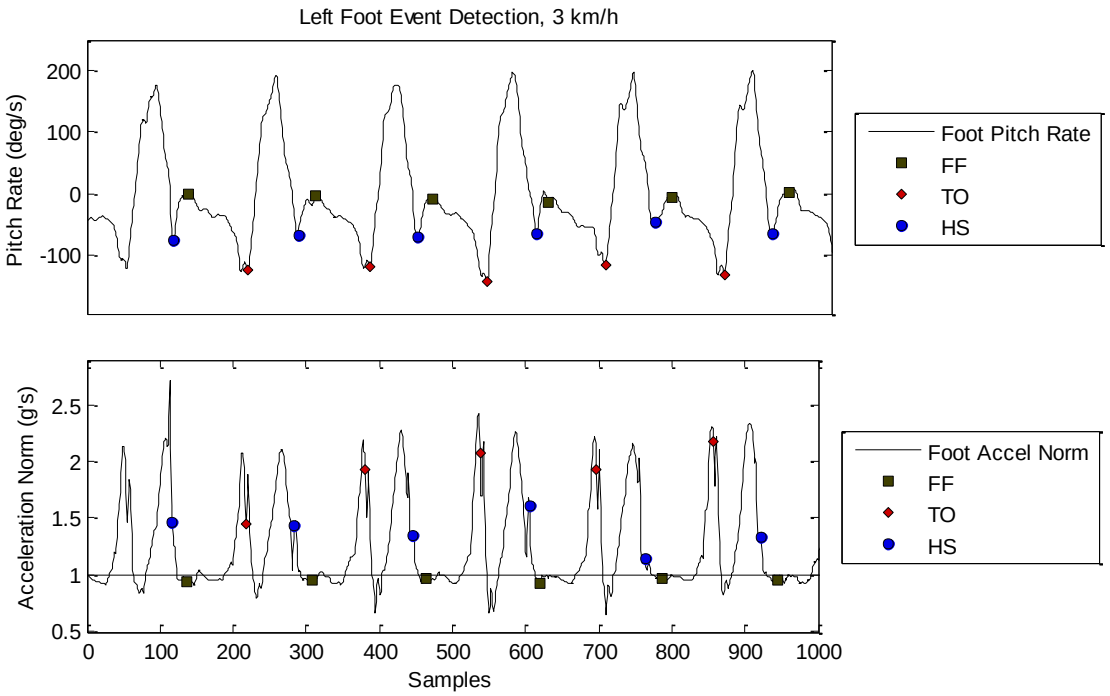
Left Foot Event Detection, 3 km/h
Pitch Rate (deg/s)
200
100
0
-100
Foot Pitch Rate
FF
TO
HS
Acceleration Norm (g's)
2.5
2
1.5
1
0.5
Foot Accel Norm
FF
TO
HS
0
100
200
300
400
500
600
700
800
900
1000
Samples

b)

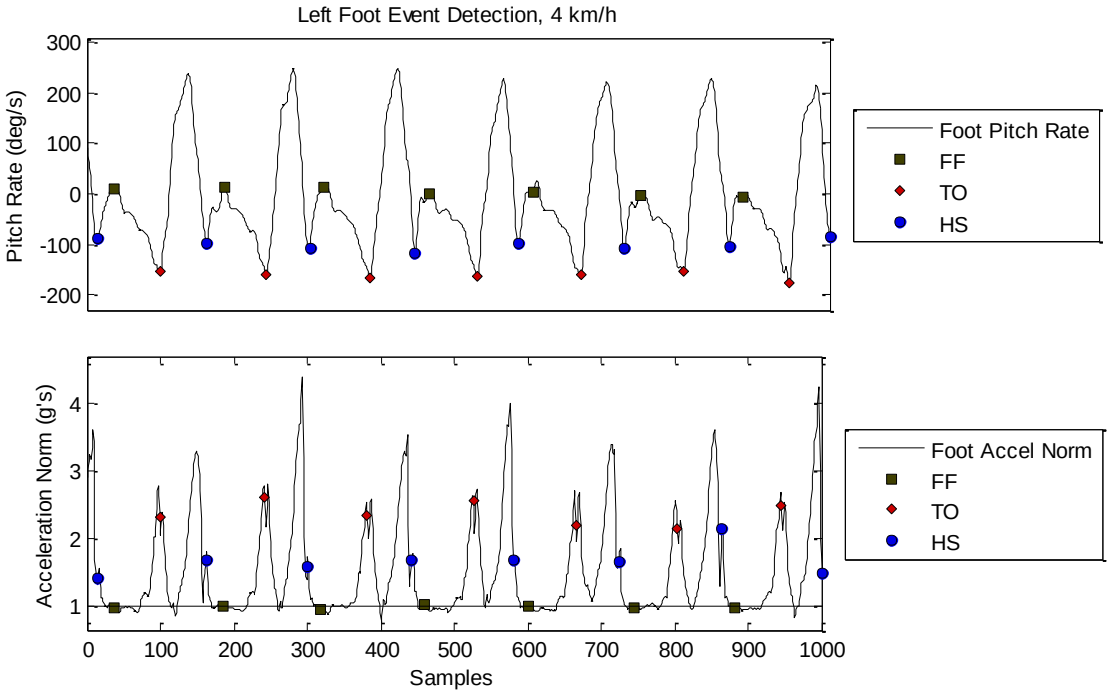
Left Foot Event Detection, 4 km/h
Pitch Rate (deg/s)
300
200
100
0
-100
-200
Foot Pitch Rate
FF
TO
HS
Acceleration Norm (g's)
4
3
2
1
Foot Accel Norm
FF
TO
HS
0
100
200
300
400
500
600
700
800
900
1000
Samples

c)

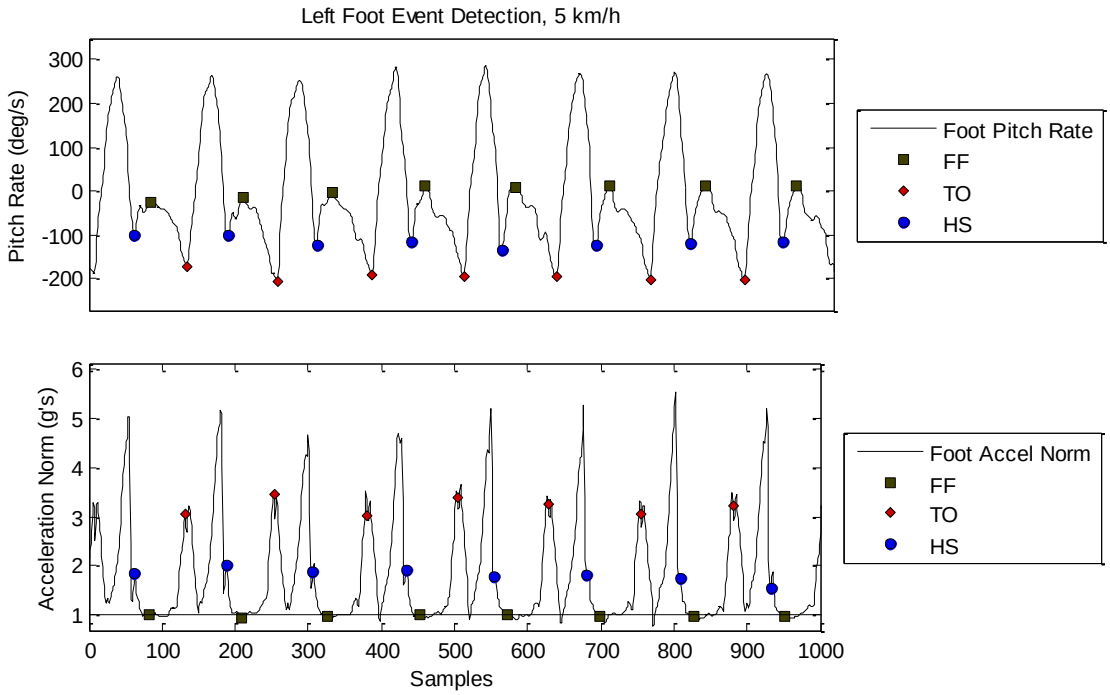

Figure 20(a-c). Sample periods of data during 3, 4, and 5 km/h incline treadmill walking, with foot strike, foot flat, foot off periods.

Acceleration norm tracked 1 g very closely during foot flat events for level walking and incline walking. On the other hand, acceleration during foot flat of running did not yield accelerations as close to 1 g but was still near the minimum acceleration for each stride cycle. For walking, level or incline, varying speed showed no noticeable differences in acceleration proximity to 1 g during foot flat. This further supports the use of foot flat as an update time for both orientation via the accelerometer and instantaneous velocities.

CONCLUSION

The method presented here is accurate over a very large dataset and rivals the best event detection methods presented in the literature, given widely accepted association of certain peaks to foot strike, foot flat, and foot off throughout the literature. Approximate foot flat

and heel strike events were identified flawlessly in over 1200 varied cycles of level running, level walking, and uphill walking on a treadmill. Unlike many machine learning approaches, ground truth knowledge and pre-determined thresholds were all that was required for execution. This work has proved that to some extent these thresholds can be generalized for inter-subject use on healthy subjects. Pathological gait could conceivably require the use of intra-subject thresholds and is grounds for additional work.

Further work needs to be done to test such a method against atypical gait such as cerebral palsy. This technique was optimized for five control subjects so errors may occur with the analysis of more varied gait. In general, significant peak ordering in the sagittal plane should remain unchanged given that all events of interest still occur in pathological gait. The addition of spastic motion may remove some clarity from the repetitive nature of pitch rate examined in this work. More aggressive filtering could combat this, as well as other sensor input from the accelerometer. Additionally, slower walking individuals may add challenges to the algorithm presented due to the thresholds used. However, adaptive thresholds could be implemented relative to the max swing-through angular velocity, which has been demonstrated to increase with walking speed.

GENERAL AND GAIT-SPECIFIC SPECTRUM ANALYSIS

The majority of this thesis deals with time-domain observation and analysis, although knowledge of the frequency domain can further improve the effectiveness of time-domain orientated methods. Spectrum analysis can provide magnitude information for distinguishing frequencies of interest for gait sensing with accelerometers and gyroscopes. The following sections analyze static and dynamic frequency spectra for the sensors used in the AFO platform. From this information, filtering thresholds will be set for upcoming methods. Additionally, insight is gained about the repeatability and variation between pre-defined walking and running speeds on a treadmill. In particular, angular velocity is highly repeatable for all speeds, whether running or walking. Frequency peak magnitude and location scales with increasing speed. However, walking acceleration is more variable without a clear relationship to walking speed.

Matlab's fast fourier transform algorithm (*fft*) was used to determine the *N*-point discrete Fourier transform (DFT) for two scenarios - a long static period and each stride cycle for a normal subject (NOA01). The *N* value was chosen empirically as *10*number of samples passed to fft (L)* for high resolution. Since DFTs are only reliable at the Nyquist frequency and below, a single-sided amplitude (*SSA*) measure was calculated up to the Nyquist frequency as follows:

$$SSA = \frac{2\left|FFT_{1:\left\lfloor\frac{N}{2}+1\right\rfloor}\right|}{L}$$

STATIC NOISE ASSESSMENT (LOW FREQUENCY)

A static data collection was performed with the AFO for approximately 17 hours to examine noise characteristics and validity of long data collections. The first five minutes of data was ignored in order to remove any sort of startup drift or external vibrations. DFTs were performed on mean removed digital time series for each of axis of each sensor to obtain SSAs. Noise characteristics were similar between the two accelerometers, as well as between the gyroscopes. Additionally, no significant differences were noticed axially for each sensor. Furthermore, subsequent analysis will deal with one axis each for the accelerometer and gyroscope of the shank sensor.

Accelerometer low-frequency noise started to increase slightly below 0.4 Hz but was very negligible (see Figure 21). Past 0.1 Hz, noise was generally uniformly small in magnitude. Given the importance of low-frequency accelerometer components in determination of gravity direction, a high-pass filter was not initially used for the accelerometer. Eventually, high-pass filtering will be necessary but will not be addressed until the *Tracking Stride Motion* section.

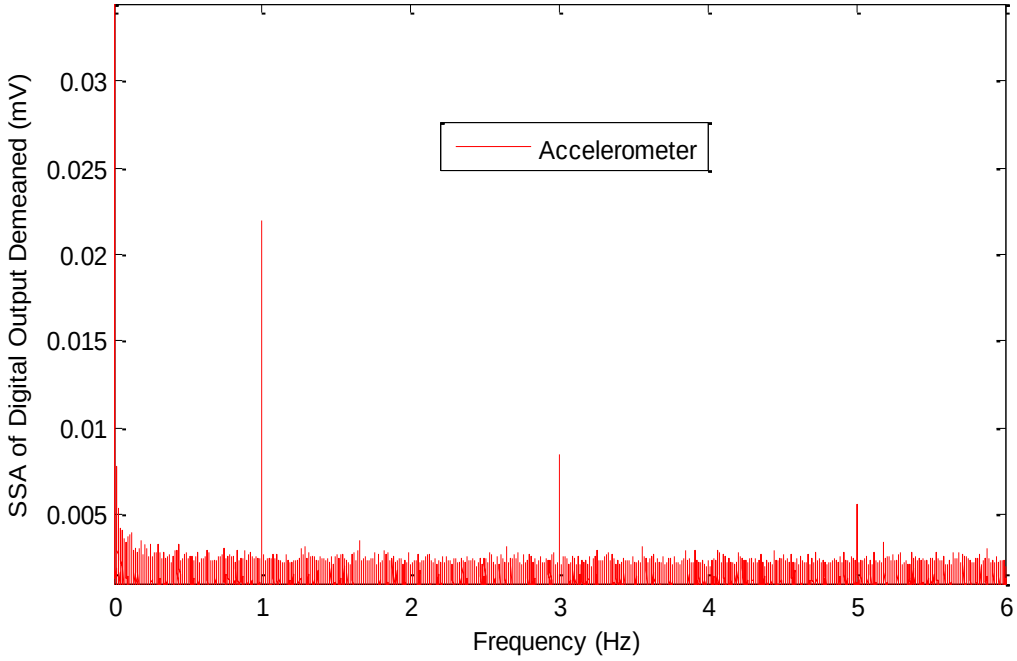

Figure 21. Single sided amplitude spectrum of a representative demeaned axial accelerometer output. Noise is consistently small in magnitude with a negligible increase starting about 0.1 Hz. Noise was similarly negligible above 6 Hz.

Low-frequency noise in the gyroscope was much more prevalent than in the accelerometer. In particular, the 0-0.4 Hz showed a significant increase in noise relative to the rest of the frequency range, with a peak occurring at 0.1 Hz. Similar to the gyroscope, noise past 0.4 Hz is uniform and small. Since the accelerometer will be used to provide updates for the drift in the gyroscope, high-pass filtering is possible without significant loss of information. Based on this analysis, a 3rd order, zero-phase, 0.4 Hz high-pass Butterworth filter seemed to remove this low frequency noise. Data was reliable for the entire collection period and displayed no inconsistencies over the long data collection. Removal of drift resulting from low-frequency noise will produce consistent outputs over long data

collections.

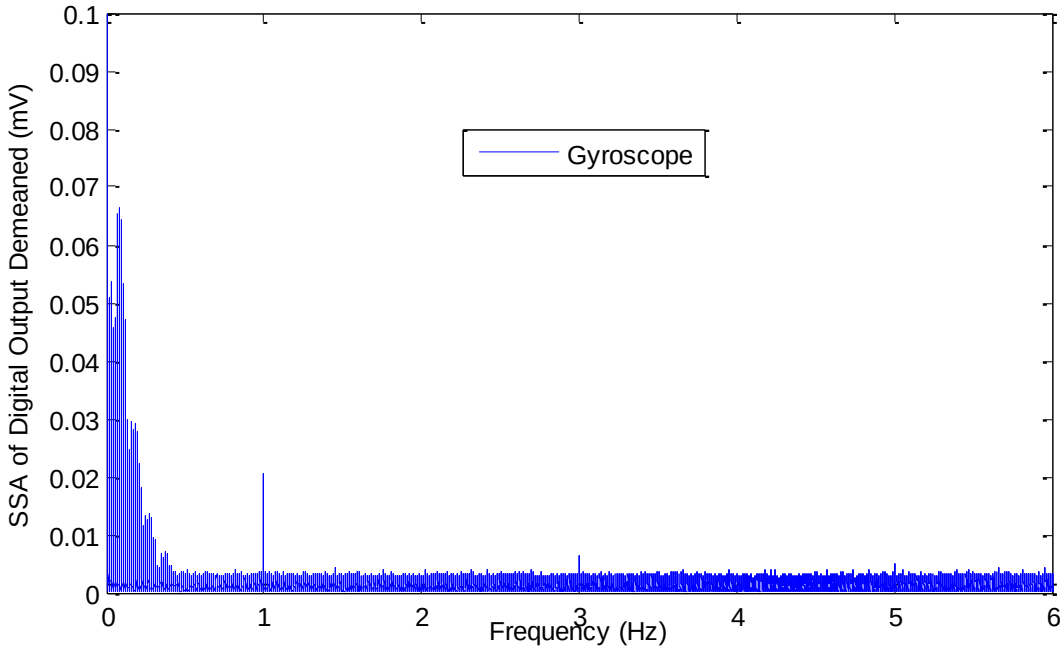

Figure 22. Single sided amplitude spectrum of a representative demeaned axial gyroscope output. Unlike the accelerometer, low-frequency noise occurs, starting around 0.4 Hz. At its highest spectral contribution, noise is more than 10 times what is observed commonly above 0.4 Hz. Like the accelerometer, noise past 6 Hz is small and uniform.

Noise was found to be consistent throughout frequency ranges above 0.4 Hz for both the accelerometer and gyroscope axes during a static trial. Low-frequency noise in the accelerometer was significantly large compared to higher frequency ranges. The gyroscope, however, produced very significant low-frequency noise below 0.4. To address this, only the gyroscope will be corrected for low-frequency error, by using a high-pass filter.

FREQUENCY OF WALKING AND RUNNING (MID-HIGH FREQUENCY)

A spectrum analysis was performed on pitch rate and accelerometer magnitude for a normal functioning subject to estimate spectrum content of normal walking and running. Previous knowledge of gyroscope noise allowed pre-filtering with a 3rd order, zero-phase, 32 Hz low-

pass Butterworth. Accelerometer data was left unfiltered. Cycle DFTs were then splined (640 point) and meaned for each constant speed period to compare variations in frequency spectra with increasing speed. Figure 23 demonstrates the results. Number of cycles included for each speed can be found in Table 6 for NOA01.

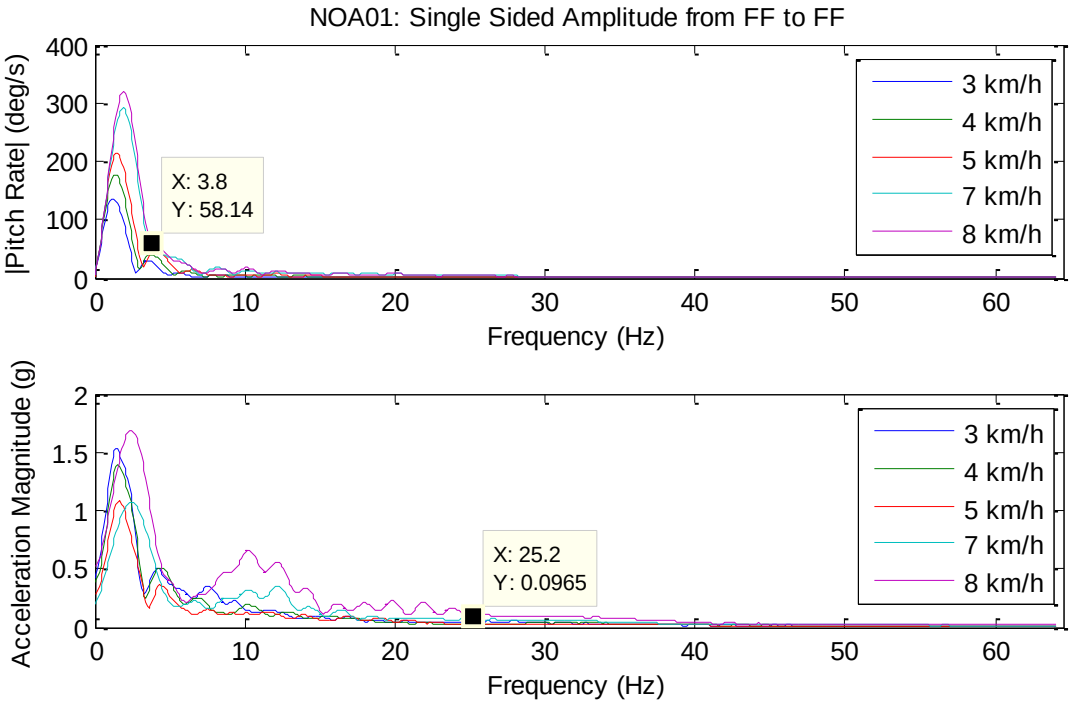

Figure 23. Single sided amplitude of foot sensor's outputs. Mean pitch rate of FF periods within each treadmill speed were passed through FFT. Data was pre-filtered by 3rd order, zero-phase, 32 Hz Butterworth.

These plots provide a number of interesting observations that can improve upcoming methods. In general, pitch rate appeared to be fairly consistent between walking and running speed variations. The large amplitude location of the spectrum only shifted from 1 to 2 Hz during the progression of 3 km/h walking to 8 km/h running. This observation is consistent with increases in gait speed being more a result of increased stride speed than decreased cadence. Running and walking both appeared to be highly repeatable at all the speeds tested.

All pitch rate activity above 5 Hz in frequency appeared to be comparable in magnitude to random noise artifacts which validates the pre-filtering of gyro data used in foot phase determination. Considering pathological gait data was not analyzed, further techniques will pre-filter gyro data with a high and low-pass, zero-phase, 3rd order Butterworth filters. A 16 Hz low-pass cut-off was chosen to allow for tracking of more spastic motions which are common and critical observations in CP gait analysis. Although a 0.4 Hz high-pass was optimal for removing low-frequency noise in static periods, this cutoff empirically demonstrated loss of important dynamic components when tested with upcoming methods. Therefore, a 3rd order, zero-phase, 0.1 Hz high-pass Butterworth filter was found to be an optimal trade-off between removal of biases and drift and conservation of low-frequency dynamics.

Accelerometer spectra showed a much stronger response than pitch rate to increasing speed. Repeatability in the higher frequency components of running seemed to be lower than walking; the ringing effect in the 10 – 25 Hz range may indicate the meaned periods demonstrated varying peak locations in this range. This is indicative of the more variable nature of running that has previously been observed in the literature, particularly at pre-defined speeds.[60,61] Spectral range also increases from 7 to 8 km/h, with some ringing past 20 Hz at small magnitudes higher than the noise ceiling. An aggressive pre-filter cut-off frequency of 20-25 Hz could be used. However, to improve generality at a small potential expense of precision, accelerometer data will be low-passed at 32 Hz for integration methods. Additionally, filtering distinctions could be made separately for running and walking but the goal of this work was to optimize generality.

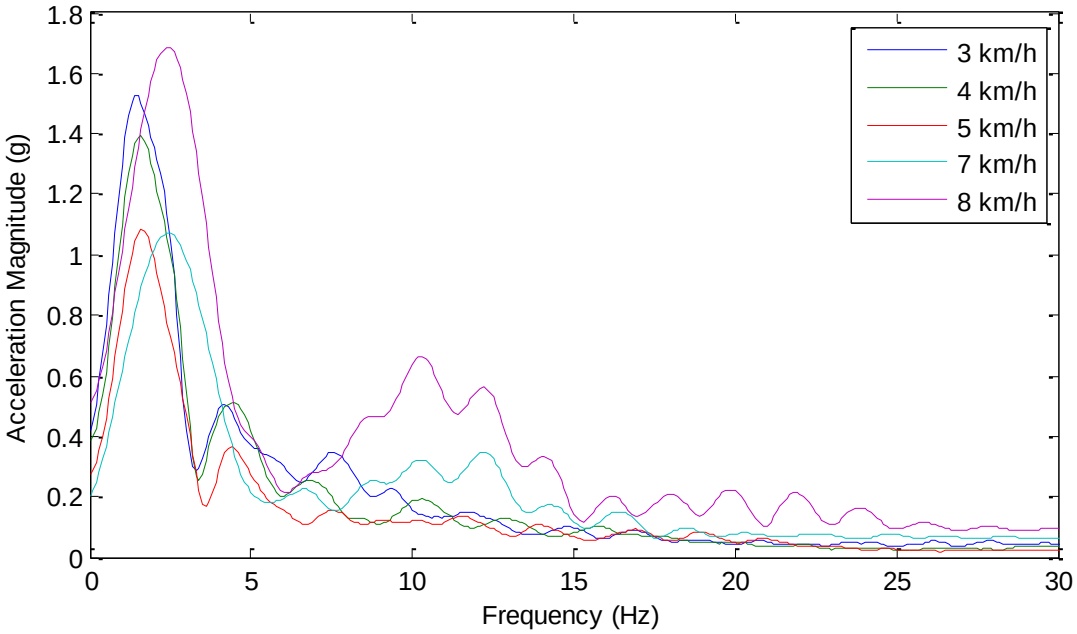

Figure 24. Magnified single sided amplitude of foot sensor acceleration magnitude.

Upon close examination (Figure 24), accelerometer spectral content varied considerably between each of the walking speeds. Magnitude contribution was consistently minimized at all frequencies for the fastest walking speed. Moreover, 3 km/h produced the maximum magnitude contribution at nearly all frequencies when compared with the other walking speeds. Previous work has suggested optimal self-selected walking speeds exist based on the criteria of energy consumption rate[62] and stride length deviations,[63] which this spectral analysis may suggest under a different criterion. Further investigation would be required to assess the significance of these results in terms of walking efficiency.

SEGMENT AND JOINT ANGLES

Joint angles, particularly ankle angle, are of great importance in clinical gait analysis. For CP in particular, sagittal ankle angle can often provide insight into osteopathic and muscular pathologies, as it both provides most of the power for walking and is the joint typically most effected by CP. This information can help physical therapists and doctors make decisions about treatment. Additionally, any global information desired from the sensors will require sample-by-sample rotations via sensor frame angle observations. Acceptable error in gait metrics such as joint angle has not been well defined by clinicians. The following section will assess motion capture's precision capabilities, as well as how sensor angle calculations compare.

Motion capture angle comparisons were performed using a custom made algorithm. The *bombadil4* and *PlugInGait* Vicon models provide accurate joint angle estimation but do not calculate reliable segment angles relative to a standing position. Instead of assessing relative ankle angle accuracy between Vicon and the AFO, each segment angle was compared for further insight. Three markers were placed on the rigid segment corresponding to each sensor in the AFO. A static standing period was used as the reference for the local coordinate frame. Due to difficulties in obtaining angles from Vicon, a rigorous comparative analysis could not be provided.

First, the Vicon sensor frame was rotated to the AFO frame *X,Y,Z* as previously described using a XZY convention. Via the three marker locations for each sensor, a plane was defined at each sample. Rotation angles were determined from each sample relative to the static reference plane using axis-angle representation. Given the relationship between axis-angle representation and *XZY* Tait-Bryan rotations, the roll, pitch, and yaw were

determined at each sample. Both Vicon angles and sensor angles were demeaned and passed through a cross-correlation algorithm (MATLAB's xcorr) to determine necessary shifting to align the data.

SEGMENT ANGLE ESTIMATION

Three methods for estimating segment angle were compared, all performed during each foot flat cycle lasting *N* samples. The first method (GO) determined segment angle purely by gyroscope strap-down integration, with zero angle resets at foot flat. Strap-down integration used angular velocity (ω) and Simpson's integration rule to produce roll (Φ), pitch (θ), and yaw (θ):

$$\Phi_i = \Phi_{i-1} + \frac{\omega_{x.i-1} + 4\theta\omega_{x.i} + \omega_{x.i+1}}{6f_s},$$

$$\gamma_i = \gamma_{i-1} + \frac{\omega_{y.i-1} + 4\theta\omega_{y.i} + \omega_{y.i+1}}{6f_s},$$

$$\theta_i = \theta_{i-1} + \frac{\omega_{z.i-1} + 4\theta\omega_{z.i} + \omega_{z.i+1}}{6f_s},$$

$$i = 2, 3, 4, \ldots N-1$$

$$\Phi_0 = \gamma_0 = \theta_0 = \Phi_N = \gamma_N = \theta_N = 0°$$

The second method (GwA0) used the same gyroscope strap-down integration as method one but used accelerometer derived orientation at foot flat to update boundary conditions for pitch and roll. As addressed in *Sensor Alignment and Reference Frames*, boundary conditions for yaw were chosen to be 0°.

$$\phi_i = atan\left(\frac{A_{z,i}}{A_{y,i}}\right), \qquad \theta_i = \text{atan}\left(\frac{-A_{x,i}}{\sqrt{A_{y,i}^2 + A_{z,i}^2}}\right),$$

$$\phi_N = atan\left(\frac{A_{z,N}}{A_{y,N}}\right), \qquad \theta_N = \text{atan}\left(\frac{-A_{x,N}}{\sqrt{A_{y,N}^2 + A_{z,N}^2}}\right),$$

$$\phi_0 = atan\left(\frac{A_{z,0}}{A_{y,0}}\right), \qquad \theta_0 = \text{atan}(\frac{-A_{x,0}}{\sqrt{A_{y,0}^2 + A_{z,0}^2}})$$

Lastly, a complementary filter (CF) was created based on Colton and Mentor's "balance filter"[64] to provide additional weighting from the accelerometer signal to improve drifting characteristics of the gyroscope. Specifically, this complementary filter balances observations from low-passed gyroscope angle from strap-down integration with orientation provided by the low-passed accelerometer data. Similar to the previous method, the accelerometer provides the boundary conditions for a cycle. In the absence of a magnetometer, complementary filters are known to be as accurate as Kalman filters but with less complexity. Kalman filters were tested, although they will not be presented here as it produced similar results as the complementary filter. A time constant τ chosen empirically to be two dictated how much weight would be distributed between the gyroscope and accelerometer. A larger value tending towards one indicated more accelerometer input as opposed to gyroscope, and vice a versa. In essence, this filter provides a pseudo low-pass and high-pass filter for accelerometers and gyroscopes, respectively, in order to extract the best information from each sensor. Estimates of orientation from the accelerometer roll (α)

and pitch (β) were fused with gyroscope estimates. Since accelerometer could not provide yaw, estimates for yaw were calculated the same as in GwA0.

$$c_g = \frac{\tau f_s}{\tau f_s + 1},$$

$$c_a = 1 - c_g,$$

$$\Phi_i = c_g\left(\Phi_{i-1} + \frac{\omega_{x.i-1} + 4\theta\omega_{x.i} + \omega_{x.i+1}}{6f_s}\right) + c_a\alpha_i,$$

$$\gamma_i = \gamma_{i-1} + \frac{\omega_{y.i-1} + 4\theta\omega_{y.i} + \omega_{y.i+1}}{6f_s},$$

$$\theta_i = c_g(\theta_{i-1} + \frac{\omega_{z.i-1} + 4\theta\omega_{z.i} + \omega_{z.i+1}}{6f_s}) + c_a\beta_i,$$

$$\alpha_i = atan\left(\frac{A_{z,i}}{A_{y,i}}\right), \qquad \beta_i = \text{atan}\left(\frac{-A_{x,i}}{\sqrt{A_{y,i}^2 + A_{z,i}^2}}\right),$$

$$\alpha_N = atan\left(\frac{A_{z,N}}{A_{y,N}}\right), \qquad \beta_N = \text{atan}\left(\frac{-A_{x,N}}{\sqrt{A_{y,N}^2 + A_{z,N}^2}}\right),$$

$$\alpha_0 = atan\left(\frac{A_{z,0}}{A_{y,0}}\right), \qquad \beta_0 = \text{atan}(\frac{-A_{x,0}}{\sqrt{A_{y,0}^2 + A_{z,0}^2}})$$

RESULTS

Despite efforts to provide a comparative analysis of these methods to ground truth data provided by Vicon, consistent problems arose with determination segment angle calculation from markers. Sagittal ground truth angles were recovered from the markers fairly well but measures of the transverse and frontal planes were not believed to be accurate. Furthermore, comparisons between the methods were not particularly insightful, except for confirmation that estimations of sagittal angle (flexion/extension) are accurate when demeaned to remove for any bias relating to initial conditions.

The alignment technique used was found to be highly effective and could be translated to other methods of validation if desired. Figure 25 shows the correlation for a representative period during level walking using the left shank sensor.

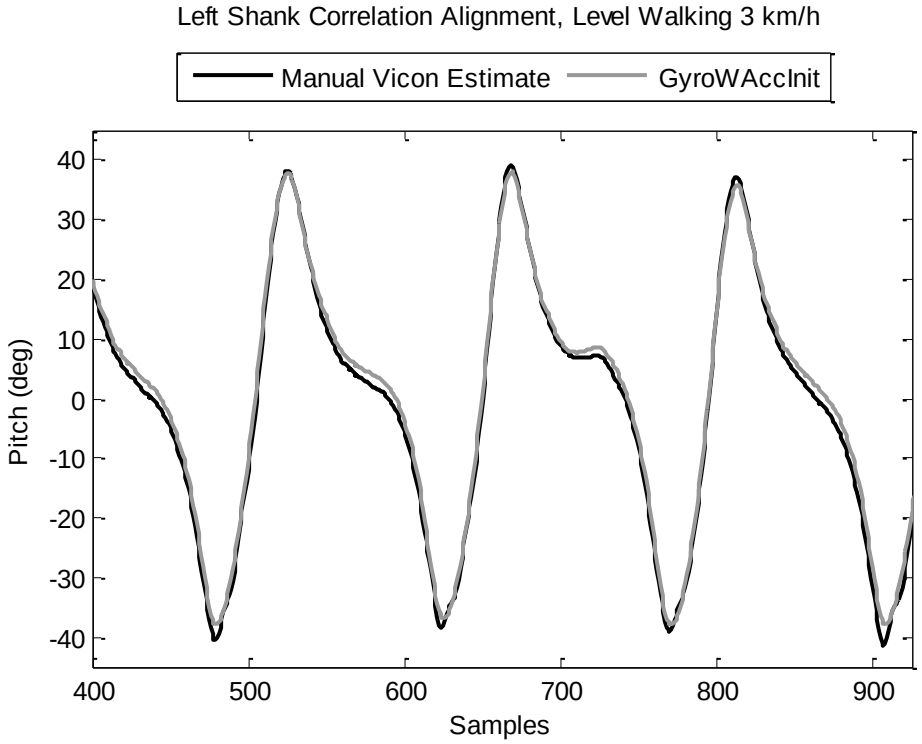

Figure 25. Vicon and sensor based pitch angle estimate aligned using a cross-correlation algorithm.

The figures below demonstrate representative results of attempted angle validation on subject NOB01. The validation method used for the shank (Figure 26) seemed to work slightly better than for the foot (Figure 27). Tests performed on other walking and running speeds are not shown. Little difference was observed between the methods when compared. Initial biases were removed from all signals. Gyroscope only method was nearly identical to gyroscope with acceleration initial conditions. After removing initial bias, GO and GwA0 were nearly identical as expected, with no noticeable drift between the two over time. The complementary filter was also not drastically different than GwA0, although discontinuities were sometimes observed due to accelerometer updating. From this analysis, temporary 1 g samples within areas of high frequency change were not reliable for orientation updating.

For these reasons along with the lack of a comparative analysis, GwA0 was used for orientation tracking.

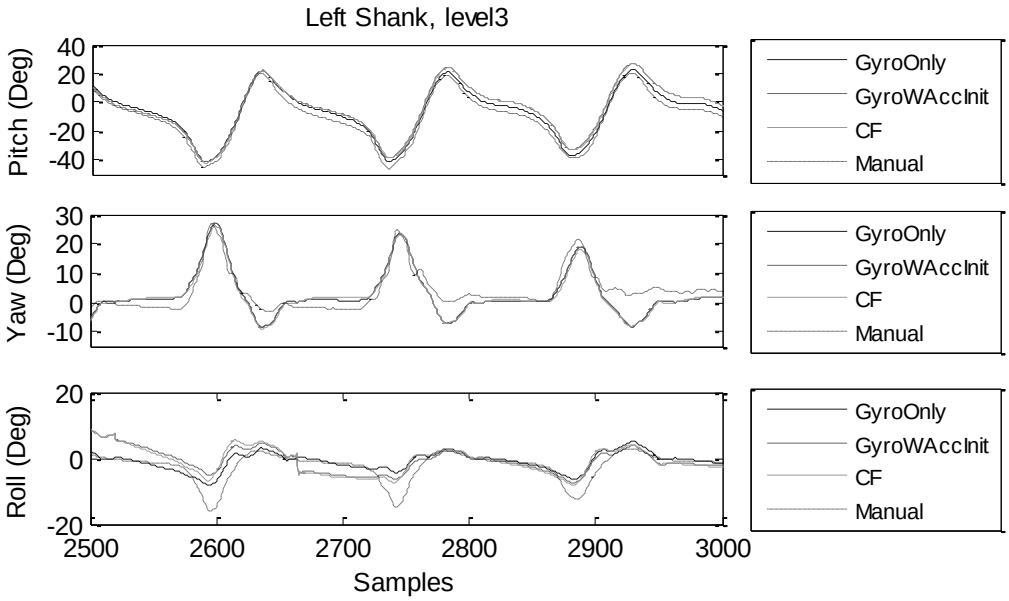

Figure 26. Vicon comparison results for the left shank during level walking at 3 km/h. Note many methods are overlapping.

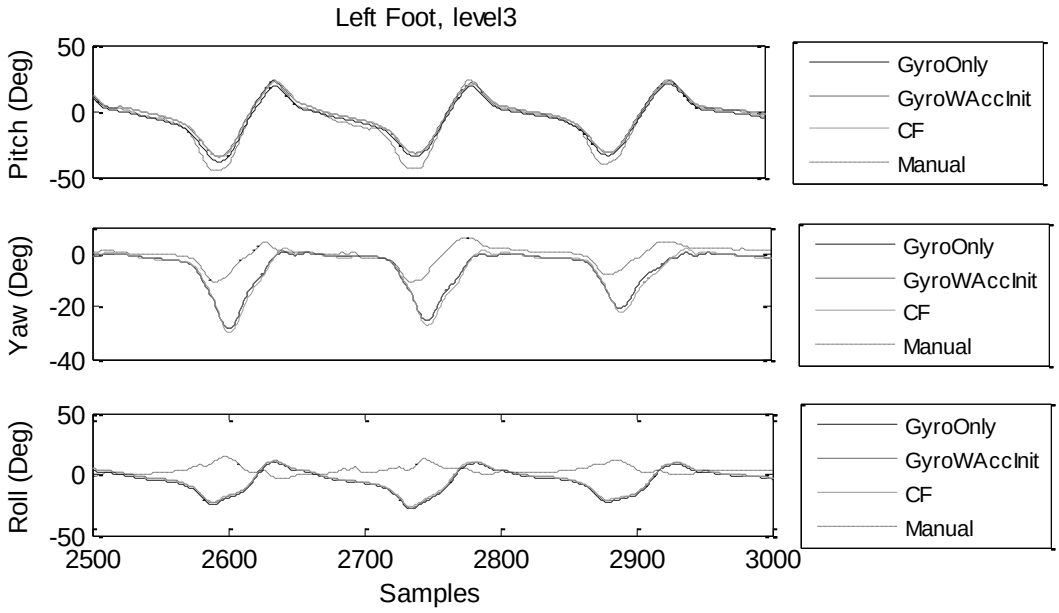

Figure 27. Vicon comparison results for the left foot during level walking at 3 km/h. Note many methods are overlapping.

Although care must be taken in considering quantitative results of this analysis, level walking produced total pitch RMSE less than 5° for level walking and running for the shank sensor. Total RMSE for each tested period is shown below in Table 7.The foot data contained was plagued by obscured markers although, similar sagittal errors were expected.

Table 7. Total RMSE errors for pitch angle in the left shank.

	Total RMSE (°)			
	Level Walking 3 km/h	Level Walking 4 km/h	Level Walking 5 km/h	Level Running 7 km/h
Pitch (Flexion/ Extension)	4.51	2.12	3.41	4.77

Validation of the segment angles ultimately produced results which were untrustworthy. Although the sensor calculations seemed trustworthy, Tait-Bryan angles of roll and yaw determined from marker position were not and the reason could not be identified. Given that the gyroscope only angles should track transient movements well, the trends observed by the sensor with gyroscope only methods should follow ground truth data but with some additional bias. This was not the case for the most part, which indicated error with the Vicon angle calculations. The other possibility is that the gyroscope and accelerometer sensors on each board were not properly aligned, contrary to this work's assumption. Still, pitch comparisons were reasonable with small error between Vicon and the sensor, which is of the most significance clinically among the three angles.

TRACKING STRIDE MOTION

Given the interest in locomotion in athletes and clinical settings, tracking gait metrics on a stride-by-stride basis in the field could provide never before observed information about environmental effects and fatigue. This section will present an extension of previous methods toward accurate tracking of linear motions during a stride.

INTEGRATION SCHEME

With the effectiveness of event detection and angle estimation established, accelerometers can provide changes in global distance during a gait cycle when integrated. A simple first principle model was constructed using Zok et al's forward and reverse integration with arctan weighting function[54] and Yang et al's solution to non-zero velocity updates[53]. Zok et al's preferred model was implemented using an empirically chosen high-pass cut-off frequency of 0.001 Hz to remove gravity induced bias. After formulation of a 132 rotation matrix *R* from roll, pitch, and yaw estimates, stride information was determined during each foot flat cycle by the following procedure

1. Global frame acceleration in $\frac{m}{s^2}$ ($\bar{A}$) from high-passed sensor frame acceleration (a) in g's

$$\bar{A} = \begin{bmatrix} A_X \\ A_Y \\ A_Z \end{bmatrix} = g \cdot R \begin{bmatrix} a_x \\ a_y \\ a_z \end{bmatrix}, \quad g = 9.8 \frac{m}{s^2}$$

2. Forward and reverse integration to instantaneous global velocity ($\bar{v}$). Angular velocities (ω) and distance from sensor to instantaneous center in the walking frame (L) were used to update initial ($\vec{v}_1$) and final velocities ($\vec{v}_p$) for the shank sensor. An

arc-tan weighting function was created using the index for the final sample (*P*) and constant *B* was set to 0.1, consistent with Zok et al.[54]

$$\vec{v}_i = \vec{v}_{i-1} + \frac{1}{6f_s}(\bar{A}_{i-1} + 4\bar{A}_i + \bar{A}_{i+1}), \qquad \overleftarrow{v}_j = \overleftarrow{v}_{j-1} - \frac{1}{6f_s}\left(\bar{A}_{j-1} + 4\bar{A}_j + \bar{A}_{j+1}\right)$$

$$\vec{v}_1 = \overleftarrow{v}_P = \omega_1 L, \;\; \vec{v}_P = \overleftarrow{v}_1 = \omega_P L$$

Shank: $L = [0.11 \quad 0.23 \quad 0]\, m$

Foot: $L = [0 \quad 0 \quad 0]\, m$ (assumed instantaneous center)

$$s_i = \text{atan}\left(\frac{2i - P}{2PB}\right), \quad w_i = \frac{s_i - s_1}{s_P - s_1}$$

$$\bar{v}_i = \vec{v}_i w_i - \overleftarrow{v}_j(1 - w_i)$$

3. Integration of instantaneous velocity ($\bar{v}$) to instantaneous position ($\bar{d}$).

$$\vec{d}_i = \vec{d}_i + \frac{1}{6f_s}(\bar{v}_{i-1} + 4\bar{v}_i + \bar{v}_{i+1}), \qquad \vec{d}_i = [0 \quad 0 \quad 0]$$

4. Stride length (*SL*), stride time (*t*) and stride velocity (*SV*)

$$SL = \left\|\vec{d}_P\right\|_2$$

$$SV = \left\|\frac{\vec{d}_P}{t}\right\|_2, \;\; t = \frac{P - 1}{f_s}$$

VALIDATION PROCEDURE

Annotated periods of level walking, level running, and incline walking data were used for the validation of stride speed for the NOA group. Subjects walked and ran for periods upward

of 30 seconds while wearing the AFO. A marker was attached to the belt of the treadmill to track its speed for duration of each period. Mean stride velocity over each entire annotated period for a constant speed was compared to the mean treadmill velocity for each subject.

Ground truth was obtained from a custom made MATLAB algorithm which extracted mean and standard deviation for the resultant treadmill speed. This method first found the largest positional range the treadmill marker in sight of the cameras for each belt cycle. The linearized slope of these periods was then calculated and averaged to produce a resultant treadmill speed. An example visualization of this technique is shown in Figure 28.

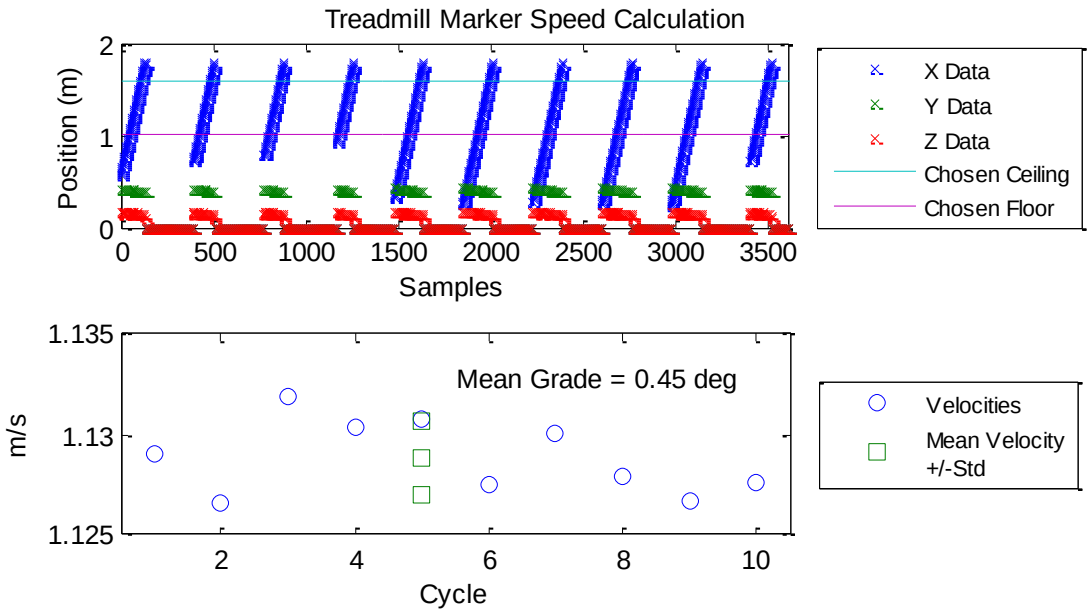

Figure 28. Treadmill velocity determination for a 3 km/h (1.11 m/s) level walking trial. Top - Determination of spatial range to be included for slope calculation during each belt cycle. Ceilings and floors are calculated on the X (approximate direction of motion) data. Bottom - Results following calculation of resultant belt cycle velocities.

The sensor data for the AFO in all periods was segmented into walking periods by foot flat as previously presented in *Event Detection*. Each of these periods was treated with the integration scheme for tracking stride motion to calculate stride length, cadence, and speed.

The mean and standard deviation over an entire annotated period was calculated and compared to the ground truth information deduced from the treadmill marker.

RESULTS

Vicon validation speed was not possible for subject NOA04 due to the marker being worn down and obscured. Some of the results for this subject will be displayed in reference to estimated treadmill speed but will not be discussed. Additionally, activities for each subject unable to be analyzed due to treadmill malfunction included: incline 3 km/h for NOA05 and all incline speeds for NOA03. Speed RMSE for each activity is shown in Figure 31. Foot based estimations were the most accurate and precise, only once surpassing 0.3 m/s RMSE for running trials. On the other-hand, shank estimations produced considerably more error. Estimation of running speed seemed to produce slightly more error than level walking, but was similar to the accuracy of incline walking. To further assess the effects of speed on error, the absolute error for each trial within an activity group was compared for each sensor. In the case of the foot sensor, error seemed to increase with increasing speed only for incline walking and level running as shown in Figure 29.

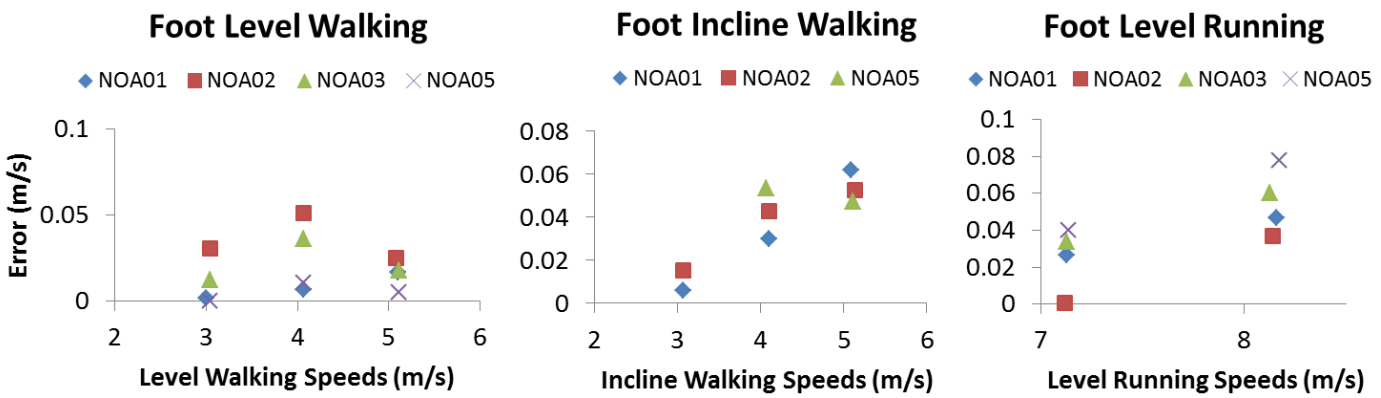

Figure 29. Absolute errors shown in each foot sensor trial.

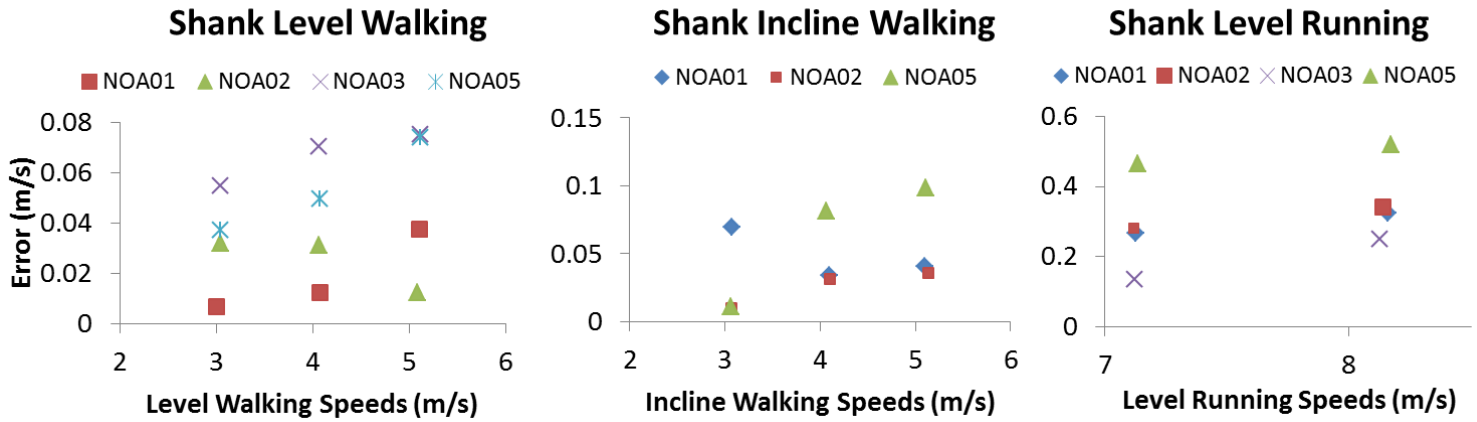

Figure 30. Absolute errors shown in each shank sensor trial.

Average Activity RMSE (m/s)

	Walking (3, 4, 5 km/h)		Incline (3, 4, 5 km/h)		Running (7, 8 km/h)	
	Shank	Foot	Shank	Foot	Shank	Foot
NOA01	0.04	0.02	0.09	0.07	0.42	0.05
NOA02	0.05	0.07	0.05	0.07	0.44	0.04
NOA03	0.12	0.04	N/A	N/A	0.28	0.07
NOA04	0.21	0.05	0.17	0.03	0.59	0.15
NOA05	0.10	0.01	0.13	0.07	0.70	0.09

Figure 31. Average RMSE for walking and running speed, broken down by subject and sensor.

The error percentage analysis demonstrated similar results and is depicted in Figure 32. The foot produced considerably less error than the shank in all activities. Error of the shank was primarily related to accuracy, as variations from the mean were small similar to the case of the foot.

Shank Sensor: Error Between Trials for Each Activity Type

	Walking (3, 4, 5 km/h)			Incline (3, 4, 5 km/h)			Running (7, 8 km/h)		
	Mean (%)	Std from Mean (%)	RMSE (%)	Mean (%)	Std from Mean (%)	RMSE (%)	Mean (%)	Std from Mean (%)	RMSE (%)
NOA01	-0.97	1.74	**2.11**	4.69	3.02	**6.49**	-13.87	0.60	**13.87**
NOA02	-2.47	1.45	**3.36**	2.12	0.83	**2.73**	-14.64	0.59	**14.65**
NOA03	-6.00	0.64	**7.38**	N/A	N/A	**N/A**	-8.93	2.91	**9.17**
NOA04	-9.37	3.55	**12.01**	-5.52	6.39	**9.30**	-19.69	1.45	**19.72**
NOA05	-4.66	0.48	**5.73**	-4.28	4.87	**7.15**	-23.20	0.39	**23.20**

Foot Sensor: Error Between Trials for Each Activity Type

	Walking (3, 4, 5 km/h)			Incline (3, 4, 5 km/h)			Running (7, 8 km/h)		
	Mean (%)	Std from Mean (%)	RMSE (%)	Mean (%)	Std from Mean (%)	RMSE (%)	Mean (%)	Std from Mean (%)	RMSE (%)
NOA01	0.52	0.73	**0.97**	2.56	1.84	**3.63**	1.70	0.51	**1.74**
NOA02	-3.33	1.41	**4.32**	3.09	1.11	**3.94**	-0.84	1.13	**1.16**
NOA03	-1.98	1.08	**2.66**	N/A	N/A	**N/A**	2.19	0.66	**2.24**
NOA04	-2.70	0.21	**3.32**	0.48	2.60	**2.67**	-4.92	0.37	**4.93**
NOA05	0.45	0.46	**0.72**	4.03	0.98	**4.09**	-2.72	1.00	**2.81**

Figure 32. Percent error measures shank (top) and foot (bottom) treadmill speed estimation.

CONCLUSION

For the foot sensor in particular, the method described consistently produced percent mean error less than 4% for level activities, save for subject NOA02 producing error around 4.5% for one trial. Running percent error was actually even lower than for level walking due to the small increase in absolute error seen going from running to walking. Speed estimation of incline walking was slightly less accurate than in level walking with mean error congregated around 4% of the treadmill marker speed. Shank estimations were much less effective and unsuitable for clinical gait analysis without further modifications. Level walking speed via the shank sensor approached those provided by the foot but the computation of incline walking and running was inaccurate. The interplay between increasing speed during walking and/or running was not clear for either the foot or the shank.

The foot based running results presented here produce smaller errors than the only validated spatio-temporal method by Yang et al.[57] Their work used a 2-d hinge model with initial velocity updates via angular velocity relationships with the shank. Considering only the shank, their method was superior as it used a different identifier for a reset condition and segmentation point for integration. However, the in-step sensor considerably surpassed the accuracy presented in their work for a shank sensor. Using comparable metrics but with five speeds and six subjects, they achieved %RMSE errors ranging from 2.87% to 5.85%. The foot method presented here achieved a %RMSE ranging from 1.16% to 2.81%. In terms of absolute error, their method produced between 0.09 m/s to 0.11 m/s absolute error. The absolute error for the foot sensor, as shown in Figure 30, ranged in absolute error from less than 0.04 m/s to a maximum of 0.078 m/s over all the trials tested. Although this foot based method was more accurate, Yang et al used more speeds, in addition to them being faster.

On the other hand, the method presented considers all 3 dimensions which could introduce error that would otherwise be lost in a 2-d model.

Additional analysis determined shank inaccuracies were most likely a result of non-zero velocity and non-zero acceleration of the shank during mid-stance period. Since the methods used here were intended for the foot sensor and its pivotal nature in gait, these inaccuracies were to be expected. Future studies incorporating new methods to provide angular updates via the accelerometer and different integration segmentations could solve the problems noted here.

A general source of error for the validation provided stems from the treadmill and motion capture. Any changes in ideal treadmill speed (acceleration) will find its way into the treadmill data. Deflection of the belt during heel strike and toe-off could cause such accelerations to occur, however small. Since no corrections are included in any algorithm to remove treadmill interactions with the sensor, these artifacts could introduce error. Additionally, the method for determining treadmill speed often had to omit treadmill belt cycles due to treadmill marker exclusion. Treadmill speed was also not calculated over instantaneous velocities but instead approximated linear periods.

The potential sources of error for the sensor based estimation are many despite best efforts to minimize them. For one, 6 parameter gyroscope calibrations using principal axis alignment were used, instead of the optimal 12 parameter LM method. The zero-velocity assumption for the foot during foot flat is supported by literature but may vary from person to person. Similarly, detected foot flat peaks are not entirely consistent due to filtering of the original data and small variations in peak shape as shown in *Event Detection*. Small initial velocities are sure to be present during mid-stance, especially on a treadmill. The assumption

here is that the velocities are small enough to ignore but eventually at some precision this assumption could introduce noticeable error; it is possible this method and others have reached that level of detail. Further studies would need to be undertaken to assess instantaneous velocities of the foot across large subject pools using an instep mounted sensor such as ours.

A stride by stride speed comparison based on Vicon heel strikes was also tested and considered but not presented. When obtaining stride velocity, a correction must be included to remove relative motion of the treadmill from the heel data. Therefore, any stride by stride comparison will produce the same mean velocity over the course of an annotated period but with slight variations on a stride per stride basis. Although this may be helpful in understanding how accurate this method is for a single stride, the validation data will not be ideal since the treadmill is not moving at a constant speed and its instantaneous speed over an entire period is very difficult to obtain. Additionally, the goal of this work is to produce long-term data collection indicative of everyday gait so extremely precise stride by stride tracking may be unnecessary.

LONGITUDINAL GAIT ANALYSIS

In order to assess the feasibility of previous activity recognition in determining subject activity months later, one subject from the NOA group returned to repeat annotated activities, as well as unannotated activity. For this session (NOB01), a variation of Archer et al's kNN approach was used to automatically identify periods of interest, e.g., walking, running and sitting. The first visit (NOA04) was used as training data for recognition of activities during the second visit (NOB01).

K-NEAREST NEIGHBOR ACTIVITY RECOGNITION

As already outlined in the background, Archer et al. employed a hierarchical kNN activity recognition method. In the original method, training and test data was partitioned from a single session of gyroscope and accelerometer data. Based on a single, pre-defined hierarchical tree, annotated labels were attached to a particular classification. A total of 12 final activity classifications were possible: unknown, level run, uphill run, downhill run, upstairs, downstairs, level walk, uphill walk, downhill walk, sitting, standing, and lying. Following training on a randomized subset of the annotated labels corresponding to the percent of training data, the rest of the data (testing subset) was classified using the kNN algorithm. Sensitivity and specificity levels were produced for both annotated and unannotated labels.

A number of modifications were made to this original method to allow for and improve use of the method for unsupervised data collection. Instead of choosing training data from the same file to be tested, the option to use training data from a separate session was included to allow for supervised in-lab training and out-of-lab recognition. Partitioning changes were also implemented to provide the most comprehensive activities possible. In

Archer's method, all annotated data corresponding to a final classification was lumped together prior to randomization. Formulation this way could cause certain annotations to be more or less weighted in the training data, or even non-existent if a certain annotation did not have much contribution. To avoid this situation, the lengths of each unique annotation within each classification group were compared. For a given classification group, an identical amount of training data was extracted from each unique annotation. This uniform and distributed amount was chosen by finding the unique annotation with the least data and finding how much of that data corresponded to the training percent specified. The purpose of this addition was to decrease the chance that a classification label became saturated with training data from a single annotation, as opposed to an even distribution.

Additionally, the hierarchical tree was modified to allow more unique classification subsets and versatility for final classifications without significant changes to the code. Intermediate classifications were minimized and final classifications were changed to an input for the method. Final classification categories were formed by matching expected annotation label names with a corresponding activity letter, similar to the pairings used in the original kNN approach. Figure 33 demonstrates the new approach.

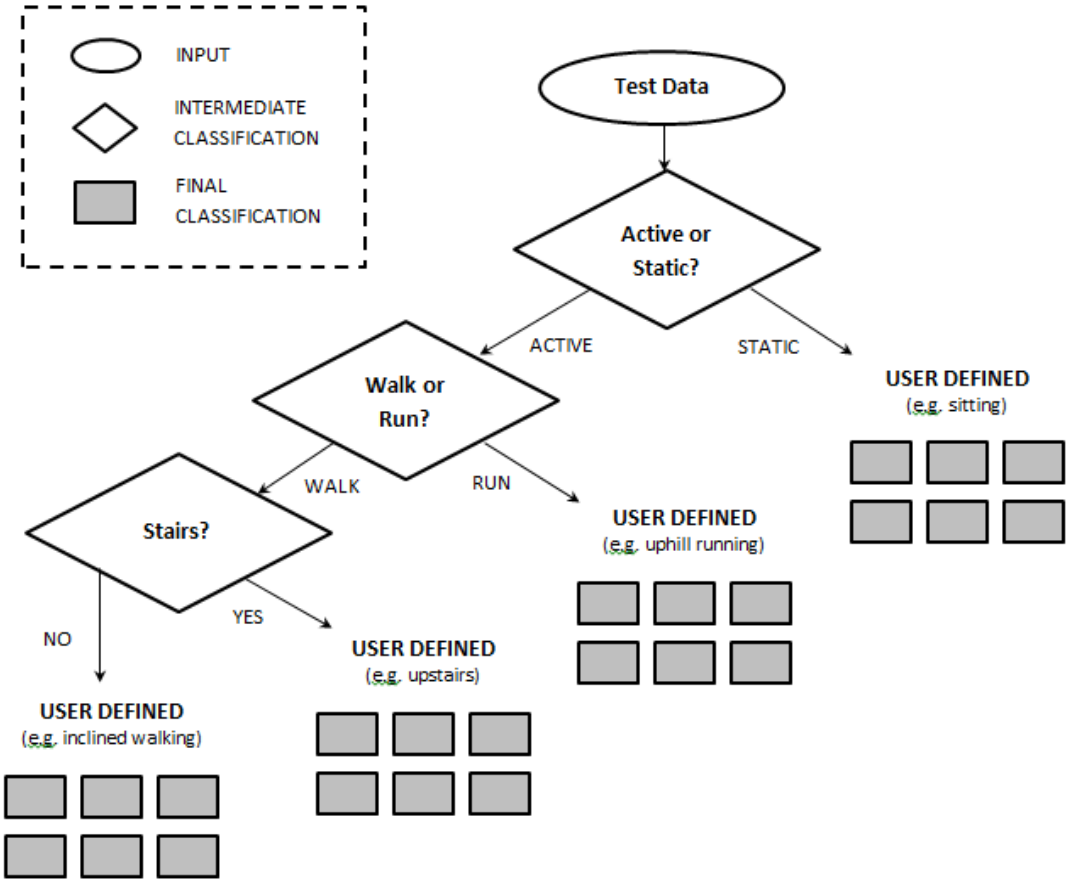

Figure 33. New hierarchical tree for kNN method

DATA COLLECTION

For the first collection (NOA03), the subject performed a number of activities that were recorded and annotated using a stop-watch synchronized with the sensor data. Variations of walking periods annotated consisted of: straight-line over-ground walking; circle over-ground walking; level and inclined treadmill walking at 3, 4, and 5 km/h; and stair climbing and descent. Running was only performed during the annotated periods and at speeds of 7

and 8 km/h on a level treadmill. Additional static activities of sitting and standing were annotated.

The follow-up collection occurred 72 days after the initial and lasted 2 hours and 36 minutes. A reduced number of annotated activities were performed at the beginning and end of the session. Straight-line over ground, stair, and treadmill walking trials were performed at the beginning of the session and identically to the first collection. Running was only performed at 7 km/h at the beginning of the collection and was not performed during any unannotated periods. The subject performed normal everyday activities following the initial activities for a couple of hours, which included over ground walking, stair walking, standing and sitting. Prior to disabling the AFO, the subject walked on a level treadmill at 3, 4, and 5 km/h for additional validation information.

USER DEFINED CLASSIFICATIONS

Two user-defined hierarchies, called activity configurations, were tested towards the purpose of long-term out-of-lab activity recognition with pre-recorded training data. If a final classification could not be reached, a label of unknown was always given. Static posture, stair walking and running classifications were identical between the two hierarchies. Final static classifications included standing or sitting; running intermediate classification always translated to a final classification of level running since incline running was not included in this test. Stair climbing and descending were the two separate final classifications possible for the stair identified trials.

The variations in user-defined hierarchies only occurred past the intermediate classification of walking, no stairs. Activity configuration 1 yielded distinct final classifications for inclined walking and level walking. Incline walking was only represented by

the various walking speeds during incline. Level walking included annotations of straight-line over ground walking, treadmill walking at various speeds, and circle walking. Note only treadmill walking was included in the training data; the rest of the level walking activities were validated in the test data. Activity configuration 2 did not differentiate between the grade of walking, producing a general walking activity prediction encompassing level and incline walking annotations. Since spatio-temporal methods may be capable of determining grade and the kinematics of level walking and everyday inclines would be similar, distinguishing grade with kNN could add unnecessary complexities and error to the recognition process. Additionally, unlike stair climbing and walking, there is not a discrete difference between incline and level walking. Other variations in the hierarchy are conceivable but these two choices seemed the most logical, given the activities passed. In the event that more activities became of interest, this system would make it simple to incorporate them.

DATA ANALYSIS

Prior to analysis of the follow-up trial, 50% and 75% partitioning of training data was used on the first collection and then tested on the remaining data for sensitivity and specificity of annotated activities. Declassification was also tested by varying the declassification constant used with the original method. Next, the training data from NOA04 was used to recognize activities during the NOB01 collection. Both the testing data for the initial and follow-up collection were performed in the context of activity configuration 1 and 2. All 23 features were used toward classification.

Initial Collection Recognition

Figure 34and Figure 35 demonstrate the sensitivity, specificity, and combined sensitivity and specificity for 50 and 75% training on the initial collection. In a practical setting, 100% of the data could be used for training but the interest here is to gauge the effectiveness of the method on untrained data. The declassification scaling constant presented in the original work was also decreased for the intention increasing specificity at the expense of sensitivity. This scaling constant decreases the allowable variation in classifiable parameters so that a lower constant increases declassifications, which can lead to higher specificity.

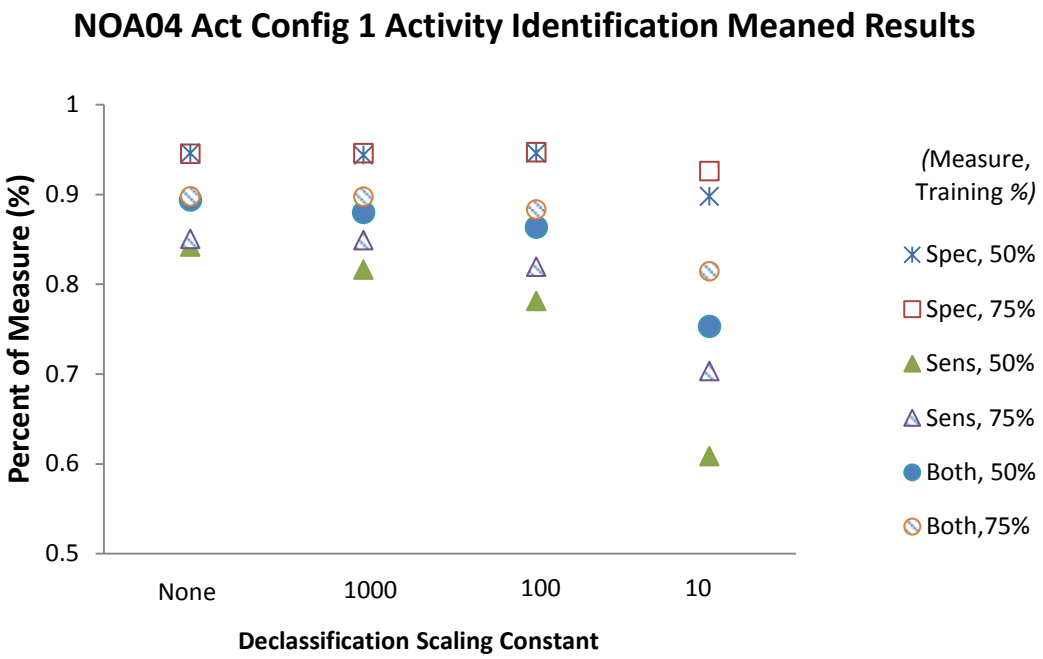

Figure 34. Activity identification results for NOA04 with activity configuration 1.

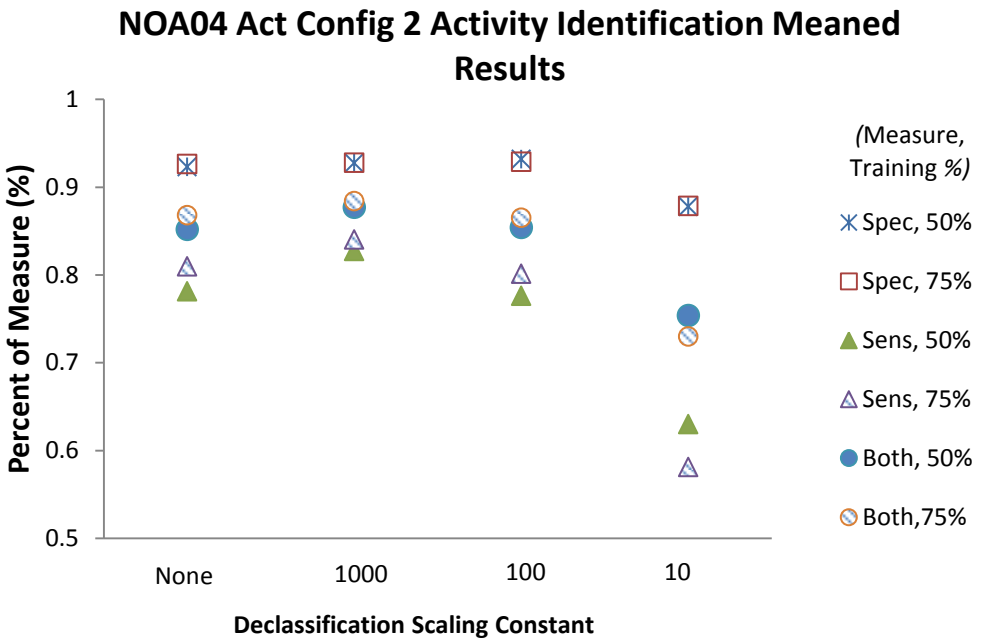

Figure 35**. Activity identification results for NOA04 with activity configuration 2.**

Activity configuration 1 yielded slightly better results in specificity and sensitivity, as well as improving more with increased training as compared to activity configuration 2. Configuration 1 followed the expected trend of decreasing sensitivity and increasing specificity as the scaling constant decreased. However, the second configuration did not follow this pattern and actually peaked in mean sensitivity and specificity. The superiority of activity configuration 1 is more than likely due to the separation of incline and level walking activities, since lumping them together as in activity configuration 2 would cause a larger spread within features resulting in more false positives.

Since the methods of this work are most related to walking and running activities, the individual results of each configuration with varying sensitivity and specificity were also analyzed. Activity configuration was clearly superior in terms of sensitivity and specificity for this comparison as well, as shown in sensitivity and specificity for running were nearly

identical between the configurations since the only modifications made were related to walking. Sensitivity and specificity were both perfect for running, except for the final declassification scaling, in which mean sensitivity and specificity combined was slightly over 70%. These results indicate the majority of errors with this classification scheme come from activities other than running and walking.

Table 8. Accuracy of activity configuration on walking recognition with varied training and training percentage and declassification.

Declass Scaling Constant	Act Config 2 Walking				Act Config 1 Walking (Level and Inclined Lumped)			
	Mean Specificity		Mean Sensitivity		Mean Specificity		Mean Sensitivity	
	50% TR	75% TR	50% TR	75% TR	50% TR	75% TR	50% TR	75% TR
None	75.41%	77.09%	100.00%	100.00%	92.50%	91.97%	100.00%	100.00%
1000	76.19%	76.88%	99.48%	100.00%	92.49%	92.30%	100.00%	100.00%
100	79.57%	78.77%	100.00%	100.00%	92.15%	93.70%	100.00%	100.00%
10	86.80%	83.77%	39.58%	65.79%	94.65%	94.92%	33.64%	39.44%

From this analysis, activity configuration with a scaling constant of 100 and 75% partitioning of training data from NOA04 was chosen as the parameters for the follow-up recognition. Although a scaling constant of 1000 produced slightly better results than 100 for annotated activities, specificity of unannotated activities would be higher with a smaller scaling constant. Since true specificity of unannotated activities is difficult to determine, these parameters were chosen on the side of caution. Additionally, walking variations are probably not well defined in the data collected so lower sensitivity are to be expected with normal walking data.

Follow-up Collection Activity Recognition

Due to the modifications to the original method, the ability to provide training data from separate files allowed identification of activities in the follow-up collection occurring months later. A 75% partitioning of test data and a declassification constant of 100 were used in the calculation of activities. All other parameters were left as the defaults originally defined by Archer.

The methodology was successful in identifying all annotated activities as shown in Table 9. Incorrect classifications of level walking were all attributed to upstairs or downstairs walking. Similarly, downstairs sensitivity errors resulted from incorrect classifications to upstairs walking. Although the annotated data was not particularly long, the results demonstrate the extensibility of training data from previous collections to new collections.

Table 9. Classification results for follow-up collection, using initial collection as training

	Final Activity Classifications				
	Standing	Level Walking	Level Running	Upstairs	Downstairs
Sensitivity	100.00%	97.66%	100.00%	100.00%	85.71%
Specificity	100.00%	94.13%	100.00%	91.72%	97.51%
Length (s)	4	256	44	15	12

To examine the unannotated everyday activities performed by the subject, activity predictions were manually examined during the period between annotated collection at the beginning and end of the session. This period lasted approximately an hour and 24 minutes. Walking predictions were filtered by removing any periods shorter than 10 consecutive identified sections of walking. All predictions followed the general consistency expected of z angular velocity trends previously described. These walking periods were much more transient in signal magnitude than treadmill walking but no issues with identification was

observed. The minimum length of walking period found was 10 s and the maximum was three minutes and 50 seconds. The maximum seems to coincide with the subject walking from the lab location to a coffee shop. Another long walking period within 30 minutes of the maximum occurrence was found possibly accounting for returning back to the lab. A total of 19 minutes of walking periods greater than 10 seconds were found over a total of 21 periods.The z frame angular velocity filtered for peak detection (5 Hz low-pass, 0.1 Hz high-pass) during the 10s period is shown below in Figure 36. The trends and associated gait events observed are similar to those seen and identified successfully in *Detection Validation*.

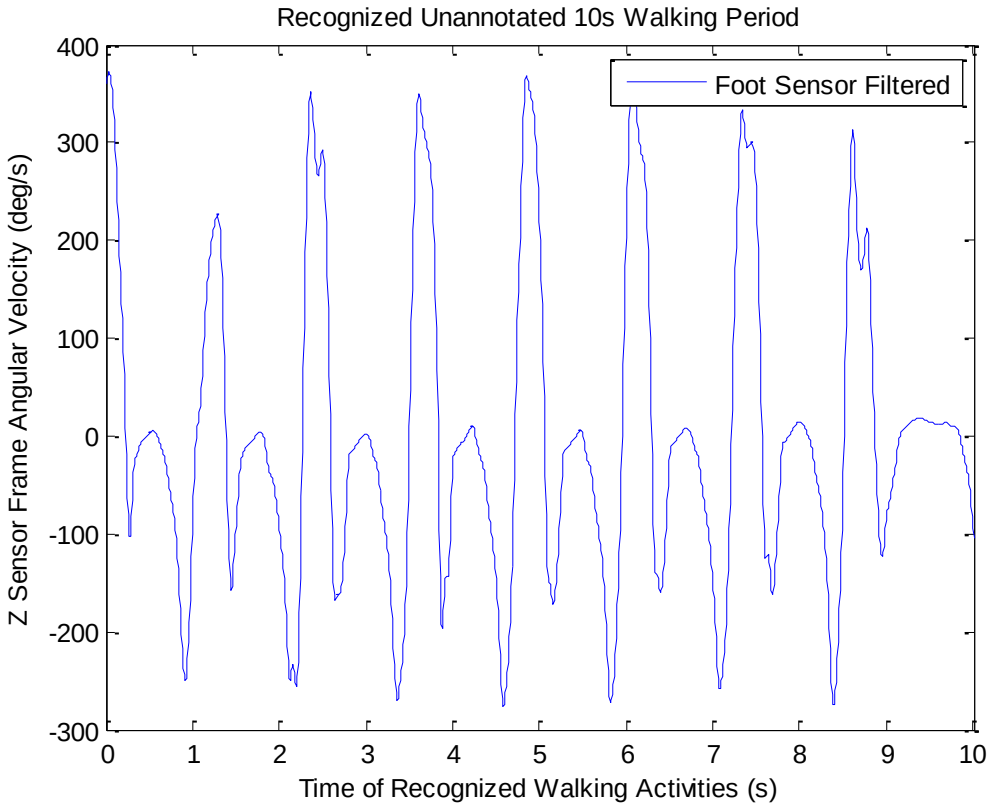

Figure 36. Lateral (*z*) angular velocity 10 second period (minimum length allowed)

Spatio-Temporal Analysis

To prove the effectiveness of the methods in this work toward analyzed unannotated, automatically recognized periods of natural motion, the aforementioned period of 10s will be analyzed. Longer periods of identified walking were generally less transient and more normal which is the motivation behind using the shorter period; longer periods were also tested effectively but will not be presented.

Peak detection properly identified all foot phases during the walking period, except for the first stride. This is an inconsequential result as that stride was ignored due to technicalities in the algorithm; if initial strides are desired, additional measures could be added to include them. Figure 37 below demonstrates the results.

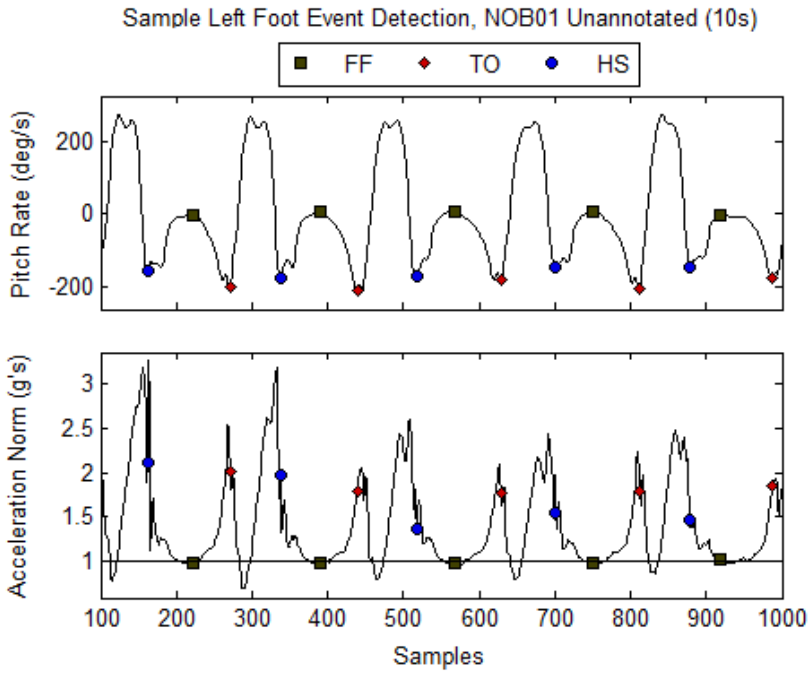

Figure 37. Peak detection results for an unannotated 10s walking period. Note a couple strides are omitted to increase clarity of the plot

Gait metrics of interest were also calculated as previously developed and defined. Table 10 shows these parameters for each stride, as well as averages over the period. The self-selected speed observed in this period fell between 2.5 and 3.8 km/h. The last two strides demonstrated a decrease in stride speed and length. Cadence was fairly consistent as expected, although it is important to note its derivation was based on foot flat.

Table 10. Gait parameters calculated for each identified stride of the 10 s unannotated period.

Stride Number	Conventional		Foot Flat Based		
	Swing Phase (s)	Stance Phase (s)	Stride Length (m)	Stride Duration (s)	Speed (m/s)
Stride 1	0.52	0.85	1.31	1.31	1.00
Stride 2	0.61	0.80	1.42	1.38	1.03
Stride 3	0.56	0.88	1.43	1.43	1.00
Stride 4	0.52	0.87	1.36	1.30	1.05
Stride 5	0.60	0.84	1.23	1.53	0.80
Stride 6	0.66	0.92	1.12	1.56	0.72
averages	**0.58**	**0.86**	**1.31**	**1.42**	**0.93**
	40.22%	59.78%			

The methods of this work in conjunction with a modified version of Archer's kNN method were proven to produce at least reasonable estimates of activities, especially walking. Peak detection and gait metric identification methods performed well and produced reasonable values for unannotated data. This section provides some evidence that this body of work may produce reasonable estimates of naturally occurring everyday activity.

CONCLUSION

The framework presented in this paper provides a foundation for an embeddable remote gait analysis system. Solutions have been proposed to all major levels of design required to observe common everyday activities with a detailed biomechanical perspective. First, an ankle-foot-orthosis instrumented with accelerometers and gyroscopes embedded proximal to the shank and foot was successfully created with the help of UVA's Inertia Team and UVA Health's Prosthetics and Orthotics. Sensor processing algorithms were validated from the bottom-up, starting with sensor calibration and ending with a trainable activity recognition system. Issues were encountered in validating segment orientation which should be addressed by future work. The results demonstrated at each level of validation were comparable, if not superior to current related literature. Additionally, the detailed description of the methodology used allows the same analysis to be applied generally to embeddable sensor systems.

Spatio-temporal methods of stride speed estimation were validated with errors below 5% for all tested conditions on the foot sensor. Inclined walking error was consistently higher than walking and running with errors around 4%. The shank sensor estimates were not nearly as accurate, ranging from 5-10% error in speed estimation. This was expected considering boundary conditions were chosen and validated specifically for the foot sensor, Future work should address more optimal modeling of the shank sensor, as well as fusion algorithms to combine sensor estimations. Work proposed by Prateek et al.[65] and Skog et al.[66] has successfully demonstrated error reduction when using multiple sensor systems and Kalman filters. Extrapolation of these methods to body attached sensor arrays could result in even more accurate gait estimations. Running estimation produced significantly reduced

error as compared to the only validated running method provided in the literature which used a shank mounted sensor. More studies should be conducted on a larger number of speeds and at higher speeds to provide a more accurate comparison to Yang et al.'s method.[57]

To test the comprehensive use of the system, a subject performed activities a couple months prior to returning for a second session in which similar activities were performed. The k-Nearest-Neighbor based activity recognition provided high accuracy and sensitivity results for activities during both collections. Annotated walking in particular was identified with over 90% specificity and sensitivity in the first trial and 98% specificity and 94% specificity for the second trial. Recognized walking periods greater than 10 seconds during the follow-up collection produced recognizable walking data with no visual errors. Longer periods of walking were found to produce more consistent stride information than short periods. Furthermore, measure of cadence, stride length, stride speed, swing phase, and stance phase were extracted for one 10s walking period using spatio-temporal methodology.

Although one long-term simulation was performed using an initial and follow-up collection with unannotated data analysis, the effectiveness of the hardware and methods have not been assessed during intended use exceeding 5 hours. A static trial of 17 hours was performed and data quality was not adversely affected but the consequences of heavy use could affect the durability or reliability of hardware. Similarly, changes in sensor properties over long collections could provide problems for signal processing techniques.

Data was also recorded on a number of cerebral palsy (CP) patients but could not be processed in time to present for this work. This is a considerable limitation of the work given the ultimate goal of use with CP. However, preliminary investigations into sensor

outputs during walking in functional CP suggest extensibility of spatio-temporal methods. Since the pivotal nature of the foot at mid-stance should not change even in severe cases of equinus gait, the most expected challenge with extension of this work to CP is identification of gait events and boundary conditions. Foot flat in control groups was an ideal boundary condition due to the smooth transition occurring from heel strike to foot flat, as well as the large range by which foot flat can be inconsequentially chosen. For CP, particularly level III and higher GMFCS, the margin for error in foot flat identification or some other ideal boundary condition may be smaller. The foot flat term may also no longer be representative since spastic plantar-flexion may physically limit the ability to flatten the foot throughout a stride.

FUTURE WORK

A new platform is currently being tested by the Inertia Team specifically for use in children's AFOs. With help from Prosthetics and Orthotics, children affected by cerebral palsy will be fitted for AFOs similar to what they would normally wear but with very small form factor sensors embedded in the instep and shank. Following molding of an everyday AFO with the sensor platform inside, children will be able to visit our gait lab following doctor visits to calibrate and train the sensors for activity recognition prior to returning home. Once home, data will be collected continuously over the course of an entire day while they walk, run, stand, sit and perform many other activities. This procedure will allow both validation of the methods used, as well as clinically relevant observations never before available. Future work for this platform will also develop an interface for the children or their parent to plug in the AFO at night and automatically offload their daily data to a cloud. Cloud storage will allow for direct access of the files to be processed by the methods demonstrated, at which point remote gait analysis will finally be available for clinical analysis.

The spatio-temporal methods presented could also be refined, particularly with the addition of a magnetometer to the current sensor combination of an accelerometer and gyroscope. This will allow more accurate determination of segment and joint angles, as well as directionality of linear motion. Work implementing magnetometers with accelerometers and gyroscopes is well established and more accurate than accelerometer/gyroscope systems. Some such systems utilizing Kalman filters are even capable of providing angle boundary condition updates without the need of a specific, repeatable reset condition (foot flat) as used here. As presented here, directionality of stride length was not validated or tested directly given the inability to explicitly determine toe-out angle and relative insignificance of directional components of a stride in clinical analysis. With a magnetometer and more advanced orientation tracking, numerous works have already demonstrated the ability to track directionality of long distance walking. The addition of such capabilities would be particularly useful in extension of these methods to hiking, competitive running, or other athletics.

LIST OF COMMONLY USED TERMS

AFO	ankle-foot-orthosis
Master	TEMPO node placed in the shank of the AFO
Slave	TEMPO node placed in the instep of the AFO
CP	cerebral palsy
IMU	inertial measurement unit
MEMS	microelectromechanical sensor/system
LM	Levenberg-Marquardt least squares method
GN	Gauss-Newton least squares method
GN-MRP	Gauss-Newton least squares method with matrix rank partitioning
FF	IMU determined foot flat during gait cycle, commonly mid-stance
FO	IMU determined foot off during gait cycle, commonly toe-off
FS	IMU determined foot strike during gait cycle, commonly heel strike
TEMPO	"Technology Enabled Medical Precision Observation" technology developed by University of Virginia's Inertia Team
ADC	digital output of analog sensor

REFERENCES

1. Bennett, B. C. *et al.* Center of Mass Movement and Energy Transfer During Walking in Children With Cerebral Palsy. *Arch. Phys. Med. Rehabil.* **86,** 2189–2194 (2005).

2. Archer, C. M., Lach, J., Chen, S., Abel, M. F. & Bennett, B. C. Activity classification in users of ankle foot orthoses. *Gait Posture* **39,** 111–117 (2014).

3. Cuccurullo, S. Physical Medicine and Rehabilitation Board Review. (2004). at <http://www.ncbi.nlm.nih.gov/books/NBK10277/>

4. Perry, J. *Gait Analysis: normal and pathological function*. (SLACK, Inc., 1992).

5. Self-selected gait speed: A critical clinical outcome | Lower Extremity Review Magazine. at <http://lowerextremityreview.com/article/self-selected-gait-speed-a-critical-clinical-outcome>

6. Sullivan, K. J., Knowlton, B. J. & Dobkin, B. H. Step training with body weight support: Effect of treadmill speed and practice paradigms on poststroke locomotor recovery. *Arch. Phys. Med. Rehabil.* **83,** 683–691 (2002).

7. Baumhauer, J. F., Alosa, D. M., Renstrom, A. F., Trevino, S. & Beynnon, B. Test-retest reliability of ankle injury risk factors. *Am J Sports Med* **23,** 571–4 (1995).

8. Zatsiorsky, V. M. *Kinematics of Human Motion*. (Human Kinetics, 1998).

9. Schopp, P., Klingbeil, L., Peters, C. & Manoli, Y. Design, geometry evaluation, and calibration of a gyroscope-free inertial measurement unit. *Sens. Actuators Phys.* **162,** 379–387 (2010).

10. Gong, J. & Lach, J. Reconfigurable differentiall accelerometer platform for inertial body sensor networks. in *2013 IEEE Sens.* 1–4 (2013). doi:10.1109/ICSENS.2013.6688327

11. Powell, H. C., Hanson, M. A. & Lach, J. A Wearable Inertial Sensing Technology for Clinical Assessment of Tremor. in 9–12 (2007).

12. Hanson, M. A., Powell, H. C., Barth, A. T., Lach, J. & Brandt-Pearce, M. Neural Network Gait Classification for On-Body Inertial Sensors. *Wearable Implant. Body Sens. Netw. 2009 BSN 2009 Sixth Int. Workshop On* 181–186 (3). doi:10.1109/BSN.2009.48

13. Q.Li, J.A.Stankovic, M.Hanson, A.Barth & J.Lach. Accurate, Fast Fall Detection Using Gyroscopes and Accelerometer-Derived Posture Information. *Int. Workshop Body Sens. Netw.* 138–143 (2009).

14. Chen, S., Cunningham, C. L., Lach, J. & Bennett, B. C. Extracting spatio-temporal information from inertial body sensor networks for gait speed estimation. in *Body Sens. Netw. BSN 2011 Int. Conf. On* 71–76 (IEEE, 2011).

15. Chen, S., Cunningham, C. L., Bennett, B. C. & Lach, J. Enabling longitudinal assessment of ankle-foot orthosis efficacy for children with cerebral palsy. in *Proc. 2nd Conf. Wirel. Health* 1–10 (ACM, 2011).

16. Barth, A. T., Hanson, M. A., Powell, H. C. & Lach, J. TEMPO 3.1: A Body Area Sensor Network Platform for Continuous Movement Assessment. in 71–76 (2009).

17. Preece, S. J. *et al.* Activity identification using body-mounted sensors--a review of classification techniques. *Physiol. Meas.* **30,** R1–33 (2009).

18. Archer, C. Activity Classification in Users of Ankle Foot Orthoses. (2013).

19. Stakkeland, M., Prytz, G., Booij, W. E. & Pedersen, S. T. Characterization of Accelerometers Using Nonlinear Kalman Filters and Position Feedback. *IEEE Trans. Instrum. Meas.* **56,** 2698 –2704 (2007).

20. Batista, P., Silvestre, C., Oliveira, P. & Cardeira, B. Accelerometer Calibration and Dynamic Bias and Gravity Estimation: Analysis, Design, and Experimental Evaluation. *IEEE Trans. Control Syst. Technol.* **19,** 1128 –1137 (2011).

21. Cai, Q., Song, N., Yang, G. & Liu, Y. Accelerometer calibration with nonlinear scale factor based on multi-position observation. *Meas. Sci. Technol.* **24,** 105002 (2013).

22. Lötters, J. C., Schipper, J., Veltink, P. H., Olthuis, W. & Bergveld, P. Procedure for in-use calibration of triaxial accelerometers in medical applications. *Sens. Actuators Phys.* **68,** 221–228 (1998).

23. Wong, M. S. *et al.* The effect of rigid versus flexible spinal orthosis on the gait pattern of patients with adolescent idiopathic scoliosis. *Gait Posture* **27,** 189–195 (2008).

24. Grip, N. & Sabourova, N. Simple non-iterative calibration for triaxial accelerometers. *Meas. Sci. Technol.* **22,** 125103 (2011).

25. Gietzelt, M., Wolf, K.-H., Marschollek, M. & Haux, R. Performance comparison of accelerometer calibration algorithms based on 3D-ellipsoid fitting methods. *Comput. Methods Programs Biomed.* **111,** 62–71 (2013).

26. Beravs, T., Podobnik, J. & Munih, M. Three-Axial Accelerometer Calibration Using Kalman Filter Covariance Matrix for Online Estimation of Optimal Sensor Orientation. *IEEE Trans. Instrum. Meas.* **61,** 2501–2511 (2012).

27. Zhang, H., Wu, Y., Wu, W., Wu, M. & Hu, X. Improved multi-position calibration for inertial measurement units. *Meas. Sci. Technol.* **21,** 015107 (2010).

28. Olivares, A., Olivares, G., Gorriz, J. M. & Ramirez, J. High-efficiency low-cost accelerometer-aided gyroscope calibration. in *Int. Conf. Test Meas. 2009 ICTM 09* **1,** 354–360 (2009).

29. Skog, I. & Händel, P. Calibration of a MEMS inertial measurement unit. in *Proc XVII IMEKO WORLD Congr. Rio Jan.* (2006).

30. Fong, W. T., Ong, S. K. & Nee, A. Y. C. Methods for in-field user calibration of an inertial measurement unit without external equipment. *Meas. Sci. Technol.* **19,** 085202 (2008).

31. Park, S. K. & Suh, Y. S. A zero velocity detection algorithm using inertial sensors for pedestrian navigation systems. *Sensors* **10,** 9163–9178 (2010).

32. Brégou Bourgeois, A., Mariani, B., Aminian, K., Zambelli, P. Y. & Newman, C. J. Spatio-temporal gait analysis in children with cerebral palsy using, foot-worn inertial sensors. *Gait Posture* **39,** 436–442 (2014).

33. Pappas, I. P. I., Popovic, M. R., Keller, T., Dietz, V. & Morari, M. A reliable gait phase detection system. *IEEE Trans. Neural Syst. Rehabil. Eng.* **9,** 113–125 (2001).

34. Pappas, I. P. I. *et al.* A reliable gyroscope-based gait-phase detection sensor embedded in a shoe insole. *IEEE Sens. J.* **4,** 268–274 (2004).

35. Kose, A., Cereatti, A. & Della Croce, U. Estimation of traversed distance in level walking using a single inertial measurement unit attached to the waist. *Conf. Proc. Annu. Int. Conf. IEEE Eng. Med. Biol. Soc. IEEE Eng. Med. Biol. Soc. Conf.* **2011,** 1125–1128 (2011).

36. Luinge, H. J. & Veltink, P. H. Inclination measurement of human movement using a 3-D accelerometer with autocalibration. *IEEE Trans. Neural Syst. Rehabil. Eng.* **12,** 112–121 (2004).

37. Pedley, M. Tilt Sensing Using a Three-Axis Accelerometer. (2013). at <http://cache-uat.freescale.com/files/sensors/doc/app_note/AN3461.pdf>

38. Chalmers, E. *et al.* Inertial sensing algorithms for long-term foot angle monitoring for assessment of idiopathic toe-walking. *Gait Posture* **39,** 485–489 (2014).

39. Bonnabel, S., Martin, P. & Salaun, E. Invariant Extended Kalman Filter: theory and application to a velocity-aided attitude estimation problem. in *Proc. 48th IEEE Conf. Decis. Control 2009 Held Jointly 2009 28th Chin. Control Conf. CDCCCC 2009* 1297–1304 (2009). doi:10.1109/CDC.2009.5400372

40. Bachmann, E., Calusdian, J., Hodgson, E. & Yun, X. In situ heading drift correction for human position tracking using foot-mounted inertial/magnetic sensors. in *2012 IEEE Int. Conf. Robot. Autom. ICRA* 5425–5430 (2012). doi:10.1109/ICRA.2012.6225007

41. Foxlin, E. Pedestrian tracking with shoe-mounted inertial sensors. *IEEE Comput. Graph. Appl.* **25,** 38–46 (2005).

42. Li, W. & Wang, J. Effective Adaptive Kalman Filter for MEMS-IMU/Magnetometers Integrated Attitude and Heading Reference Systems. *J. Navig.* **66,** 99–113 (2013).

43. Cooper, G. *et al.* Inertial sensor-based knee flexion/extension angle estimation. *J. Biomech.* **42,** 2678–2685 (2009).

44. Petruska, A. J. & Meek, S. G. Non-drifting limb angle measurement relative to the gravitational vector during dynamic motions using accelerometers and rate gyros. in *2011 IEEERSJ Int. Conf. Intell. Robots Syst. IROS* 3632–3637 (2011). doi:10.1109/IROS.2011.6094612

45. Favre, J., Jolles, B. M., Aissaoui, R. & Aminian, K. Ambulatory measurement of 3D knee joint angle. *J. Biomech.* **41,** 1029–1035 (2008).

46. Olivares, A., Górriz, J. M., Ramírez, J. & Olivares, G. Accurate human limb angle measurement: sensor fusion through Kalman, least mean squares and recursive least-squares adaptive filtering. *Meas. Sci. Technol.* **22,** 025801 (2011).

47. Öhberg, F., Lundström, R. & Grip, H. Comparative analysis of different adaptive filters for tracking lower segments of a human body using inertial motion sensors. *Meas. Sci. Technol.* **24,** 085703 (2013).

48. Mazzà, C., Donati, M., McCamley, J., Picerno, P. & Cappozzo, A. An optimized Kalman filter for the estimate of trunk orientation from inertial sensors data during treadmill walking. *Gait Posture* **35,** 138–142 (2012).

49. Yang, S. & Li, Q. Inertial Sensor-Based Methods in Walking Speed Estimation: A Systematic Review. *Sensors* **12,** 6102–6116 (2012).

50. Peruzzi, A., Della Croce, U. & Cereatti, A. Estimation of stride length in level walking using an inertial measurement unit attached to the foot: a validation of the zero velocity assumption during stance. *J. Biomech.* **44,** 1991–1994 (2011).

51. Sabatini, A. M., Martelloni, C., Scapellato, S. & Cavallo, F. Assessment of walking features from foot inertial sensing. *IEEE Trans. Biomed. Eng.* **52,** 486–494 (2005).

52. Li, Q., Young, M., Naing, V. & Donelan, J. M. Walking speed and slope estimation using shank-mounted inertial measurement units. in *IEEE Int. Conf. Rehabil. Robot. 2009 ICORR 2009* 839–844 (2009). doi:10.1109/ICORR.2009.5209598

53. Yang, S., Zhang, J.-T., Novak, A. C., Brouwer, B. & Li, Q. Estimation of spatio-temporal parameters for post-stroke hemiparetic gait using inertial sensors. *Gait Posture* **37,** 354–358 (2013).

54. Zok, M., Mazzà, C. & Della Croce, U. Total body centre of mass displacement estimated using ground reactions during transitory motor tasks: application to step ascent. *Med. Eng. Phys.* **26,** 791–798 (2004).

55. Kose, A., Cereatti, A. & Della Croce, U. Bilateral step length estimation using a single inertial measurement unit attached to the pelvis. *J. NeuroEngineering Rehabil.* **9,** 9 (2012).

56. Lee, J. B., Mellifont, R. B. & Burkett, B. J. The use of a single inertial sensor to identify stride, step, and stance durations of running gait. *J. Sci. Med. Sport* **13,** 270–273 (2010).

57. Yang, S., Mohr, C. & Li, Q. Ambulatory running speed estimation using an inertial sensor. *Gait Posture* **34,** 462–466 (2011).

58. Kwakkel, S. P., Lachapelle, G. & Cannon, M. E. GNSS Aided In Situ Human Lower Limb Kinematics During Running. in 1388–1397 (2008). at <http://www.ion.org/publications/abstract.cfm?jp=p&articleID=8051>

59. Bergamini, E. *et al.* Estimation of temporal parameters during sprint running using a trunk-mounted inertial measurement unit. *J. Biomech.* **45,** 1123–1126 (2012).

60. Kadaba, M. P. *et al.* Repeatability of kinematic, kinetic, and electromyographic data in normal adult gait. *J. Orthop. Res.* **7,** 849–860 (1989).

61. Queen, R. M., Gross, M. T. & Liu, H.-Y. Repeatability of lower extremity kinetics and kinematics for standardized and self-selected running speeds. *Gait Posture* **23,** 282–287 (2006).

62. Zarrugh, M. Y., Todd, F. N. & Ralston, H. J. Optimization of energy expenditure during level walking. *Eur. J. Appl. Physiol.* **33,** 293–306 (1974).

63. Sekiya, N., Nagasaki, H., Ito, H. & Furuna, T. Optimal walking in terms of variability in step length. *J. Orthop. Sports Phys. Ther.* **26,** 266–272 (1997).

64. Colton, S. & Mentor, F. R. C. The balance filter. (2007).

65. Prateek, G. V., Girisha, R., Hari, K. V. S. & Handel, P. Data Fusion of Dual Foot-Mounted INS to Reduce the Systematic Heading Drift. in *2013 4th Int. Conf. Intell. Syst. Model. Simul. ISMS* 208–213 (2013). doi:10.1109/ISMS.2013.46

66. Skog, I., Nilsson, J.-O., Zachariah, D. & Handel, P. Fusing the information from two navigation systems using an upper bound on their maximum spatial separation. in *2012 Int. Conf. Indoor Position. Indoor Navig. IPIN* 1–5 (2012). doi:10.1109/IPIN.2012.6418862